University of New Mexico
UNM Digital Repository

Chemical and Biological Engineering ETDs | Engineering ETDs

9-9-2015

Investigation of calcium orthophosphate chemical effects in a post-LOCA nuclear reactor containment

Sterling Olson

Follow this and additional works at: https://digitalrepository.unm.edu/cbe_etds

Recommended Citation
Olson, Sterling. "Investigation of calcium orthophosphate chemical effects in a post-LOCA nuclear reactor containment." (2015).
https://digitalrepository.unm.edu/cbe_etds/46

This Thesis is brought to you for free and open access by the Engineering ETDs at UNM Digital Repository. It has been accepted for inclusion in Chemical and Biological Engineering ETDs by an authorized administrator of UNM Digital Repository. For more information, please contact disc@unm.edu.

Sterling Olson

Candidate

Chemical Engineering

Department

This thesis is approved, and it is acceptable in quality and form for publication:

Approved by the Thesis Committee:

Dr. Edward Blandford , Chairperson

Dr. Kerry Howe

Dr. Sang M. Han

INVESTIGATION OF CALCIUM ORTHOPHOSPHATES CHEMICAL EFFECTS IN A POST-LOCA NUCLEAR REACTOR CONTAINMENT

by

STERLING OLSON

**B.S., NUCLEAR & RADIOLOGICAL ENGINEERING,
GEORGIA INSTITUE OF TECHNOLOGY, 2013**

THESIS

Submitted in Partial Fulfillment of the
Requirements for the Degree of

**Master of Science
Chemical Engineering**

The University of New Mexico
Albuquerque, New Mexico

July 2015

Dedication

To my father

Acknowledgements

To Dr. Blandford for providing me the opportunity and funding to pursue a masters in chemical engineering. To Dr. Kerry Howe for always having an open door and a willingness to teach. To Cody Williams for his experience in the UNM CHLE lab, work ethic, and making the lab an enjoyable place to research. To Amir Ali for always pushing me to work harder; his invaluable help navigating graduate school, and leading by example. To Daniel LaBrier for the countless revisions to my papers, and witty references to jokes of a different time. To David Pease for being my chemistry source, brainstorming partner, and your attention to detail. Seung-Jun Kim for being a friend as I transitioned into graduate school. To Floren Rubio and Joel Hughes for figuring out graduate school with me. To Chris Fullerton for introducing me to the GSI-191 bench scale laboratory, always being willing to work, and making work fun. To James Pike who was responsible for a collecting a large portion of the 4000 series data. To Lexy O'Rourke for her help in the 4000 series bench tests. Monica Padilla for her review, and thesis guideline knowledge. To Carlos Charry for first of all the uncountable nights spent studying together to get to graduate school, and secondly for the review of my thesis. Thanks to Aaron Gomez for keeping me laughing and in good spirits during the thesis writing period. Most of all thank you to Erica Brown, my editor and partner who kept me stress free, feed, and spent her nights awake with me editing this thesis. I could not have done it without everyone's help. Thank you team.

Investigation of Calcium Orthophosphates Chemical Effects in a Post-LOCA Nuclear Reactor Containment

by

Sterling Olson

B.S. Nuclear & Radiological Engineering, Georgia Institute of Technology, 2013
M.S. Chemical Engineering, University of New Mexico, 2015

Abstract

Calcium leached from NUKON fiberglass in containment following a Loss of Coolant Accident (LOCA) could lead to the formation of chemical precipitates that in turn cause head-loss increase due to filtering through a fibrous debris accumulation at the sump pump screens. Experiments conducted on the bench scale show that the level of fiberglass destruction does not affect the concentration of calcium leached. Reduced-scale experiments were conducted on three solution inventory scales (0.5 L, 31.5 L, 1136 L) with three different flow conditions, and two fiberglass concentrations to investigate calcium release from NUKON fiber. Results showed that the calcium leached at a constant temperature of 80 ^{o}C in borated-buffered solution over a 30-day period has a repeatable behavior. The calcium concentration behavior can be divided into four distinct regions as a function of time. These distinct regions are comprised of a prompt release of calcium, a metastable region, followed by an autocatalytic drop region and a final stable concentration region. The prompt release of calcium determined by the fiberglass concentration determined the maximum calcium concentration reached and the time taken to reach the metastable position. The metastable position of calcium is due to the formation of an amorphous calcium phosphate (ACP) whose solubility is decreased by the presence of magnesium, which also leaches from NUKON fiberglass. Magnesium has been shown to behave in a similar manner as calcium. The magnesium concentration initially increased to the metastable solubility limit of calcium and then drop out of solution. This drop in magnesium concentration coincides with the autocatalytic drop in calcium concentration to the final stable position. Understanding the calcium leaching from NUKON fiberglass a prototypic debris bed prepared with NUKON fiberglass and particulates was generated in a vertical head-loss column to quantify the corresponding head-loss change due to the in situ calcium leaching. The measured head-loss slope was compared to regional changes in calcium concentration and found to continually increase from 4.4” H_2O to 12.2” H_2O (Head-loss temperature corrected to 20^{o}C over an experimental period of 20 days.

Contents

List of Figures

List of Tables

Glossary

4000 Series	Separate effects calcium leaching from NUKON fiberglass
4100 Series	Effects of Fiberglass destruction on Calcium Leaching
4200 Series	Solubility limit and post-LOCA containment solution
4300 Series	Leaching experiments (3 bench, 1 tank) carried out for varying total leaching time
4300.P1	One day bench leaching experiment
4300.P3	Thirty day bench leaching experiment
4300.P2	Eight day bench leaching experiment
4300.Tank	Thirty day tank scale leaching experiment
4400	Vertical head-loss column chemical effects
ACP	Amorphous calcium phosphate ($Ca_xH_y(PO_4)_z \cdot nH_2O$, n= 3-4.5; 15-20% $\cdot H_2O$)
ANL	Argonne National Lab
BWR	Boiling water reactor
Cal-Sil	Calcium silicate

CDHA	Calcium-deficient hydroxyapatite $Ca_{(10-x)}(HPO_4)_x(PO_4)_{(6-x)}(OH)_2$
CHLE	Chemical head loss experiment
CSS	Containment spray system
DCPA	Dicalcium Phosphate Anhydrous ($CaHPO_4$)
DCPD	Dicalcium Phosphate Dihydrate ($CaHPO_4.2H_2O$)
ECC / ECCS	Emergency Core Cooling / Emergency Core Cooling System
FAP	Fluorapatite ($Ca_{10}(PO_4)_6(OH)_2$)
GL	Generic Letter
GSI-191	Generic Safety Issue - 191
H_3BO_3	Boric Acid
HAp	Hydroxyapatite ($Ca_{10}(PO_4)_6(OH)_2$
HCL	Hydrochloric acid
HL	Head loss
ICET	Integrated chemical effects test
ICP-OES	Inductively coupled plasma – optical emission spectroscopy

IN	Information Notice
IOZ	Inorganic zinc
LANL	Los Alamos National Lab
LBLOCA	Large Break LOCA
LiOH	Lithium hydroxide
LOCA	Loss of coolant accident
Log(C)	Logarithm base 10 of concentration
MCPA	Monocalcium phosphate anhydrous ($Ca(H_2PO_4)_2$
MCPM	Monocalcium phosphate monohydrate ($Ca(H_2PO_4)2{\cdot}H_2O$
NaOH	Sodium hydroxide
NaTB	Sodium tetraborate
NPSH	Net positive suction head
NRC	Nuclear Regulatory Commission
OAp	Oxyapaptite ($Ca_{10}(PO_4)_6O$
OCP	Octcalcium phosphate

PRL	proton reference level
PWRs	pressurized water reactors
Large-scale	Experiments on the column and tank scale
RHR	Residual Heat Removal
RMS	root mean square
RO	reverse osmosis
RWST	Reactor Water Storage Tank
SEM	Scanning electron microscope
SNC	Southern Nuclear Company
SRV	Safety relief valve
WEC	Westinghouse Science & Technology
TSP	Trisodium phosphate ($Na_3(PO_4)_2.12\ H_2O$).
TTCP	Tetracalcium phosphate ($Ca_{10}(PO_4)_2O$)
UNM	University of New Mexico
USI	Unresolved safety issue
WCAP	WCAP-16530-NP

α-TCP α-Tricalcium phosphate (α-$Ca_3(PO_4)_2$)

β-TCP β-Tricalcium phosphate (β-$Ca_3(PO_4)_2$)

ΔP Differential pressure

Chapter 1: Introduction and Background

1.1 Introduction

The primary objective of the work described in this thesis is to characterize the leaching of calcium from low density NUKON fiberglass in trisodium phosphate (TSP) buffered and borated post loss of coolant accident (LOCA) containment water and characterize the head-loss associated with its precipitation and filtration through a debris bed accumulated at containment sump screens. Generic Safety Issue - 191 (GSI-191) was issued by the Nuclear Regulatory Commission (NRC) in 2004 requiring licensee operators of pressurized water reactors (PWRs) to perform plant specific analysis and possible modifications due to the concerns associated with debris accumulation at sump screen in the event of a LOCA. Specifically, the potential accumulation of containment debris at the emergency core cooling system (ECCS) sump strainer, could prevent recirculation of coolant water to the reactor core. The ECCS pump is designed to return water released into containment back into the reactor to prevent the core from overheating through continued recirculation of released coolant. Pumping water from post-LOCA containment floor may transport debris generated in the accident from jet impingement in the break vicinity, and latent debris to the sump screens, forming a bed and leading to head-loss across the sump screen debris bed. If head-loss increases and subsequently lowers the available net positive suction head (NPSH) below the design margin, the ECCS may not be able to adequately cool the reactor. The formation of chemical precipitates may lead to further head-loss through filtration of corrosion products across the debris bed; this additional head from generated precipitates is known as chemical effects.

Major contributors to corrosion products in post-LOCA containment include aluminum, calcium, and zinc. A fiberglass thermal insulation product NUKON, is a major contributor to released materials, the most significant being calcium. Calcium and the other elements released by NUKON can interact with containment materials to form precipitates. To the author's knowledge, no research on the separate effects of calcium leached from NUKON in a TSP buffered containment has been reported in the general literature. In an effort to understand the behavior of calcium leaching from fiberglass, leaching experiments were carried out in numerous bench scale investigations, and two large-scale experiments,

under variable flow conditions from the bench experiments. The research presented here reproduced the behavior of calcium on all spatial scales out to 30 days and identified four distinct behavioral regions. This research was able to provide an explanation for the four observed regions, and link the behavior of calcium, to the behavior of magnesium also leached from NUKON fiberglass. Ultimately, a test was run in a vertical head-loss column using a prototypical debris bed. The head-loss behavior was compared to the change in head-loss over a 20 day period. This research quantifies the separate effects behavior of calcium leached from NUKON in post-LOCA containment and sets a foundation for separate effects leaching from NUKON at high temperature. Furthermore the research provides insight for future researchers to continue investigations of calcium leached from NUKON fiberglass in post-LOCA containment.

1.2 Loss of Coolant Accidents in PWRs

Figure 1 shows the normal operation of the primary loop of a typical PWR. The primary PWR major components include a reactor vessel which houses the reactor core, steam generators to transfer heat to a secondary loop, reactor coolant pumps, a pressurizer to maintain a high pressure within the primary loop, and accumulators to supply immediate water to the reactor in the case of a loss of coolant accident. The reactor coolant enters the loop through the cold leg, flows through the down-comer, and into the pressure vessel lower plenum. The water is then circulated from the lower plenum, up the center of the reactor core where the fuel rods exchange heat to the water due to fission. The heated water exits the vessel through the hot leg heading toward the steam generator, where heat is then exchanged to a secondary loop. The secondary loop sends high quality steam to a steam turbine to produce power. Following the turbine low quality steam is condensed and sent back to the steam generator as feed water (Levy, 1999).

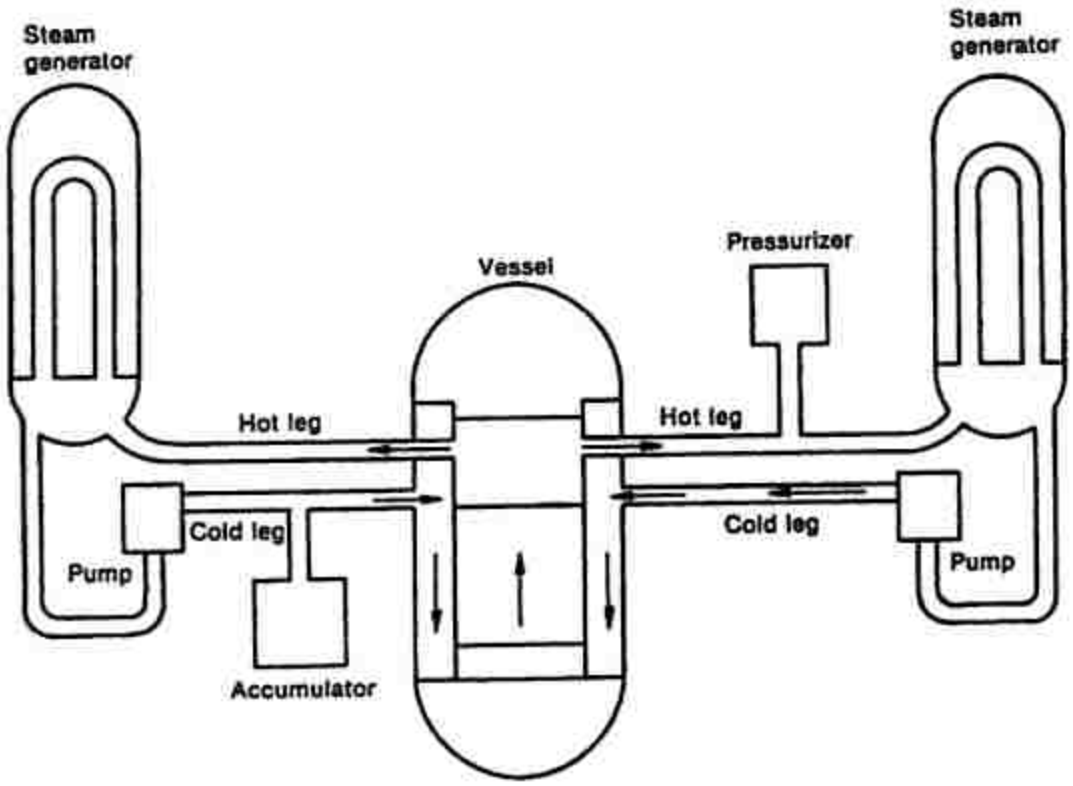

Figure 1: Typical Pressurized Water Configuration

The LOCA is an accident scenario where a break in the primary coolant loop occurs in either the hot or cold leg. Immediately following the pipe break, the reactor enters a sequence known as the blowdown phase. During this stage of the LOCA, subcooled water escapes through the pipe break at a maximum of 315ºC and 2200 psi (Lahti 2013). Stagnation of water occurs in the core due to the differences in flow conditions favoring flow out of the pipe break over flow through the pump. The reactor rapidly depressurizes and the water in the upper plenum, hot leg, and pressurizer reach saturation pressure and temperature, causing consequential flashing into steam. A preset low pressure point is reached at which point control rods are inserted, and the primary coolant pumps trip, but continue to rotate in a coast-down mode (Levy, 1999).

The blowdown phase is terminated at the initiation of water insertion from the intact accumulator loop, and the reactor enters a phase known as the Emergency Core Cooling (ECC) bypass or refill. During this stage, borated water flows from the accumulator into the lower plenum. Some of the influent accumulator flow is swept out through the break

leading to the lower plenum undergoing a series of influent water build ups, and effluent water sweep outs, until the reactor vessel depressurizes more, at which point water will remain in the lower plenum. At this point the recirculation period of the LOCA initiates, in which the ECCS pumps water from the Reactor Water Storage Tank (RWST) into containment through the containment spray system (CSS) (Levy, 1999).

The initiation of the ECCS pumps leads to the safety concern known as GSI-191, specifically addressing the issue of debris accumulation on the PWR sump screens and the induced loss of NPSH by the ECCS pump. As shown in Figure 2, debris can be removed by jet impingement in the vicinity of the break. Flow from the break may induce the transport of removed debris to containment floor. Suction from the ECCS may further induce transport of accident debris and latent containment debris to the sump pump screens. Increased head-loss across this debris bed due to this accumulation could lead the NPSH to fall below the pump design margin, preventing the ECCS from properly cooling the reactor (Lee et. al. 2008). There is further concern that an increased loss in NPSH could occur due to the particulate generation from interactions between containment materials and chemicals leading to the formation of chemical precipitates. Chemical precipitates may be filtered by debris at the sump screen leading to a decrease in NPSH known in the industry as chemical effects (Bum 2013).

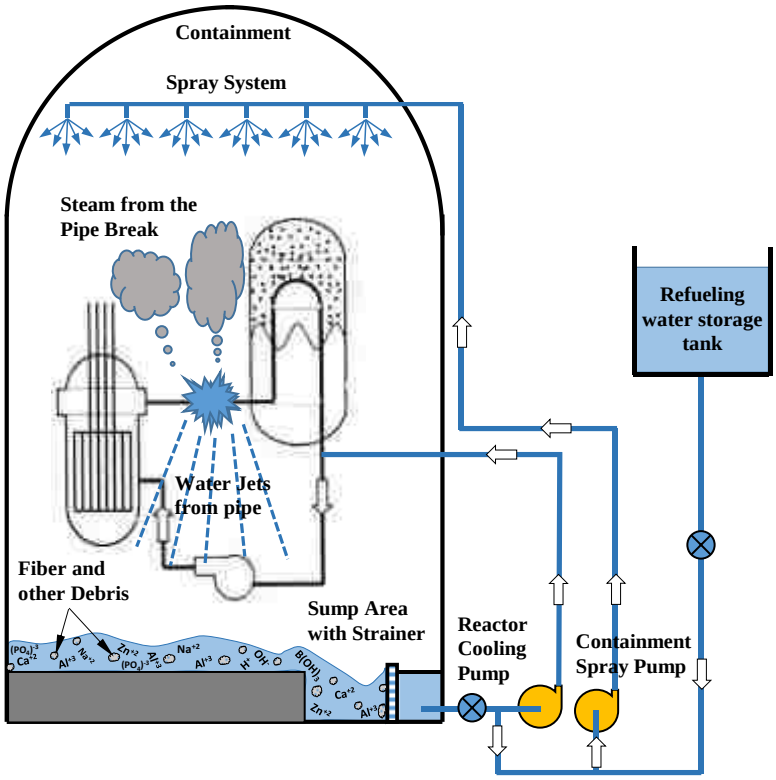

Figure 2: Hypothesized GSI-191 LOCA Scenario (Ali, 2014)

1.3 History of Generic Safety Issue – 191

Most nuclear power plants were originally licensed such that the ECCS must maintain recirculation in the event of a LOCA with up to 50% of the sump screens (PWR) or suction strainer (boiling water reactor (BWR)) area blocked. In the late 1970s the NRC began questioning the design basis of the 50% blockage criterion with the filing of unresolved safety issue (USI) A-43 (Hart 2004) addresses the NPSH falling below design specifications due to the accumulation of LOCA generated debris on the sump screens. At the time no recirculation system strainer had been designed with regard to the head-loss and the strainer structural integrity due to the associated increase in pressure. The NRC ultimately considered the original 50% blockage to be non-conservative and decided each plant should be evaluated on a plant specific basis in 1985 with the issuance Generic Letter (GL) 85-22. This required all plants to conduct an analysis and eventually led to all plants replacing existing thermal insulation with a new type of insulation, thus closing USI A-43.

This resolution promoted the idea that post-LOCA debris accumulation was solely an insulation problem (the less fibrous material the lower the chance of a potential blockage). This reasoning remained predominate until incidences of BWR strainer blockages occurred beginning in 1993 (Hart 2004).

On April 26, 1993 the NRC issued Information Notice (IN) 93-34 in response to the second of two strainer blockages at Cleveland Electric Illuminating Company's BWR Perry-1 plant. The first incident had happened in February of 1992 when miscellaneous fibers in the suppression pool were pulled into the Residual Heat Removal (RHR) suction strainer causing a sudden decrease in NPSH to 0 psig. This incident was relatively unpublicized and not considered significant until the second Perry-1 blockage incident occurred following a Swedish safety incident at Barseback-2. In the summer of 1992, the Swedish BWR Barseback-2 experience a strainer blockage, due to a safety relief valve (SRV) discharging and subsequently sending 220 pounds of mineral wool (thermal insulation) into the suppression pool and leading to possible cavitation in 1 of 2 operational suction strainers. This incident at Barseback-2 lead to the backfitting of Swedish BWRs to increase suction strainer area. Due to the Barseback-2 incident the second incident at Perry-1 brought the concern of debris accumulation at strainer screen into the NRC's focus as well as the United States public eye.

The second incident at Perry-1 in February 1993 was caused by an intentional discharge of the SRV, and the RHR system. In this event, no thermal insulation was added to the suppression pool by SRV release or any other known source, but miscellaneous fiber did accumulate on the strainer. Following the fibrous accumulation on suction strainers, the fibers then filtered out iron oxide particulate coming from the main steam and feedwater carbon steel piping and equipment. The very thin layer of filter fibers led to very high head-loss; accumulating to the point of suction strainer deformation. This incident was not immediately understood but eventually changed the industry's understanding of USI A-43 (Hart 2004).

This shift in perception with regards to the decrease of fibrous material in containment, came about because the source of the fiber was never identified, nor listed in

documented fibrous material logs. The fiber would later be known as "latent" fibrous material, and the resolution to USI A-43 was to reduce and control the fibrous insulation in containment was now deemed inadequate. To understand the events leading to 0 NPSH at the Perry-1, the NRC hired an outside consulting company to develop a head-loss correlation which considered not only fibrous material but particulates as well. This correlation is known as the NUREG-6224 correlation (more colloquially known as the 6224 correlation) and remains the industry standard to this day. The 6224 correlation predicts head-loss as a function of water velocity, water viscosity, particulate type and quantity. It was determined, from the 6224 correlation, that the relationship between head-loss and fiber quantity to be highly nonlinear, and non-monotonic, however linear with respect to particulate quantity. This correlation gave a clearer explanation to how high head-loss developed at Perry-1 due to a thin debris film, and large particulate quantity. The 6224 correlation further challenged the understating to the resolution to USI A-43 in that for the same flow conditions and particulate amount would result in a lower head-loss for increased fiber quantity. This head-loss correlation led to the issuance of bulletin 96-03 in May of 1996, which led to every BWR back-fitting units with new, large surface area suction strainers (Hart 2004).

Throughout the late 1990s, the NRC issued a number of reports for BWRs considering major contributors of particulates in the suppression pool to be paint chips and concrete. The relevance of these sources were not well understood with respect to PWRs due to their main difference such as the suppression pool, containment configuration, less carbon steel piping, and the difference in post-LOCA water chemistry. PWR investigation started with the issuance of GSI-191 in June of 2004. An initial case study conducted by Los Alamos National Lab (LANL) identified for a Large Break LOCA (LBLOCA) 60 of 69 US PWRs were either "likely" to "very likely" to have a sump screen blocked by mixed debris (Hart 2004). Since its issuance, GSI-191 has created a tremendous amount of industry research in the form of thermodynamic modeling [4,5], materials transport testing (Lee et. al 2008), bench scale materials leaching tests (Lane et. al 2006), vertical head-loss testing (Park et. al., 2006), and integrated tank testing of representative post LOCA materials (Dallaman et. al., 2006). Due to the overwhelming amount of collected data with

respect to GSI-191, this review will focus only on the research conducted with relevance to the release of calcium from NUKON fiberglass.

1.4 Historical GSI-191 Calcium Research

Previous calcium testing for GSI-191 has been carried out primarily at three testing locations: Westinghouse Science & Technology (WEC) (Lane et. al 2006), the University of New Mexico (UNM) (Dallaman et. al., 2006), and Argonne National Lab (ANL) (Park et. al., 2006). Of the three primary metals (Al, Ca, & Zn) calcium research has received the least emphasis to date. Significant containment calcium sources include concrete and piping insulation such as calcium silicate (Cal-Sil), a drywall-like piping insulation and NUKON fiberglass. The WEC program focused on bench scale separate effects leaching to study all documented containment materials. UNM conducted a series of scaled containment leaching experiments known as the integrated chemical effects test (ICET) representing a range of prototypical containment material and chemistry. ANL used results obtained from ICET program and chemical surrogate procedures developed at WEC known as WCAP-16530-NP (Lane et. al 2006) to investigate and quantify the expected head-loss due to the generation of these chemicals in different amounts. Additionally, thermodynamic modeling has been conducted (McMurrary et. al., 2006; Jain et. al., 2005) as it is an inexpensive and quick method to simulate a large number of containment conditions. The thermodynamic modeling presented herein sought to validate data obtained in ICET testing to understand the relevance of results obtained from selected thermodynamic modeling software.

The WEC research (Lane et. al., 2006) focused on benchtop leaching tests at two temperatures (87.8°C (190°F), 96.1 (205°F)), three values of pH (4.1, 8, 12) and three time scales out to a maximum of 90 min. These tests were conducted without the presence of TSP, but TSP was added to the end of some leaching tests. Following the addition of TSP filtered samples found precipitates not previously present. Using the total metals data versus leaching time obtained in the bench test, a liner regression was used to fit coefficients to a leaching model known as WCAP-16530-NP (WCAP). A sensitivity analysis using WCAP to model the initial release of 1 gram of NUKON fiberglass in a 500 mL solution has shown that the release rate is dependent on temperature but relatively unaffected by pH. The WCAP model has been found unrepresentative of calcium leaching from NUKON fiberglass in a TSP buffered environment. The modeling of the NUKON fiberglass leaching as well as the many other separate effects leaching experiments conducted in WCAP-16530-np provided insight to results obtained from integrated testing efforts.

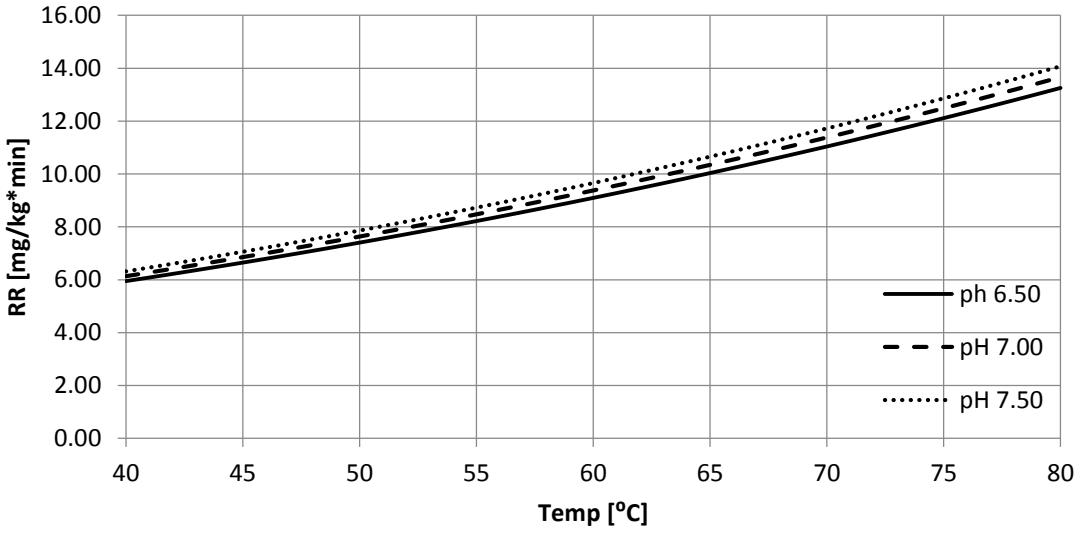

Figure 3: WCAP-16530 Calcium Release Rate for 1 g of NUKON™ at time zero

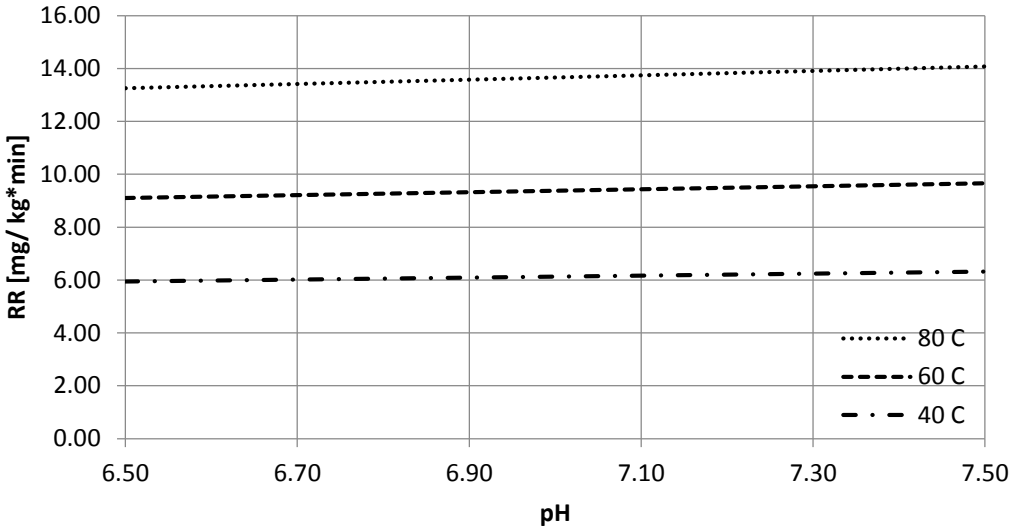

Figure 4: WCAP-16530 Calcium Release Rate for 1 g of NUKON™ at time zero

In a concurrent effort with Westinghouse separate effects bench scale leaching testing, the integrated chemical effect testing (ICET) (Dallaman et. al., 2006)was being conducted under the provision of LANL with the purpose of monitoring the chemical system for an extended time observing for the presence, composition, and physical characteristics of chemical products formed. The ICET (Dallaman et. al., 2006) series conducted leaching experiments in a large tank to replicate a scaled post-LOCA containment environment, including materials that would exist in the vapor and submerged spaces, ECCS spray systems, and recirculating solution (Figure 5). The ICET series was designed to investigate a variety of containment materials and quantities representing multiple plant environments as shown in Table 1 and Table 2. The buffering agents include TSP, sodium tetraborate (NaTB), and sodium hydroxide (NaOH) and insulation materials include calcium-silicate (Cal-Sil) and NUKON fiberglass. All ICETs are conducted to represent the recirculation LOCA phase. The initial chemical environment contained 2800 mg/L boron, 100 mg/L hydrochloric acid (HCL), and 0.7 mg/L lithium hydroxide (LiOH). The tests were conducted for 30 days at a constant temperature of 60^{o}C. The start of the test includes a 4 hour spray period which interacts with representative amount of unsubmerged containment material in order, to simulate the CSS system response during

the LOCA. Water is continuously circulated from the bottom of the tank and back into the tank through headers on the north and south side of the tank.

Table 1: ICET Experimental Conditions (Dallaman et. al., 2014b)

Experimental scale	*250-gallon tank test*
pH	**See* Table 2 *for test-specific pH target values*
Temperature	*60°C*
Testing Duration	*30 days*
Chemicals	**See Table 2 for test-specific buffer and insulation information* *Aluminum (118 ft^2)* *Galvanized steel (268 ft^2)* *IOZ coated steel (154 ft^2)* *Copper (200 ft^2)* *Uncoated steel (6 ft^2)* *Concrete(0.0014 pounds per ft^3water)* *Insulation Material (CalSil or NUKON) 0.54 g/L*
Source of Ca	*Fiberglass, Concrete, Cal-SIl*

Table 2: Expected pH, buffer and insulation used for ICET (Dallaman et. al., 2014b)

Experiment	pH	Buffer	Insulation	NUREG 6914 volume
ICET 1	*10*	*NaOH*	*NUKON*	*Volume 2*
ICET 2	*7*	*TSP*	*NUKON*	*Volume 3*
ICET 3	*7*	*TSP*	*Cal-sil (80%) and NUKON (20%) mix*	*Volume 4*
ICET 4	*10*	*NaOH*	*Cal-sil (80%) and NUKON (20%) mix*	*Volume 5*
ICET 5	*8.5*	*NaTB*	*NUKON*	*Volume 6*

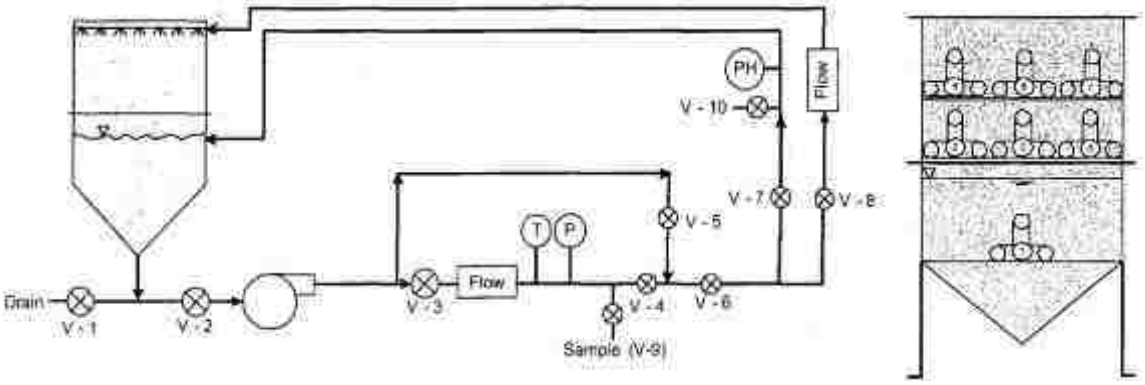

Figure 5: ICET- Test loop Schematic and coupon rack arrangement inside the tank (Dallaman et. al., 2006)

Most relevant to the research presented here was ICET 2 (Dallaman et. al., 2006), conducted using a TSP buffer at a temperature of 60°C, with a NUKON concentration of 0.54 g/L. The NUKON used in this test was heat treated on one side at 600°F for 1 day leading to the browning of one side. This burning represented prototypical heat experience in the power plant. The fiberglass was then run through a leaf shredder twice. There was a total of 4.58 ft^3 enclosed in a stainless steel mesh bag. One quarter of the NUKON was placed in the containment spray (unsubmerged) area and the other three quarters were submerged. The mesh bags reduced the movement of fiberglass through the tanks. Results of this test indicated that the test fluid remained Newtonian at all times of the test, at room and test temperatures. Analytical measurements found the presence of calcium, magnesium, silica, and sodium present in solution but not aluminum. Fiberglass examined at the $15^{th}$and 30^{th} day showed a web-like material present on the fiberglass which increased between the 15 to 30 day period. The calcium in solution remained constant at approximately 8 mg/L through the duration of the test (Figure 6). This behavior was found the match the behavior observed in the testing conducted for this research. Ultimately, the question of the chemical effects on head-loss was conducted at ANL where scenarios were run in which representative amounts of chemicals leached in ICET were used to measure head-loss across a debris bed using surrogate methods developed by the WEC bench tests.

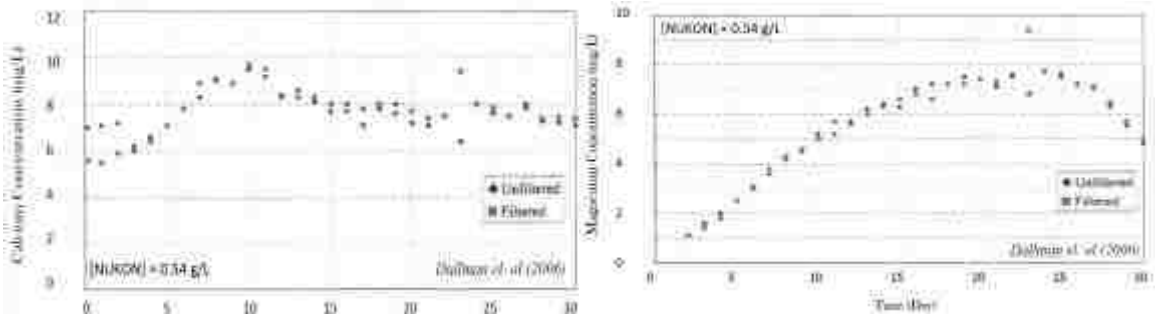

Figure 6: ICP-AES analysis for filtered and unfiltered samples of Ca & Mg during the ICET-2 30 day testing period (Dallaman et. al., 2006)

The question of the effects of LOCA-specific chemistry on sump screen head-loss was addressed by tests performed at ANL. The testing matrix considered the relative amounts of debris and precipitates arriving at the screen. The possible precipitates were dependent on containment sump residence time, transport time to the screen, initial containment pH, containment sump temperature, and the buffer dissolution rate. Tests were designed based on scenarios in which representative amounts of chemicals leached (based on ICET results) were used to measure head-loss across a debris bed using surrogate methods developed by Westinghouse bench tests. A series of the ANL experiments focused on calcium chemical effects, using two types of insulation: Calcium-Silicate and NUKON fiberglass. The loop contained a total of 119 L, a residence time of 4 minutes and loop velocities ranging from 0.02 – 2 ft/s, as well as heating and cooling capabilities (Figure 7). Fiberglass beds prepared for head-loss testing were of the blended form, which yields highly inconsistent head-loss results for replicate experiments.

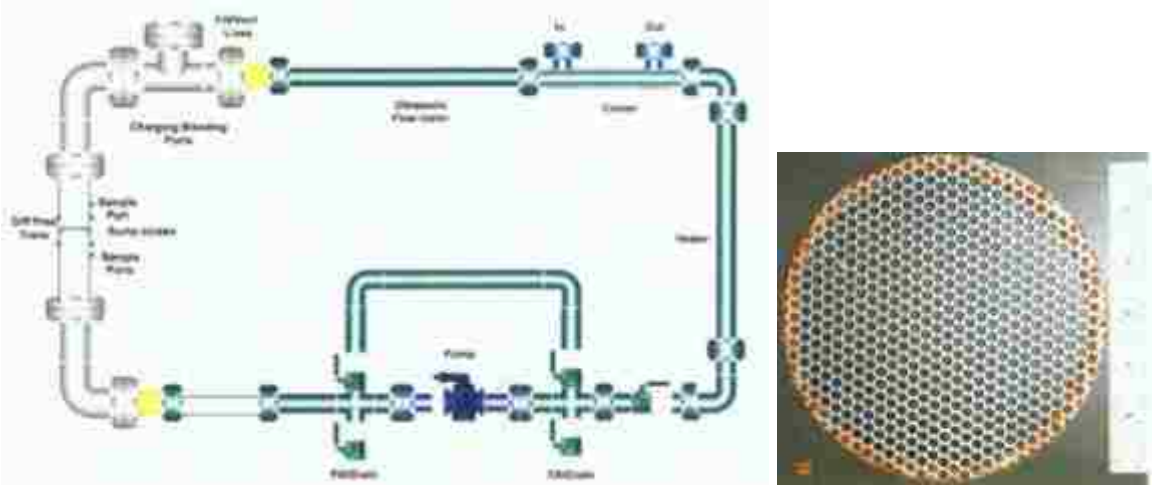

Figure 7: Schematic of the ANL test loop & vertical column perforated plate with 51% flow area, 3/16" holes, & ¼" staggered centers

ANL concluded that the relationship between head-loss and fiberglass amount is highly nonlinear and monotonic, as was previously determined in the 6224 correlation (Bum 2013). ANL further concluded that there was variable time between 1 to 4+ days to reach an equilibrium concentration of calcium. Deeper insight from these head-loss tests can be obtained by considering which calcium precipitate forms, how it may form and the precipitates properties such as size, shape, and stabilizing agents. These types of understandings have proved somewhat difficult due to the many complications of the containment system, but simulations run by thermodynamic software help provide insight to these types of questions.

LOCAs result in rapid changes in the time, temperature, pressure, chemistry, and pH conditions in containment. The materials in containment lead to further complications by interactions among materials present in the lower region of containment. Thermodynamic modeling provides an important role due to its ability to provide quick, cheap results for varying containment parameters. Following the measurements of corrosion rates, calculations of exposed surface area, and exposed time, thermodynamic simulations were run to investigate if debris generation and head-loss can be subsequently increased due to interactions between exposed materials and the ECCS/ CSS. The simulations utilized a number of different chemical speciation thermodynamic modeling software.

For each tested software, blind and predictive studies were simulated and compared to investigate if a particular program outperformed the others when compared to the results of ICET. The software comparison showed that the programs were most sensitive to the initially provided database and the chemical species it contained. No one software outperformed the others for all cases but some proved easier to manipulate parameters than others. Accuracy of the models was increased when using informed bench measurements when compared to the ICET testing, but no exact replication of experimental results could be simulated for all species. Important containment materials considered included copper, galvanized steel, aluminum, NUKON, and concrete.

Important thermodynamic modeling findings show that the dominate phases formed were controlled by the presence of NUKON, aluminum, and concrete. The majority of the predicted dominate solid phases consisted of potentially amorphous silicate phases such as sodium aluminum silicate, calcium magnesium silicate, calcium silicate, and silica. Sodium aluminum silicate was always dominant, and could lead to the formation of a gel like substance in alkaline solutions. Based on the dissolution rate of NUKON the average fiber insulation at 60^{o}C and an average of 7 μm diameter would leach in 180 hours. Furthermore, the leached contribution from NUKON is ~10,000 times more than that for concrete walls. Important findings for the thermodynamic modeling are summarized below.

Table 3: Constituent comparisons for thermodynamic modeling results at neutral and basic pH

Characteristic	pH = 7 (Trisodium Phosphate Moderator)	pH = 10 (Sodium Hydroxide Moderator)
Dominant Solid Phases	$Ca_5(OH)(PO_4)_3$ and $NaAlSi_3O_8$ with $Fe_3(PO_4)_2 \cdot 8H_2O$ (60 °C [140 °F]), Fe_3O_4, and $Fe_7Si_2O_5(OH)_4$ (150 °C [302 °F])	$NaAlSi_3O_8$ and $Ca_2Mg_5Si_8O_{22}(OH)_2$ with $Ca_3Fe_2Si_3O_{12}$ (60 °C [140 °F]) and $Fe_3Si_4O_{10}(OH)_4$ (150 °C [302 °F])
Temperature Dependencies	Redistribution of iron and zinc phases	Redistribution of iron phases
Sensitivity—Aluminum	Increasing aluminum leads to increasing $Al(OH)_3$ (60 °C [140 °F]) and AlO(OH) (130 °C [266 °F])	Increasing aluminum leads to increasing $Al(OH)_3$ (60 °C [140 °F]) and increases $NaAlSi_3O_8$ (130 °C [266 °F])
Sensitivity—Carbon Steel	Increasing iron leads to increasing $Fe_3(PO_4)_2 \cdot 8H_2O$ (60 °C [140 °F]), Fe_3O_4, and $Fe_7Si_2O_5(OH)_4$ (130 °C [266 °F])	Increasing iron leads to increasing $Fe_7Si_2O_5(OH)_4$ (60 °C [140 °F]) and $Ca_3Fe_2Si_3O_{12}$ (130 °C [266 °F])
Sensitivity—Zinc	Increasing zinc leads to increasing $Zn_3(OH)(PO_4)_2 \cdot 2H_2O$ (60 °C [140 °F]), $Zn_3(OH)(PO_4)_2 \cdot 2H_2O$, and $ZnO \cdot Fe_2O_3$ (130 °C [266 °F])	Increasing zinc leads to increasing $ZnO \cdot Fe_2O_3$ and Zn_2SiO_4
Sensitivity—Copper	No corrosion, no influence	No corrosion, no influence
Sensitivity—Concrete	Increasing concrete leads to increasing $Ca_5(OH)(PO_4)_3$ and SiO_2	Increasing concrete leads to increasing $CaSiO_3$
Sensitivity—Fiber Insulation	Increasing fiber insulations leads to increasing $NaAlSi_3O_8$	Increasing fiber insulations leads to increasing $NaAlSi_3O_8$ and $Ca_2Mg_5Si_8O_{22}(OH)_2$
Long-Term Trends (time)	Major solid constituents: $Ca_5(OH)(PO_4)_3$, $NaAlSi_3O_8$, $Ca_2Mg_5Si_8O_{22}(OH)_2$, $Fe_7Si_4O_{10}(OH)_2$, SiO_2, and Zn_2SiO_4	Major solid constituents: $NaAlSi_3O_8$, $Ca_2Mg_5Si_8O_{22}(OH)_2$, $Ca_3Fe_2Si_3O_{12}$, $CaSiO_3$, and Zn_2SiO_4

1.5 Research Motivation

Calcium testing conducted by Westinghouse bench tests were not leached in the presence of TSP and were only allowed to leach for a maximum of 90 minutes, leading to an unreliable leaching equation for NUKON fiberglass leaching in a TSP buffered solution and inconclusive results to solution behavior beyond 90 minutes (Jain et. al., 2005). To the author's knowledge, separate effects testing of calcium leached from NUKON fiberglass in the presence of TSP at high temperature has not been reported. Furthermore, to the author's knowledge, no combination of vertical head-loss through a prototypic debris bed and measurements of metals in solution has been conducted. This research was conducted to characterize chemical effects from calcium precipitation leached from NUKON fiberglass in LOCA conditions where consulting team partners provided input conditions for Southern Nuclear Company (SNC) Vogtle LOCA conditions.

Chapter 2: Precipitation Chemistry and Thermodynamic Modeling

2.1 Background

Post-LOCA containment scenarios encompasses a large array of variable materials and subsequent chemical conditions, depending of the type of break (e.g. large, small, double guillotine, etc.) and the plant design (e.g. materials used, plant layout, etc.). Historical approaches to investigating this problem include the testing of separate and integrated effects and thermodynamic modeling. This section presents background information on important post-LOCA containment chemicals and thermodynamic modeling basis for the conducted experiments. Additionally, this section will outline the chemistry basics of multi-protic acids, calcium orthophosphates, and present thermodynamic models which will predict the concentration of calcium orthophosphate present in experiments conducted during the course of this research.

2.2 Post-LOCA Solution

2.2.1 Orthophosphates

Orthophosphates are added to the post-LOCA environment in the form of a dry chemical, TSP ($Na_3(PO_4)_2 \cdot 12\ H_2O$). An orthophosphate is comprised of one phosphorous joined to four oxygens (PO_4^{3-}). Examples of other phosphates include meta- (PO_3^-), pyro- ($P_2O_7^{4-}$) and poly- ($(PO_3)_n^{n-}$) (Dorozhkin, 2007). Orthophosphates are triprotic acids, having three pK_a values which determine the phosphate's level of protonation for a particular pH, increasing protonation with decreased pH. The behavior of orthophosphate deprotonation can be observed in Equations 1, 2, 3, and graphically in Figure 8, with the most protonated species (H_3PO_4) dominating at low pH, and the most deprotonated species (PO_4^{3-}) dominating at high pH. The point at which the concentrations of an acid and its conjugate base are equal it at the point which pH equals pK_a.

$$H_3PO_4 \leftrightarrow H_2PO_4^- + H^+ \qquad pK_{a1} = 2.16 \qquad (1)$$

$$H_2PO_4^- \leftrightarrow HPO_4^{2-} + H^+ \qquad pK_{a2} = 7.20 \qquad (2)$$

$$HPO_4^{2-} \leftrightarrow PO_4^- + H^+ \qquad pK_{a3} = 12.35 \qquad (3)$$

When phosphates are present in sufficiently high concentrations in calcium containing carbonate systems, orthophosphates dominate precipitation reactions (Bachra et. al., 1965). To demonstrate the high orthophosphate concentration in comparison to carbonate, a $\log_{10}$(Concentration) (log(C)) vs. pH diagram was generated for prototypic phosphate values for a LBLOCA of 5.83 mM TSP and a typical fresh water carbonate level of 0.97 mM. The true post-LOCA accident scenario would be expected to have much lower values of carbonate. One should note this graph makes a simplifying assumption that the system is closed, which is not the case in a LOCA. A prototypic post-LOCA containment solution is seeking an equilibrium with containment gases, but this graph demonstrates that if one were to consider carbonate levels as high as those found in typical fresh water, the phosphate level is still an order of magnitude higher than the carbonate system.

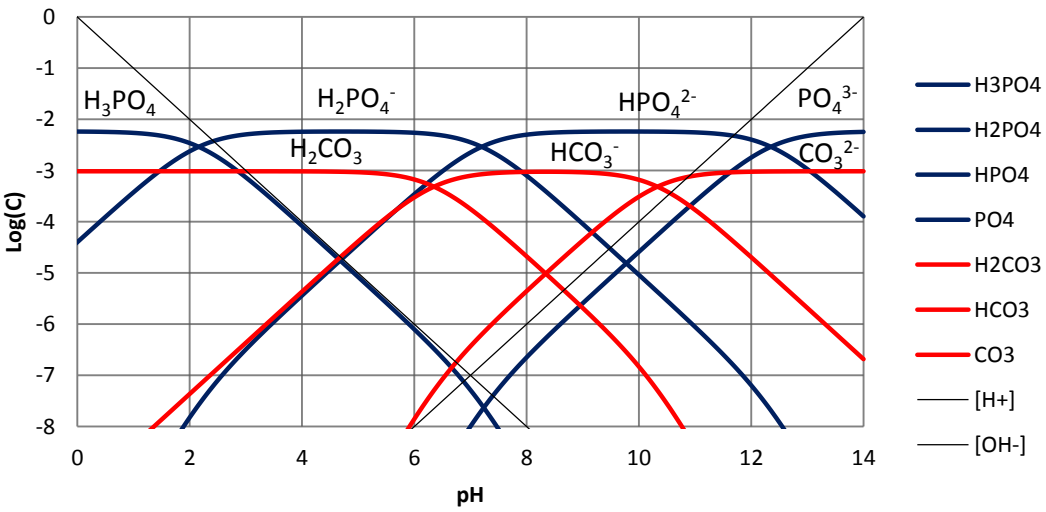

Figure 8: Log(C) vs. pH for prototypic phosphate and typical carbonate levels

2.2.2 Orthophosphate & Boric Acid

The two main constituents in post-LOCA water chemistry are TSP and boric acid. Modeling these two constituents provide insights into the expected solution pH and illustrate the accompanying dominant boric acid concentration. Boric acid is a weak acid used to control reactor activity, and is present in varying quantities during normal reactor operation. Unlike orthophosphate, boric acid is a monoprotic acid with a pK_a of 9.24 (Equation (4)). The log(C) vs. pH diagram in Figure 9 includes a prototypical post-LOCA concentration of H_3BO_3 (221.3 mM), provided for a break taking place when boric acid is at a concentration near the higher concentration during reactor operation (provide by outside consulting partners (Olson, 2014a)). The 5.53 mM of phosphate buffer addition from the dissolution of TSP allows for an estimation of pH using a graphical method, which is generated from mass balance on the hydronium concentration by a method known as the proton condition.

$$H_3BO_3 \leftrightarrow H_2BO_3^- + H^+ \qquad pK_{a1} = 9.24 \qquad (4)$$

The solution pH may be estimated by establishing a proton reference level (PRL) for each species of interest e.g. H_3BO_3, PO_4^{3-}, and H_2O. The PRL is used as a reference to define the amount of pronation for each conjugate acid or base associated in comparison to the chosen reference level. The protonated and deprotonated species that are higher and lower than the reference level are shown in Table 4. Notice that because the $H_2PO_4^-$ and H_3PO_4 species are two and three times as protonated as the PRL, each of these constituents are multiplied by a coefficient equal to the amount by the amount more protonated. This leads to the slight change observed in the relative maximums of the orthophosphate species seen in Figure 9.

Table 4: PRL table displaying the species applied in a graphical charge balance used to determine the solution pH

PRL	**H_3BO_3**	**PO_4^{3-}**	**H_2O**
>PRL	-	$[HPO_4^{2-}]$ $[2 * H_2PO_4^-]$ $[3 * H_3PO_4]$	$[H]^+$
<PRL	$[H_2BO_3^-]$	-	$[OH]^-$

The pH may be estimated graphically by beginning to trace from 2 points in Figure 9; (1) starting from the species that dominates at pH 0 ($[H^+]$) and (2) from pH 14 ($[OH^-]$). The pH is then found by tracing the dominating species defined by the PRL (Table 4), from low pH in the positive x-axis direction and the high pH in the negative x-axis direction, until the two curves intersect. If one subsequently follows each intersected dominating species curve, until the species intersect, the predicted pH is approximately 7.5, where the $H_2BO_3^-$ curve meets the $H_2PO_4^-$ curve. This estimate leads to an inaccurate result in this case because at boric concentrations greater than 0.025 M, boron will form polynuclear complexes with itself (Austria, 2008), which cannot be predicted by a simple mass and charge balance model. Further due to the multiple intersecting lines it is difficult to say that one species equals another. As will be discussed later, the expected pH will be 7.1 at 80^{o}C from equilibrium modeling, using a software package Visual MINTEQ (Gustafsson, 2012) and insights from shakedown bench testing. Nonetheless, the diagram describes the species concentrations dependence on pH and demonstrates that H_3BO_3 is the dominant boron species and HPO_4^{2-} is the dominant orthophosphate species in the region around pH 7.1.

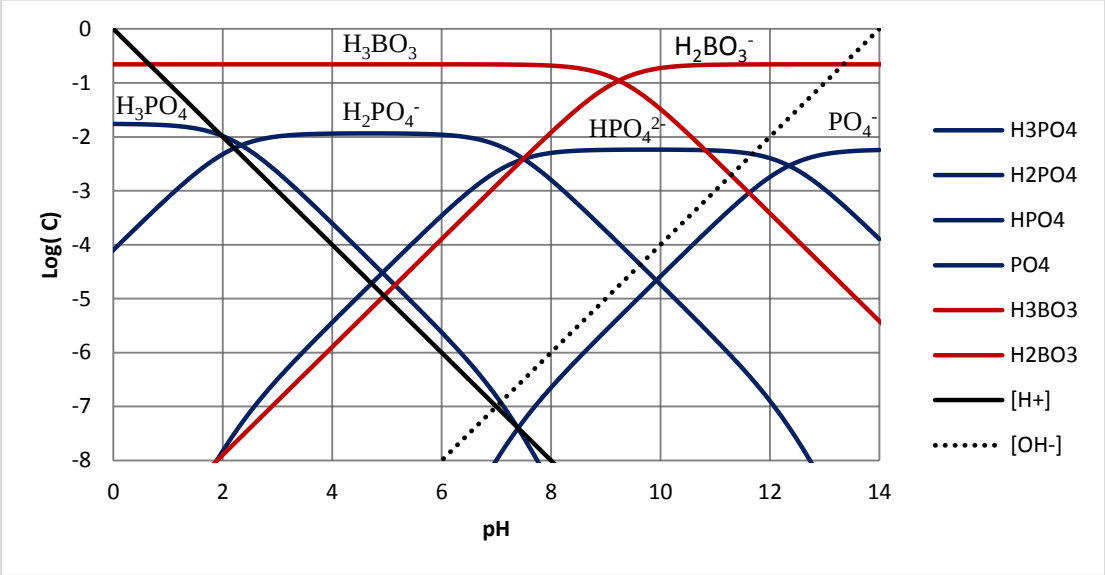

Figure 9: Log(C) vs. pH for prototypic phosphate and boric acid concentrations

2.3 Calcium Orthophosphates

There are 11 known calcium orthophosphates without ion substitutions, made up of three major elements: calcium, phosphorus and oxygen. Orthophosphates may also include a hydrogen as an acidic orthophosphate anion, or incorporate water into the lattice. All calcium orthophosphates are soluble in acids and insoluble in alkaline solution. Each phase is dependent on solution pH, temperature, and the Ca/P molar ratio. Looking to Table 5, the lower the Ca/P molar ratio the more soluble the precipitate, and more likely the precipitate is to form in acidic conditions. The triprotic equilibrium of phosphate, leads to variations in pH altering relative concentrations of the 4 polymorphs of the orthophosphoric acid. This change in relative polymorph concentrations directly impacts composition and amount of calcium orthophosphate formed (Dorozhkin, 2007) a discussion of relevant calcium orthophosphates follows. The acidic conditions necessary for the formation of monocalcium phosphate monohydrate (MCPM) and monocalicum phosphate anhydrous (MCPA) are not predicted in post-LOCA containment conditions, and are therefore excluded from further discussion. Further, Fluorapatite (FAp) and

tetracalcium phosphate (TTCP) will not be considered for this analysis due to lack of fluoride source in containment, and TTCP cannot be precipitated from aqueous solution (Dorozhkin, 2007.)

Table 5: Existing calcium orthophosphates and their major properties (Dorozhkin 2010)

Ca/P molar ratio	Compound	Formula	Solubility at 25 °C, −log (K$_s$)	Solubility at 25 °C, g l^{-1} [a]	pH stability range in aqueous solutions at 25 °C
0.5	Monocalcium phosphate monohydrate (MCPM)	$Ca(H_2PO_4)_2·H_2O$	1.14	~18	0.0–2.0
0.5	Monocalcium phosphate anhydrous (MCPA)	$Ca(H_2PO_4)_2$	1.14	~17	[c]
1.0	Dicalcium phosphate dihydrate (DCPD), mineral brushite	$CaHPO_4·2H_2O$	6.59	~0.088	2.0–6.0
1.0	Dicalcium phosphate anhydrous (DCPA), mineral monetite	$CaHPO_4$	6.90	~0.048	[c]
1.33	Octacalcium phosphate (OCP)	$Ca_8(HPO_4)_2(PO_4)_4·5H_2O$	96.6	~0.0081	5.5–7.0
1.5	α-Tricalcium phosphate (α-TCP)	α-$Ca_3(PO_4)_2$	25.5	~0.0025	[c]
1.5	β-Tricalcium phosphate (β-TCP)	β-$Ca_3(PO_4)_2$	28.9	~0.0005	[c]
1.0–2.2	**Amorphous calcium phosphate (ACP)**	**$Ca_xH_y(PO_4)_z·nH_2O$, n = 3–4.5; 15–20% H_2O**	[b]	[b]	~5–12 [c]
1.5–1.67	Calcium-deficient hydroxyapatite (CDHA)[d]	$Ca_{10-x}(HPO_4)_x(PO_4)_{6-x}(OH)_{2-x}$ (0 < x < 1)	~85.1	~0.0094	6.5–9.5
1.67	Hydroxyapatite (HA, HAp or OHAp)	$Ca_{10}(PO_4)_6(OH)_2$	116.8	~0.0003	9.5–12
1.67	Fluorapatite (FA or FAp)	$Ca_{10}(PO_4)_6F_2$	120.0	~0.0002	7–12
1.67	Oxyapatite (OA or OAp)	$Ca_{10}(PO_4)_6O$	~69	~0.087	[c]
2.0	Tetracalcium phosphate (TTCP or TetCP), mineral hilgenstockite	$Ca_4(PO_4)_2O$	38–44	~0.0007	[c]

[a] These compounds cannot be precipitated from aqueous solutions.
[b] Cannot be measured precisely. However, the following values were found: 25.7 ± 0.1 (pH 7.40), 29.9 ± 0.1 (pH 6.00), 32.7 ± 0.1 (pH 5.28). The comparative extent of dissolution in acidic buffers is: ACP > α-TCP > β-TCP > CDHA > HA > FA.
[c] Stable at temperatures above 500 °C.
[d] Always metastable.
[e] Occasionally, CDHA is named precipitated HA.
[f] In the case x = 1 (the boundary condition with Ca/P = 1.5) the chemical formula of CDHA looks as follows: $Ca_9(HPO_4)(PO_4)_5(OH)$.

2.3.1 Dicalcium Phosphate Dihydrate (DCPD) & Dicalcium Phosphate Anhydrous (DCPA)

DCPD ($CaHPO_4·2H_2O$) is the most soluble of calcium orthophosphates considered in this review and is known by the mineral name brushite (Dorozhkin, 2007). Brushite has the fastest formation kinetics of all calcium orthophosphates. These rapid nucleation kinetics are believed to be due to the higher solubility, caused by the hydration layers of water. Brushite has been proposed as a precursor phase to both Hydroxyapatite (HAp) and octacalcium phosphate (OCP). The structure consists of chains of $CaPO_4$ (Figure 10) with layers of water populating the lattice in between. The interface has two separated water bilayers: (1) highly ordered layer incorporated into the DCPD crystal structure, and (2) exhibits no order, and is only seen layering in the direction perpendicular to the $CaPO_4$ layers. Magnesium ions have been found to disrupt brushite crystal formation favoring thermal hydrolysis to monetite (Shadanbaz, 2014). DCPA, known as the mineral monetite,

is similar to DCPD in that it can precipitate from solution, but is less soluble, attributed to the lack of water molecules in its structure (Dorozhkin, 2007).

DCPD is also reported to transform to DCPA at temperatures above 80°C.

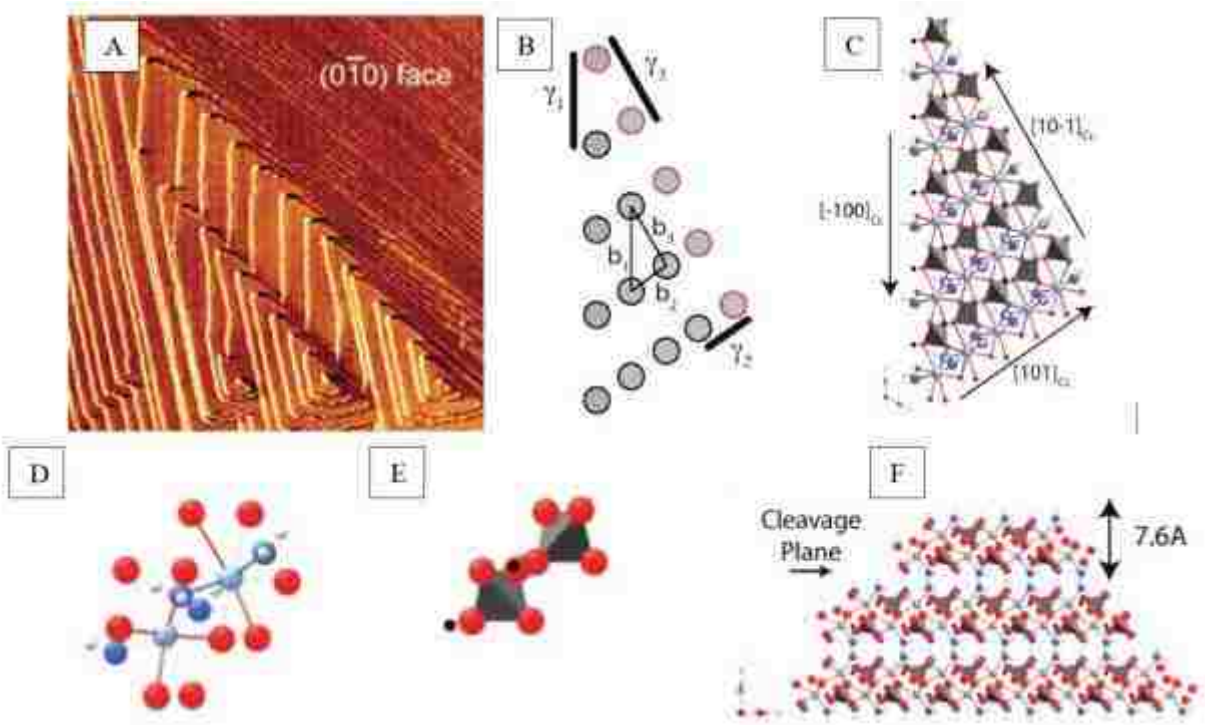

Figure 10: A) Scanning probe microscopy (SPM) image of growing hillocks on brushite surface. B) Brushite formation shown for one atom; dark lines indicate the newly created edge length. C) overview of brushite atomic structure (Ca (light blue), O from HPO_4 (red), O from water (dark blue), P coordinated with 4 O (grey tetrahedrons), and H (white). D) calcium cluster E) phosphate cluster F) side view of (C) (Qiu & Orme, 2008)

2.3.2 Octacalcium Phosphate

Octacalcium phosphate (OCP) has been identified as metastable with respect to HAp and a possible precursor phase to the formation of HAp and calcium deficient Hydroxyapatite (CDHA). The crystal structure of OCP is remarkably similar to that of HAp (Gustafsson, 2012), with arrangements of calcium and orthophosphate ions separated by hydrated layers such as those in DCPD. OCP's crystal structure is that of apatite separated by hydrated layers. Conversion of OCP to HAp can occur within the crystal structure when water molecules enter the hydration layer. OCP to HAp is most commonly accomplished by the hydrolysis reaction shown in equation 1 (Gustafsson, 2012):

$$Ca_8H_2(PO_4)_6 * 5H_2O + 2Ca^{2+} \rightarrow Ca_{10}(PO_4)_6(OH)_2 + 4H^+ \quad (5)$$

In neutral solutions hydrolysis of amorphous calcium phosphate (ACP) to OCP has been observed. It has also been proposed that OCP is as an intermediate phase between ACP and HAp (Gustafsson, 2012). In an experiment carried out at constant temperature (26°C), and constant pH 8.50 (Feenstra & De Bruyn, 1979), the extent of reaction exhibits three slopes (Figure 11). The extent of reaction was found by an iterative method of calculating the level of supersaturation for each solubility product, here considering only OCP, TCP, HAp, and DCPD. The experiment concluded that it is not unlikely that ACP behaves as a template for heterogeneous nucleation of OCP which in turn serves as a template for epitaxial growth of HAp.

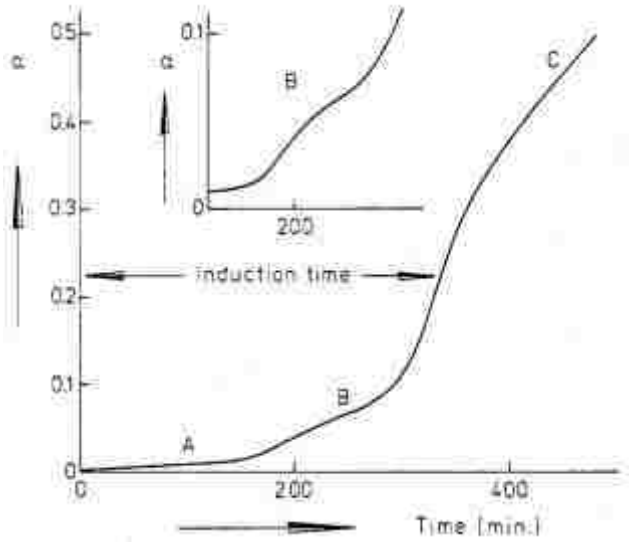

Figure 11: Growth curve of pH 8.50 at 26°C plotted as extent of reaction versus time (Feenstra & De Bruyn, 1979)

2.3.3 α -Tricalcium Phosphate (α-TCP) & β-Tricalcium Phosphate (β-TCP)

β-TCP cannot be precipitated from aqueous solutions, and exists only from the decomposition of another calcium orthophosphate at high temperature such as heating CDHA to temperatures above 800°C, or interactions of acidic calcium orthophosphate such as DCPD with a base CaO (Dorozhkin, 2007). If heated to temperature above 1125°C β-TCP can transform to α-TCP. α-TCP can be stabilized by the presence of silica at temperatures between 800-1000°C. β-TCP is less soluble than α-TCP in room temperature

water, and α-TCP is known to react more quickly than β-TCP. Although they have the same chemical composition each phase differs in crystal structure (Dorozhkin, 2007). Solubility data (Figure 12) from recent research shows the solubility of β-TCP to be lower than previously reported (Pan & Darvell, 2009).

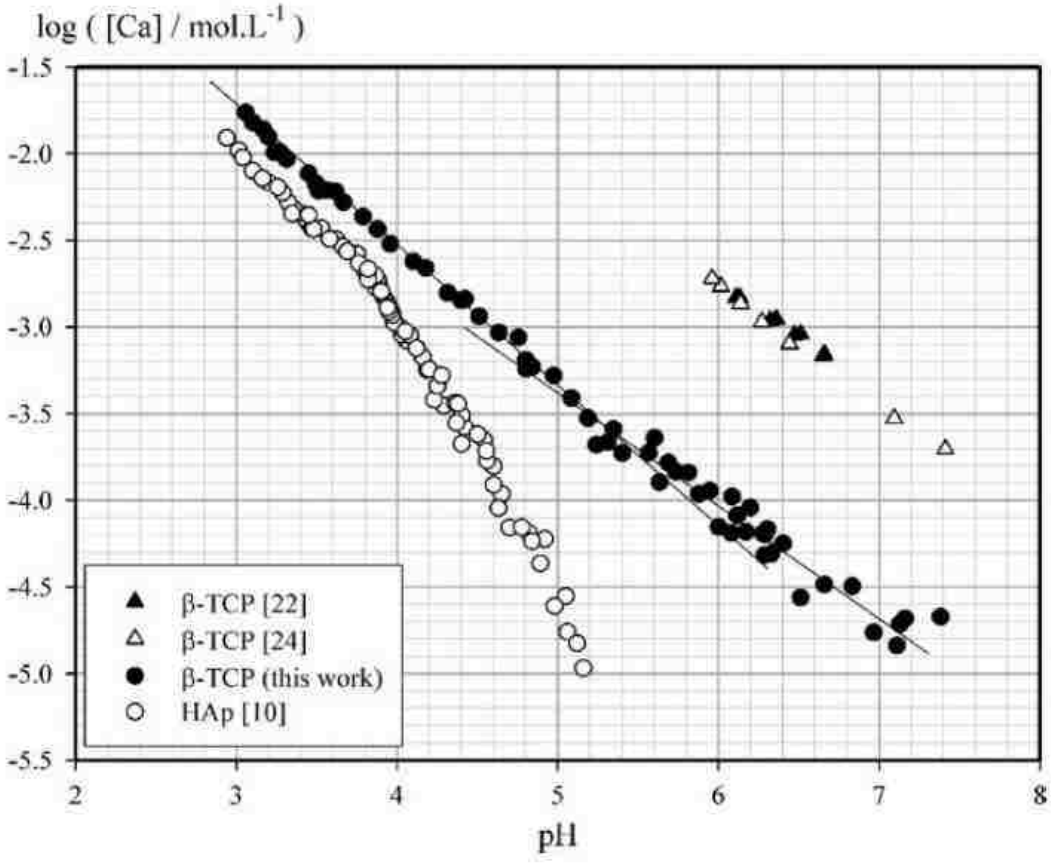

Figure 12: Titration curves for β-TCP in 100 mM KCl solution at 37.0 ±0. ºC. HAP results for comparison. Regression lines added for only to show change in slope.

2.3.4 Amorphous Calcium Phosphate (ACP)

ACP appears spherical (diameter ca. 30-100 nm), with the particle size of ACP depending on containment pH, Ca/ PO_4 concentration, and temperature. ACP is the first precipitate formed from the rapid mixing of supersaturated calcium and orthophosphates; the affinity for ACP is believed to be due ACP having lower surface energy than OCP and HAp. The transformation of ACP to HAp is a solution mediated first-order reaction which is regulated by both the dissolution of ACP and the nucleation of HAp. The rate of the autocatalytic transformation of ACP to HAp, at a given temperature, is determined by the solution pH,

independent of the type of buffering or calcium/ phosphate salts used, etc. (Posner et. al., 1975). The interfacial surfaces of the emerging crystalline HAp act as sites for heterogeneous nucleation (Eanes et. al., 1965). Inspection by X-Ray diffraction demonstrated for an ACP solution seeded with apatite crystals, the precipitate converted exclusively to HAp, suggesting that once a HAp seed crystal is present the solution, only HAp is formed (Neuman & Mulryan, 1971). ACP is characterized by its lack of long range order, but is known to have short range apatite order, similar to that of HAp, known as the Posner's cluster. The level of amorphization is proportional to the concentration of the calcium and orthophosphate. Amorphization has also been found to increases with increasing pH and low temperature. While ACP to HAp is the dominate transformation path of ACP, high temperatures are one example which would cause ACP to form another precipitate such as CDHA. The sequence of ACP to CDHA in the SEM imaging below shows the circular cluster formation of ACP, and its transformation e.g. to CDHA.

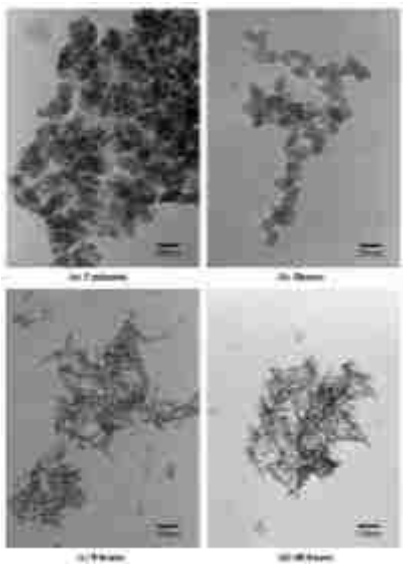

Figure 13: Bright-field transmission electron micrographs of ACP to CDHA transformation at reaction times of a) 5 min, b) 3 hour, c) 9 hour, and d) 48 hour (Dorozhkin 2010)

2.3.5 Calcium-deficient Hydroxyapatite (CDHA)

CDHA can be formed by adding calcium and orthophosphates to a boiling water solution. The ACP will initially precipitate, but restructure and transform to CDHA, leading to similarities in the crystal structure and similarities in properties. The lack of defined stoichiometry promotes the existence of other ions such as Mg^{2+}, Cl^{-}, or Na^{+}. The variable

Ca/P ratio found in CDHA has been explained by multiple methods including: surface adsorption, lattice substitution, and intercrystalline mixtures of HAp and OCP. The exact structure and unit cell of CDHA is not known. A simple approximation of the structure of CDHA is HAp with vacancies filled with Ca or ^{-}OH ions (Dorozhkin, 2009).

2.3.6 Hydroxyapatite (HAp)

The most thermodynamically stable product of the reaction of calcium and orthophosphate salts in neutral or basic solution is a needle-like crystalline precipitate known as hydroxyapatite (HAp; $Ca_{10}(PO_4)_6(OH)_2$) (Posner & Betts, 1975; Wang & Nancollas, 2008). The formation of HAp is always proceeded by the formation of Amorphous Calcium Phosphate (ACP; $Ca_xH_y(PO_4)_z \cdot nH_2O$, n=3-4.5 (Dorozhkin 2010)) in highly supersaturated solutions, and unless stabilized, the amorphous phase transforms autocatalytically to HAp by the process of solution and re-nucleation (Posner & Betts, 1975). Figure 14 and Figure 15 show images of HAp crystal formation by different growth techniques with and without the presence of magnesium. As discussed next magnesium is an important metal in formation of calcium orthophosphates. This investigation of crystal growth found that magnesium was evenly dispersed across all calcium orthophosphate samples and that magnesium substitution in HAp increased proportionally to the amount of magnesium added. Magnesium was found to result in a similar needle-like structure expect from HAp but would exhibit plate-like crystallite agglomerate formations as well (Qiu & Orme, 2008).Figure 14: TEM image of 1) HAp and 2) Magnesium Hydroxyapatite; SEM micrograph images of 3) HAp and 4) Mg-HAp

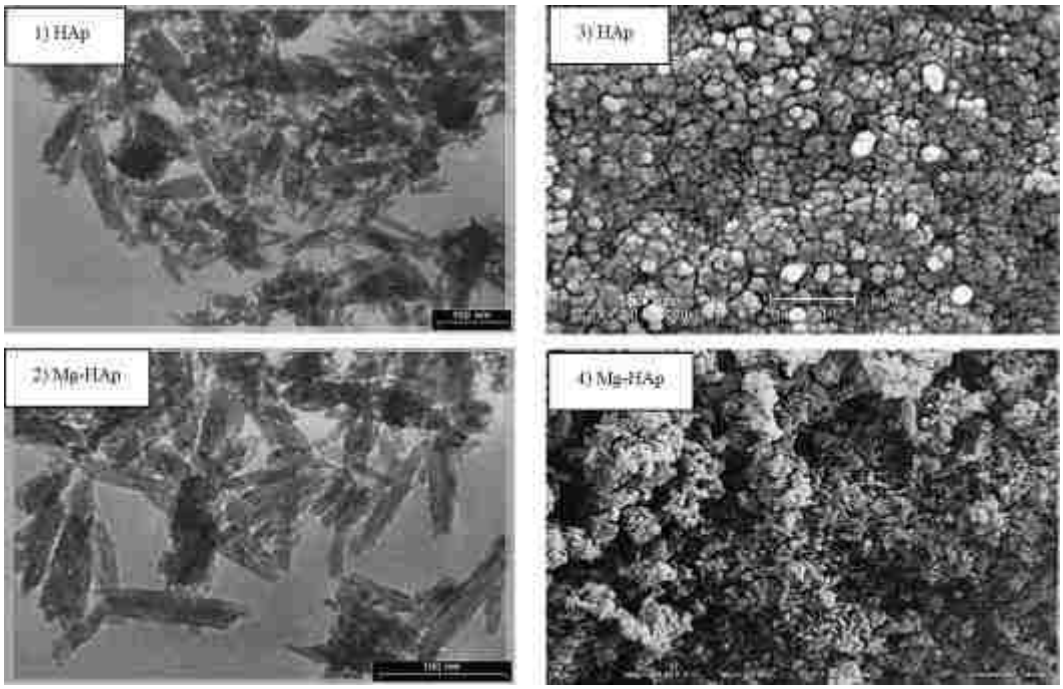

Figure 14: TEM image of 1) HAp and 2) Magnesium Hydroxyapatite; SEM micrograph images of 3) HAp and 4) Mg-HAp (Farzadi et. al., 2014)

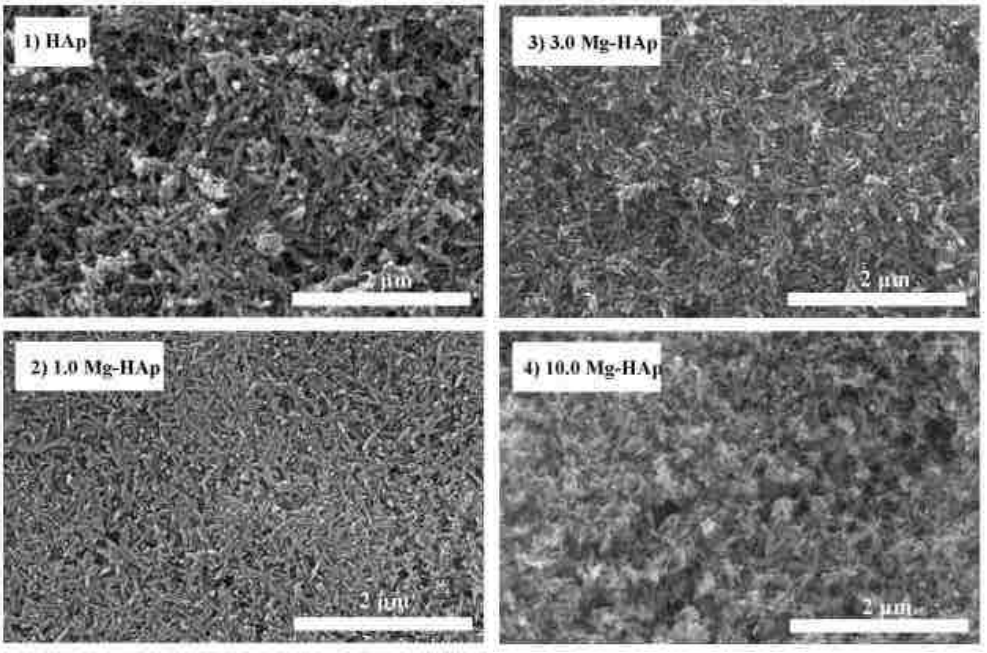

Figure 15: FE-SEM microphotoaphs of as-synthesized powders dried at 105°C for20 hours formed with increasing Mg concentrations (Stipniece, 2014)

2.4 ACP Stabilization

As previously mentioned it is possible to stabilize ACP. A known ACP stabilizer is magnesium, a second column element with a 2^+ charge similar to calcium (Tomazic et. al. 1975). Table 6 below shows that in addition to calcium NUKON fiberglass contains magnesium. The leaching of magnesium into solution has been confirmed from leaching tests in prototypic post LOCA conditions bench tests conducted at UNM (discussed in chapter 4). The presence of magnesium either in the ACP or in the solution affects the transformation kinetics, by decreasing the ACP solubility. Posner states that below a 0.2 Mg:Ca molar ratio the time to reach HAp is increased, but, once HAp nucleation begins, the first-order transformation reaction proceeds with the same rate constant as in the absence of magnesium (Posner & Betts, 1975). Other researchers have found that magnesium's presence will increase the time it takes to reach HAp transformation, up to a limit set by Posner of 0.2 Mg:Ca molar ratio, above which no transformation to HAp will occur [20,23].

Table 6: NUKON elemental composition by weight percent by EDX analysis (Lane et. al., 2006)

Material	Weight Percent									
	C	O	Mg	Al	Si	K	Ca	Fe	Na	Mn
NUKON	26.65	46.46	0.82	1.43	14.39	0.33	2.95	0.15	6.98	0.03

The ACP—HAp conversion process has been visualized as occurring in three steps (Boskey & Posner, 1974):

(i) ACP dissolution yielding a saturated solution of ions or ion clusters

(ii) the first HAp nuclei forms from these ions

(iii) secondary nucleation leading to the autocatalytic proliferation of HAp

Analysis of precipitates formed from mixing salts has shown that magnesium ions were excluded from matured crystalline HAp (Neuman & Mulryan, 1971). Close to 90% of magnesium was located in readily accessible surface positions. When HAp seed was added to ACP solutions and allowed to transform, magnesium did not poison the seed or

change the crystal growth, further suggesting magnesium is a surface limited ion (Neuman & Mulryan, 1971). These results suggest that step (iii) is unaffected by the presence of magnesium. Furthermore, the size of the HAp crystal and conversion time from ACP to HAp is independent of magnesium concentration, thus further implying that Step (iii) is not suspect for the longer induction time associated with the presence of magnesium. The lack of magnesium on the HAp crystals surface also suggests that it is Step (i) the dissolution of ACP, which is affected by magnesium (Boskey & Posner, 1974). This suggests that magnesium attaches on the ACP surface positions and slows the absorption/ desorption process with calcium. As magnesium and calcium are both group two alkaline earth metals it is not surprising that magnesium may interfere with calcium nucleation sites.

In conclusion, ACP is always a precursor product formed before HAp. HAp formation can be prolonged or prevented depending on the concentration of magnesium. Magnesium and calcium are both present in NUKON fiberglass and are known to leach form the fiberglass. Magnesium prevents the formation of HAp by preventing adsorption/ desorption on the ACP surface nucleation sites. Decreases in magnesium concentration would allow calcium to adsorb/ desorb without the interference, leading to the formation of a more thermodynamically stable product. This formation could lead immediately to HAp or reach an intermediate phase of OCP. The understanding of the relation between magnesium and calcium precipitation will provide resolution to questions about the behavior of calcium in post LOCA containment solution.

2.5 Thermodynamic Modeling

In regards to the research conducted herein, the primary measurement tool used to investigate calcium leaching from NUKON fiberglass was inductively coupled plasma – optical emission spectroscopy (ICP-OES) total metals by EPA 200.7, which provides an accurate measurement of the total calcium concentration and other elements in solution. Thermodynamic modeling of the system provides insight into the solubility of calcium in solution by assuming the presence of specific calcium orthophosphates in solution. Using the thermodynamic modeling software Visual MINTEQ (Gustafsson, 2012), chemical

equilibrium modeling was conducted investigating the formation of calcium orthophosphate precipitates.

Simulations were run using prototypical post-LBLOCA TSP and H_3BO_3 concentrations, provided by an outside consulting source (Olson, 2014a). The borated and buffered concentrations are representative of all experimental solutions used in the testing herein, prior to the addition of NUKON. Therefor Visual MINTEQ modeling included a total of three species: Na^+ (17.49 mM), $(PO_4)^{3-}$(5.83 mM), and H_3BO_3 (221.3 mM). An initial model using the species above and calculating the pH using mass and charge balance returned a pH of 7.1 at 25ºC. Another simulation was run at the experimental temperature of 80ºC, which returned a pH of 6.5. pH 6.5 is below any measured pH from solutions of borated and buffered water in shake-down testing. The pH of 7.1 is much closer to the observed pH in solution, proposed inaccuracy due to either or both lacking enthalpies, or lack of proper modeling of the high concentrations of the acids. The pH of 7.1 will be used as the baseline for future discussion in this section. The modeling consists of performing pH sweeps for the borated buffered solution. First calcium is considered in solution and the dissolved amount is output to show the pH at which precipitation is predicted by Visual MINTEQ. Second, no calcium is modeled in the simulated solution and solubility product equilibrium constant (K_{sp}) of varying calcium orthophosphates are considered to back calculate the expected amount of calcium in solution, for comparison to testing results in later sections.

To investigate the expected pH at which calcium is predicted to form calcium orthophosphates, dissolved calcium is modeled to include the total available calcium from NUKON fiberglass in a LBLOCA that releases the maximum amount of NUKON into containment. The maximum expected NUKON concentration, provided by an outside consulting company, of 1.18 g/L was multiplied by the total available calcium in NUKON listed in Table 6, amounting to a total of 0.87 mM calcium. The pH of the solution was swept, and the dissolved calcium species were output. The presence of calcium was observed to decrease as pH increased indicating the formation of an insoluble product beginning at a pH of 5.5 (Figure 16). Visual MINTEQ predicts the formation of the most insoluble product by calculating the saturation index of expected soluble phase. Therefore

if the saturation indices were plotted for the available calcium orthophosphates, Visual MINTEQ would predict the formation of HAp.

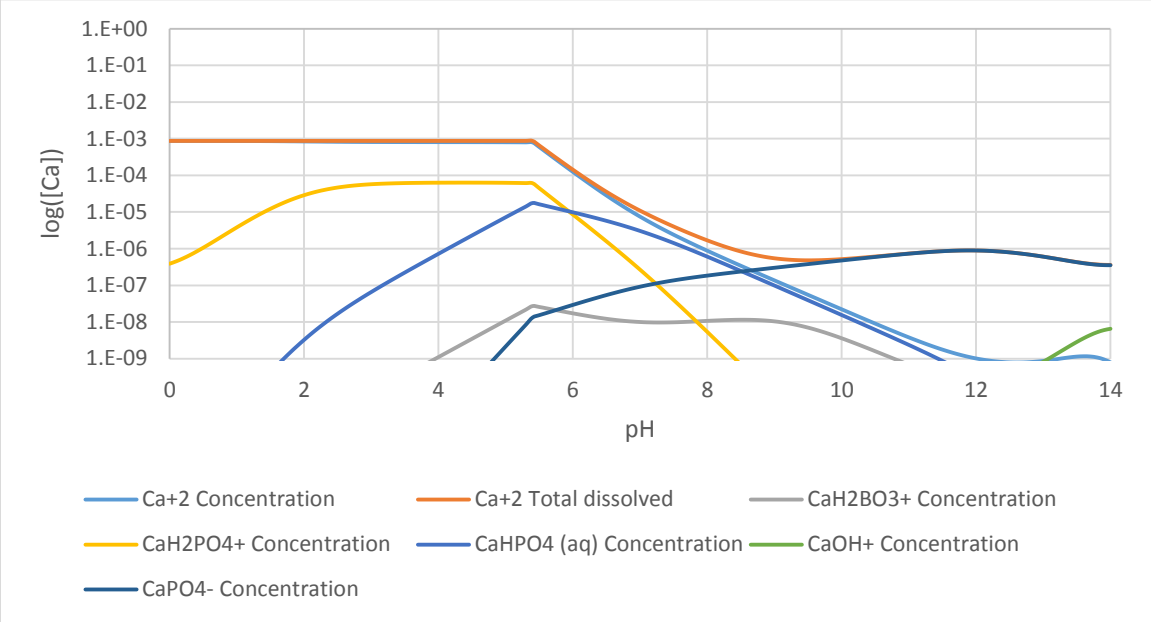

Figure 16: Visual MINTEQ dissolved calcium species for 0.87 mM Ca, 221.3 mM H_3BO_3, & 17.5 mM PO_4^{3-}

To determine the calcium concentration in solution for a given solubility product, Visual MINTEQ was used to find the ionic concentration as well as the activity of orthophosphate species at varying pH. Using Table 5 a solubility product for any species may be calculated by considering the dissolution of the solid phase. This investigation includes only calcium orthophosphates that are stable at a pH from 5-10, and that include only calcium, orthophosphate, hydronium or hydroxide. The K_{sp} is defined as the activity

of the dissolved product divided by activity of the reactant. As the only reactant is a solid phase its activity coefficient is not considered in the calculation of K_{sp} shown below.

$$A_aB_bC_c\ (s) \leftrightarrow\ aA\ (aq) + bB(aq) + cC(aq) \tag{6}$$

$$K_{sp} = \{A\}^a\{B\}^b\{C\}^c \tag{7}$$

If for example one were to consider OCP, its solubility product could be calculated as follows:

$$Ca_8(HPO_4)_2(PO_4)_4 * 5H_2O \leftrightarrow 8Ca + 2HPO_4 + 4PO_4 \tag{8}$$

$$K_{sp} = \{Ca\}^8\{HPO_4\}^2\{PO_4\}^4 \tag{9}$$

The solubility product of OCP is dependent upon the activity of two orthophosphate species. As previously discussed the activities of orthophosphates is pH dependent. The previously defined system (5.83 mM H_3BO_3 and 5.53 mM TSP) was simulated for a series of defined pH values and using Visual MINTEQ, for which the resultant species activity of each orthophosphate, as well as the ionic strength was calculated and output. Using the Davies equation (Benjamin, 2014) the activity coefficient was calculated from the ionic concentration.

$$\gamma_{Davies} = 10^{-A*z^2\left(\frac{I^{1/2}}{1+I^{1/2}}-0.3I\right)} \tag{10}$$

A is a fitting parameter dependent on the dielectric constant and temperature, but an *A* value of 0.5 (water at 25°C) was used for all calculations. The charge of calcium resulted in a z^2 of 4, and *I* represents ionic strength output from Visual MINTEQ. Finally the calcium concentration may be obtained by rearranging Equation (6) to solve for calcium activity and dividing by the calculated activity coefficient. This procedure was carried out for seven calcium orthophosphates listed in order of increasing calcium to phosphate molar ratio as arranged in the following figures Figure 17-Figure 23 and listed for the expected

pH at two temperatures in Table 5. The generated graphs show that in the neutral pH region, slight variations in pH could lead to a significant change in the expect calcium solubility limit.

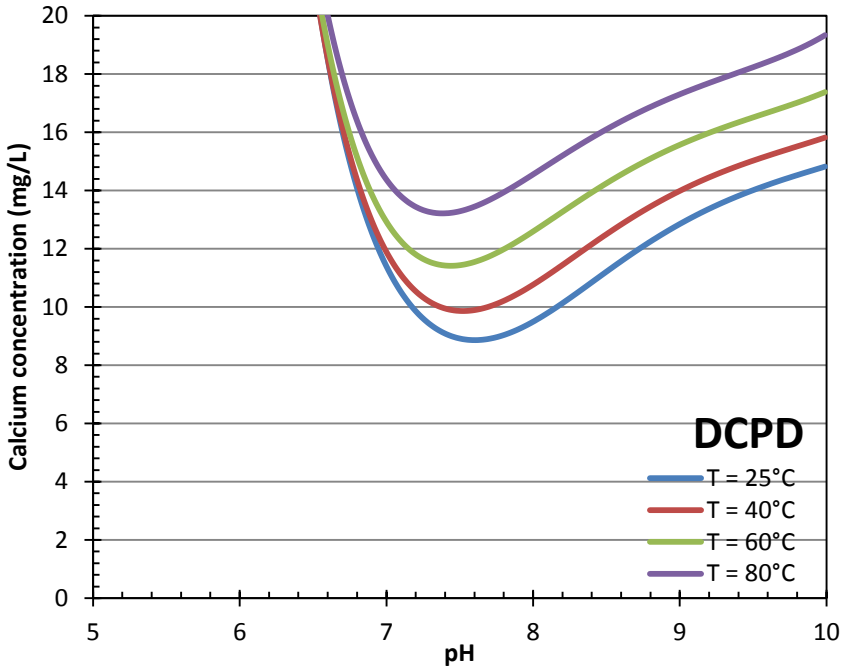

Figure 17: Calcium in solution considering DCPD to control solubility

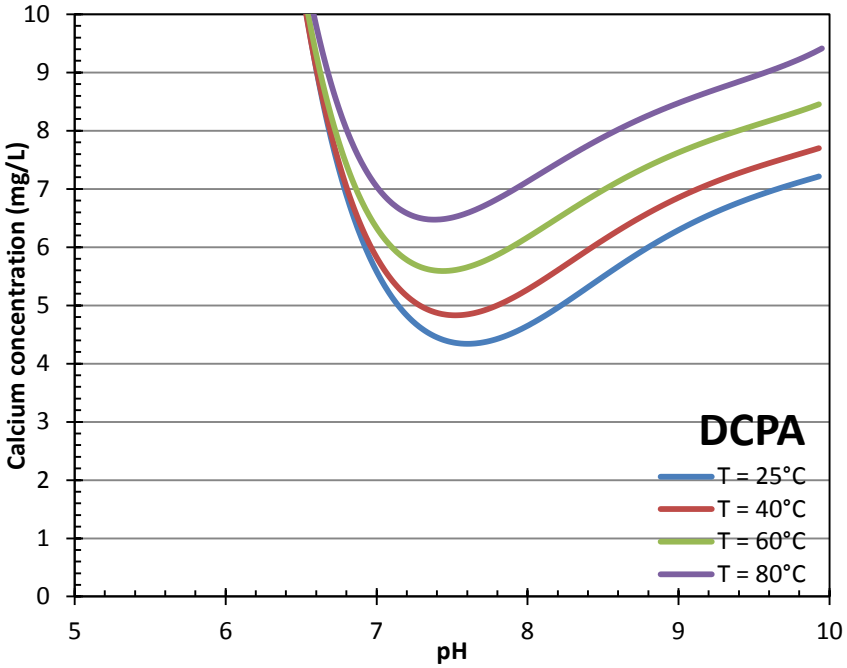

Figure 18: Calcium in solution considering DCPA to control solubility

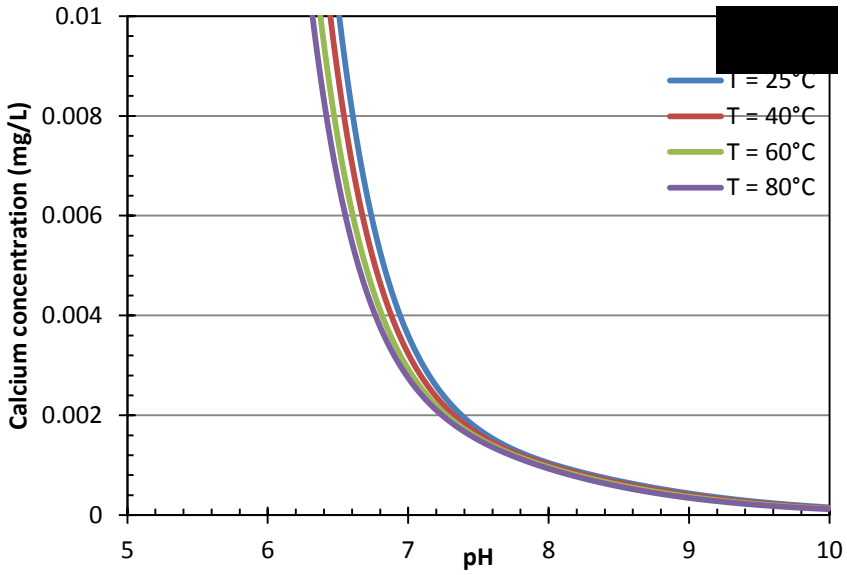

Figure 19: Calcium in solution considering OCP to control solubility

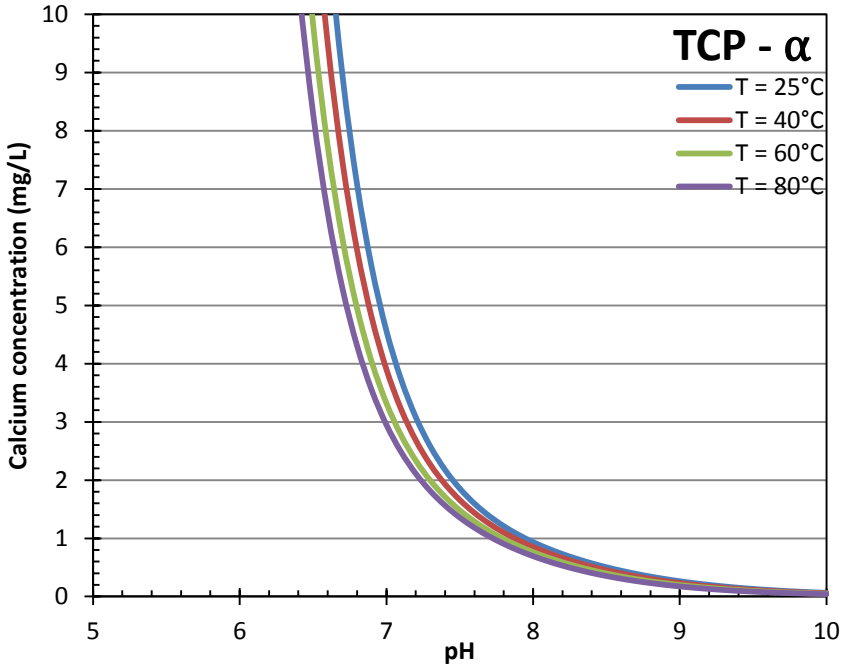

Figure 20: Calcium in solution considering TCP-α to control solubility

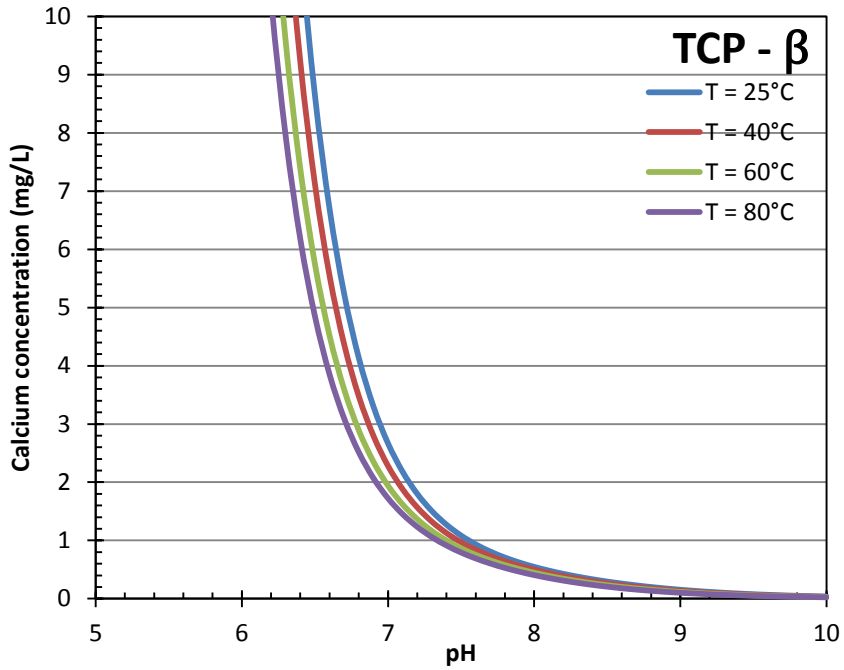

Figure 21: Calcium in solution considering TCP-β to control solubility

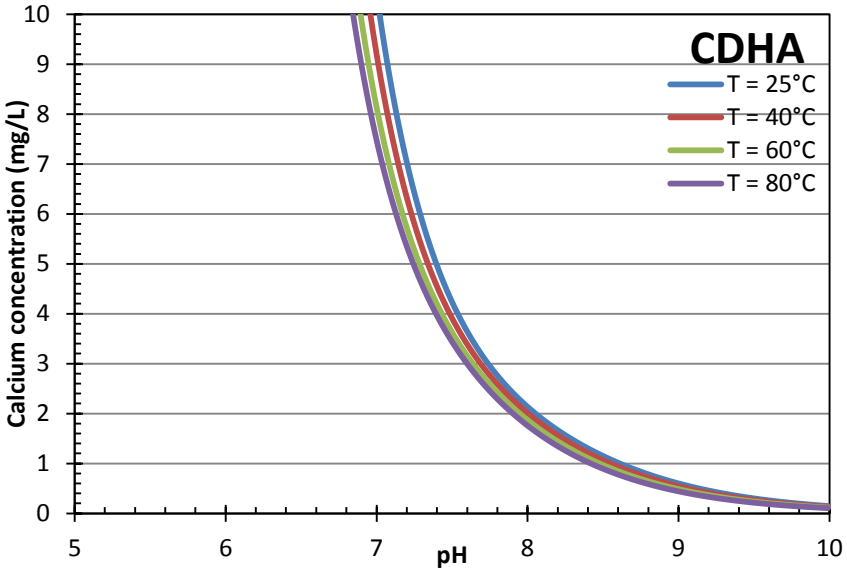

Figure 22: Calcium in solution considering CDHA (x=1) to control solubility

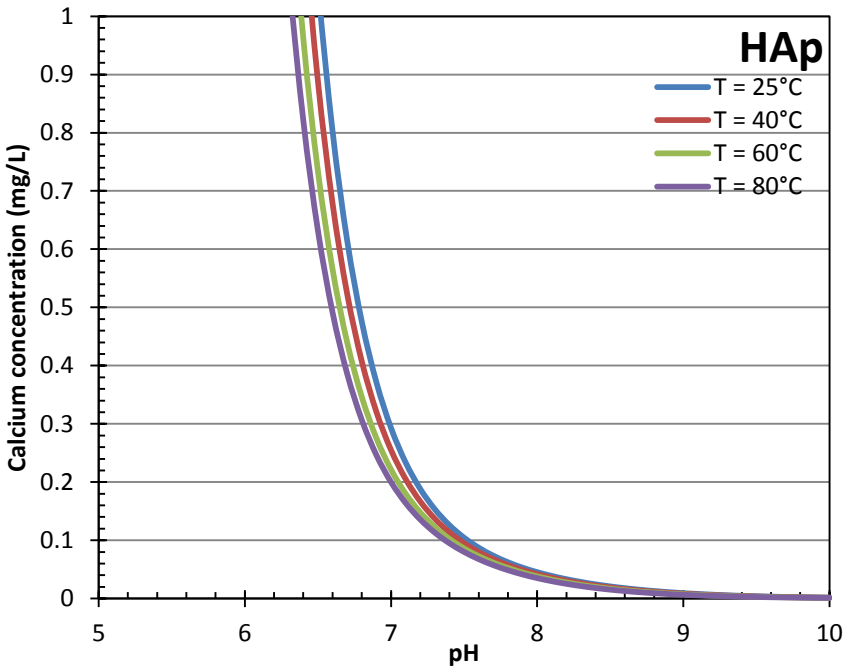

Figure 23: Calcium in solution considering HAp to control solubility

Each of these modeled species could control the solubility of calcium at neutral pH. These graphs will be referenced in the chapter 5 for insight into which calcium orthophosphate is controlling calcium solubility. As mentioned previously, pH 7.1 is the baseline pH, therefore Table 7 was populated to list the concentration of calcium for each species at the predicted pH and 25^{o}C and experimental temperature.

Table 7: Summary of calcium solubility assuming a specific calcium orthophosphates at baseline pH and experimental temperature used in all leaching experiments

Calcium Orthophosphate	**[Ca] [mg/L] for pH 7.1 at 25ºC**	**[Ca] [mg/L] for pH 7.1 at 80ºC**
DCPD	10.5	13.8
DCPA	5.53	6.76
OCP	0.00354	0.00239
α -TCP	3.73	2.48
β -TCP	2.61	1.45
CDHA (x=1)	10.2	6.29
HAp	0.491	0.164

In conclusion, the thermodynamic modeling has shown that precipitation should occur at pH values greater than 5.5. The calcium solubility in solution, when controlled by a variety of possible calcium orthophosphates, has been determined for a range of temperatures and pH values. The importance of these graphs is twofold: (1) the primary measurement made in the leaching experiments was ICP-OES total metals, (2) finding a particular precipitate is difficult due to the presence of fiberglass in solution. The presence of fiberglass leads to difficulties in separating precipitates due to the large volume of fiberglass, as well as the fiberglass fines which settle out of the main fiberglass body during testing. These fines also appear in scanning electron microscope SEM imaging, leading to difficulties between selecting a precipitate versus a fiberglass fine. For post-LOCA containment the true temperature profiles of interest vary over the break period and a more detailed analysis should include effects of temperature change overtime. Due to the high TSP content the system is calcium limited, a system not typically studied for calcium orthophosphate research which may lead to results which vary from the described behavior of calcium orthophosphates properties above. This foundation of calcium orthophosphate behavior will assist in understanding the behavior of calcium in solution in experimental results presented herein.

Chapter 3: Experimental Setup & Testing Conditions

3.1 Introduction to Testing

Calcium leaching experiments were carried out on the three scales: bench, tank, and column with respective solution volumes of 0.5 L, 1135 L, and 31.5 L. For the purposes of this research, the column and tank scale experiments are referred to as reduced-scale testing. Separate effects calcium testing was initiated with bench scale investigations to measure the effects of fiberglass destruction on the release of calcium from NUKON fiber. Bench testing continued through investigation of the solubility of calcium in solution using a $CaCl_2$ as a calcium surrogate. Bench testing was completed with an investigation into the behavior of calcium at leaching periods of 1, 8, and 30 days. A large-scale containment tank facility was utilized next to investigate the scaling effects related to the experiment findings of the bench scale. Prototypic concentration of fiberglass for a LBLOCA, with the greatest amount of submerged NUKON, was leached for 30 days. This tank test investigated the possible effects of scaling and fiberglass concentration gradients. A final test was conducted in a heated vertical head-loss column to measure head-loss across a prototypic fibrous debris bed, and attain a baseline of chemical effects from calcium precipitation. In the next two sections, the bench, tank, and column facilities will be explained in further detail in addition to the experimental conditions of each test.

3.2 Bench Facility

Bench testing was conducted using replica experiments in 1 L Nalgene bottles placed in a constant temperature thermal bath supported by a shaker table. Each measurement made on the bench scale represents an identical but separate experiment. Chemicals prepared for bench scale experiments were massed using an Analytical balance (OHAUS AR1140, readability: 0.0001 g, repeatability: 0.0001 g). pH measurements in the lab were made using a ThermoOrion, model 720A+ pH meter (precision: 0.05 to .1 pH). The experiment took place within 1 L Nalgene polypropylene bottles. Samples were placed in 125 mL bottles with 0.4 mL Nitric acid. If samples required filtering, solution was removed from

the Nalgene using a 2 oz disposable syringe and docked in to an AquaPrep Device device with a 0.45 μm Thermopor membrane.

There were two heat baths used in bench testing (Figure 24), which were referred to as Unit 1 (22" x 22" x 8", capacity of 20 sample bottles) and Unit 2 (22" x 34" x 8", capacity 32 experimental bottles). The heated baths were filled with sufficient deionized water to ensure the entirety of the enclosed 500 mL sample solution was submerged. Heat was exchanged to the sample bath from water heated by a TECHNE TU-20D Tempunit Thermoregulator rod type heater in a separate heat exchanger bath. Water from the heat exchanger bath was pumped through copper pipes configured in a square "U" pattern across the bottom of the heat bath with 4" separation distance. The shaker tables were a VWR Digital Shaker (Models: DS2-500-1(24x24", 50 kg max load) and 15000 (24x36", 68 kg max load) which had a variable speed drive capable of controlling the rotational speed of the table.

Figure 24: Bench Scale Controlled Temperature Baths; Unit 1: 20 sample capacity (top left), Unit 2: 32 sample capacity (top right); Heat baths on shaker tables (bottom)

3.3 Tank Facility

The tank tests were run in the same tank as described for the ICET (Figure 5). The tank is stainless steel and 1.2 m x 1.2 m x 5 m. The tank was heated using the two 10 kW rod type heaters to perform high-temperature tests. Solution within the tank was circulated using a 5 HP motor on a variable frequency drive. Water was circulated through a flowmeter followed by inline "T" split with a gate valve for diverting flow for samples. Water was pumped back into the tank by two submerged headers on opposite sides of the tank through 36 evenly spaced 3/8" nozzles.

NUKON fiber samples were secured in a stainless steel box (9" x 13.5" x 8.5") and two stainless steel bags (1' x 1.5'); bags were secured using stainless steel screws inserted through holes punched through the mesh. The fiber sample containers were completely

submerged inside of the tank; all containers were hung from racks inside the tank in a symmetric pattern, placed in front of the tank headers.

Figure 25: CHLE Tank Apparatus (left), Stainless steel mesh box to secure fiberglass in tank (right)

3.4 Column Facility

The vertical head-loss column as shown in Figure 26, consists of a circulation pump, vertical testing column, control valves, and measuring instrumentations. The upper and lower portions of the 6-in diameter vertical columns were constructed of stainless steel and were sealed at the top with a blind flange. The blind flanges could be removed to introduce debris into the head loss assembly. The middle section of the assembly was constructed of 1/8-in thick polycarbonate to visualize the debris beds. A perforated stainless steel plate was installed inside of the polycarbonate tubing for the accumulation of debris materials. The plate was supported by a polycarbonate ring located 6-in from the lower edge of the section where the debris bed accumulates. The stainless steel screen contained 0.094-inch holes. A differential pressure (ΔP) transducer was piped to ports above and below the screen support to measure the pressure loss through the debris bed. Each column had a flow meter and control valves to monitor the flow rate and adjust the approach velocity in each column (Figure 26). Debris materials were added manually to the columns by pouring prepared fiber with particulate mixture from the open lid of each column. The preparation of this debris bed is described in the following section.

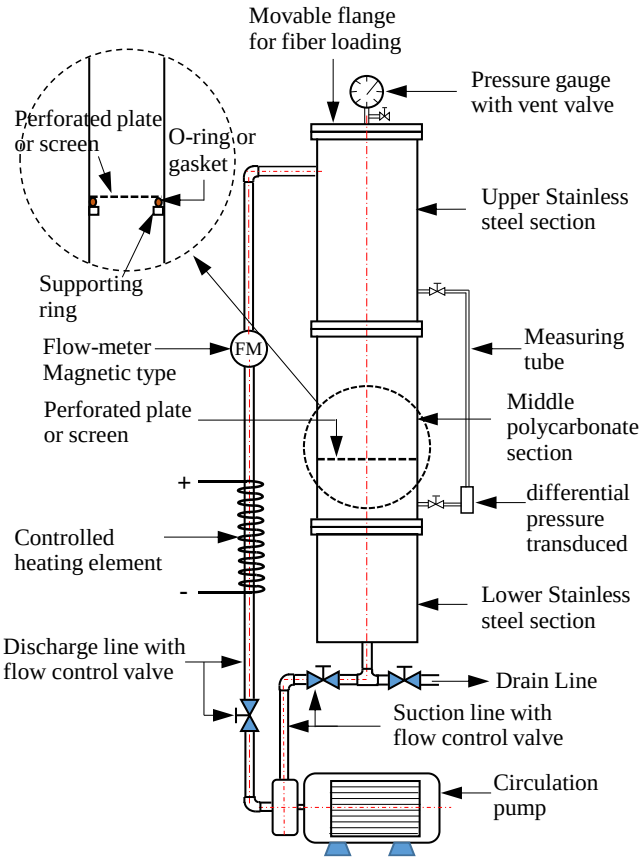

Figure 26: Vertical Head Loss piping Schematic

3.5 Preparation of Debris Beds

The debris bed generated for this testing was designed to be reproducible and prototypic to LOCA scenarios, following guidelines set by the NEI procedure to simulate mostly class 1 and 2 as described in NUREG/CR-6224 (Zigler, 1995). Large pieces of NUKON fiberglass (Figure 27a) were separated by hand into thin layers and placed in five gallon bucket (Figure 27b) with 1 liter of reverse osmosis (RO) water. Fiberglass layers were separated using RO water run through a Cleanforce 1800-psi 1.5 gpm Axial Cam Heavy-Duty Electric pressure washer (Model # CF1800HD) with a 40 degree small diameter fan type tip. The nozzle was maintained slightly below the water surface for 2.5-3 minutes (Figure 27c), followed by a period where the washer wand oscillated between clockwise and counterclockwise motions to keep the disturbance in the water sufficient to separate the fiberglass. The fiberglass pressure washing preparation was completed when water

nears the top of the 5 gallon bucket. The degree of fiberglass separation is confirmed via visual inspection by taking a mixture sample from the 5-gallon bucket. The sample is poured into a clear glass baking dish and inspecting the fiber in baking dish using a light table. Using a glass stir rod, the fiberglass solution is swirled gently to reveal any clumps and confirm that the fiber distribution is prominently NUREG/CR-6224 Class 1 and 2 debris.

The solution was then filtered from the 5 gallon bucket, through a fine mesh to preserve the total fiber mass (Figure 27d), and placed into a glass beaker with 3 liters of RO water (Figure 27e). Using a glass rod, the fiberglass was pulled to the beaker wall and shaken for a few seconds to break any agglomerated fibers (Figure 27f). The water/fiber mixture was then circulated for about 20 minutes using a magnetic stirrer (Figure 27g). A separate beaker was used for mixing the epoxy paint, inorganic zinc (IOZ), and latent particulates with 1 L of RO water. The mass and type of these particulates were determined by other teams based on a detailed analysis for different LOCA scenarios and determined the transported debris The particulate-loaded mixture was then combined with the fiber-loaded mixture (Figure 27h); this combined mixture was stirred for another 10-15 minutes on the magnetic stirrer. The debris mixture was prepared to be loaded to the vertical column (Figure 26).

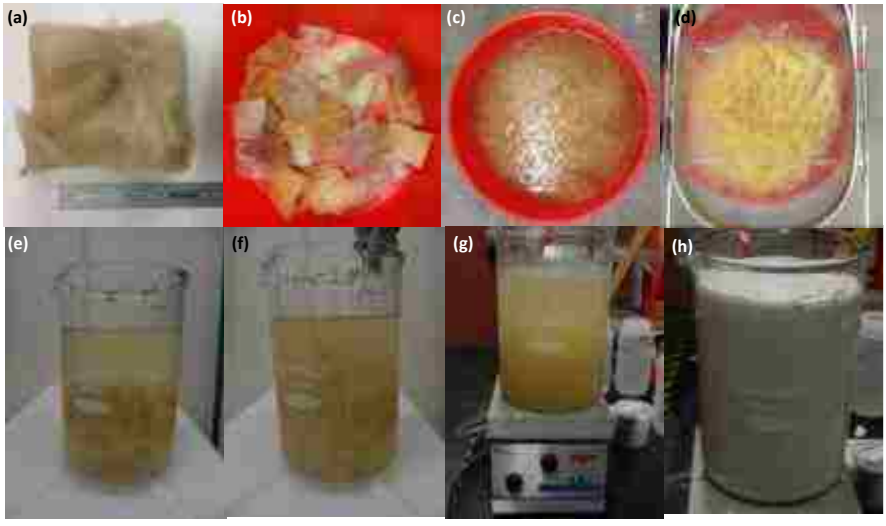

Figure 27: Debris mixture preparation process

3.6 Experimental Conditions

All tests were performed using a solution consisting of 221.3 mM boric acid (H_3BO_3 and 5.83 mM TSP ($Na_3PO_4 \cdot 12H_2O$ yielding a pH near 7.1; test solutions were maintained at a temperature of 80°C. NUKON fiberglass used in this experiment was thermally treated by the manufacturer (PCI Inc.) at 600°F for 24 hours on one side, prior to its arrival at UNM to replicate the high heat conditions that the insulation would experience in the nuclear power plant facility. This heat treatment produced a two-toned portion of NUKON fiberglass: yellow ("unburnt") and brown ("burnt") (Figure 28). Efforts were made to maintain the use of equal amounts of "burnt" and "unburnt" fiberglass in all tests

Figure 28: Blanket of NUKON fiberglass showing the results of heat treatment

3.7 Bench Experimental Conditions

Bench tests consisted of 1 gram of NUKON fiberglass in 0.5 L of borated-buffered solution, resulting in a fiberglass concentration of 2 g/L (Table 8). Bulk amounts of solution were prepared and metered out in 500 mL portions using a graduated cylinder before adding to each 1 L test bottle. Solution-filled bottles were placed in the heated bath overnight to reach an experimental temperature of 80°C before adding the fiberglass. After a designated time in the bath, dependent on experimental focus, samples were taken for analysis by removing a bottle from the bath, pulling 125 mL of solution into a syringe, and then passing the solution through a 0.45 μm polymer filter in order to remove submerged particulate. The solution was stored in a nitric acid-treated bottle in a refrigerator until

taken to an outside laboratory for inductively coupled plasma – optical emission spectroscopy (ICP-OES) analysis.

Table 8: Bench Testing Conditions

RO Water		**Bench Chemicals**	
Volume	0.5 L	NUKON	2 g/L
Resistivity	17 Ω · cm	TSP	2.27 g/L
Turbidity	< 0.5 NTU	H_3BO_3	13.7 g/L

3.8 Tank Experimental Conditions

The tank experiment began by adding 1135 L of reverse osmosis (RO) water to the tank using a totalizer. The tank was heated to 80^{o}C before the addition of boric acid and TSP (Table 9). The total amount of fiberglass added to the tank was 1339 grams of NUKON; the specific amount of fiberglass used was provided by a consulting partner as a typical amount for a large break LOCA. Five fiberglass pieces (~4" thick) were cut from the bulk fiberglass sheet to fit exactly to the dimensions of the stainless steel box (Sec. 3.3). The remaining mass of fiberglass (~1 in^2 pieces) was placed in two stainless steel mesh bags.

Table 9: Tank Testing Conditions

RO Water		**Tank Chemicals**	
Volume	1136 L	NUKON	1.18 g/L
Conductivity	39 µS cm	TSP	2.27 g/L
Turbidity	0.1 NTU	H_3BO_3	13.7 g/L

3.9 Heated Vertical Column Test

The heated vertical column test investigated calcium leaching from prototypic debris beds and the effects of calcium concentration variation on the measured head-loss. The total mass of fiber utilized in this experiment was 37.17 grams in 31.5 L (fiber/water ratio of 1.18 g/L (Table 10)) in borated TSP-buffered solution. The mixed debris materials were scaled to match prototypical values used in the UNM Head Loss (HL) series (Eanes et. al. 1965). Following preparation (Sec. 3.5), the debris bed materials were added to the column at a flow velocity of 0.05 ft/s to promote debris settling. The measured head loss in

considered stable if the root mean square (RMS) value of the measured column head-loss for the early 5 minutes of each testing hours does not change by more than 1%. The velocity was decreased to the testing velocity (0.013 ft/s) once the head-loss stability criteria was met. The column temperature was set higher than testing conditions at 86.2^{o}C, to account for temperature losses anticipated during debris bed material addition, and set back to 80^{o}C following debris bed loading.

Aqueous samples were taken from the column for elemental composition analysis (using ICP-OES) once per day; spot measurements for turbidity and pH were also collected daily. Sample were collected from one of two possible locations: the column drain, located below the debris bed relative to the direction of solution flow (Figure 26, "Drain Line") or the top of the column, located above the debris bed (Figure 26, "Movable flange"). Samples extracted from the top of the column through the drain line (Figure 26) were filtered through a 0.45 μm filter; samples extracted from the bottom of the column were not filtered. The advantages of taking samples from the bottom were regarding turbidity due to a small portion of unmixed epoxy paint floating at the top of the column, leading to misleading turbidity results despite efforts to avoid epoxy paint particulate in the solution. The disadvantage of taking a sample from the bottom was a slight increase in the velocity through the bed and resulted in slight disturbance in the head loss. Supplementary additions (125 mL) of borated-buffered solution were added daily to maintain a constant inventory of solution in the column throughout testing.

Table 10: Column Testing Conditions

RO Water		**Column Chemicals & Debris Bed**	
Volume	31.5 L	NUKON	1.18 g/L
Conductivity	22.5 μS cm	TSP	2.28 g/L
Turbidity	0.1 NTU	H_3BO_3	13.8 g/L
Supplementary Bulk Solution		Epoxy Brown	0.612 g/L
TSP	2.22 g/L	Epoxy White	0.612 g/L
H_3BO_3	13.6 g/L	Latent dust/dirt	0.0686 g/L
		IOZ	0.0695 g/L

Chapter 4: Methods and Results

4.1 Introduction to Calcium Testing and the 4000 Series

The calcium testing is a subset of the chemical head loss experiment (CHLE) program known as the 4000 series. The 4000 series test plan divides data collection into four subseries (4100, 4200, 4300, and 4400) (Olson, 2014a). The 4100 series investigated the effects of fiberglass destruction on calcium release into solution by considering two fiberglass preparation methods: unadulterated fiberglass samples with no preparation, and blended fiberglass samples. Following the 4100 series, the 4200 tests sought to experimentally determine the solubility limit of calcium in prototypical post-LOCA water chemistry, using calcium chloride ($CaCl_2$) as a surrogate. The following 4300 series determined the behavior of calcium released through leaching from NUKON fiberglass. Once the calcium behavior is well understood, a heated vertical loop head-loss experiment measured the chemical effects of calcium (4400 series). The 4400 series was designed to simultaneously measure behavioral changes in solution chemistry and head-loss though a prototypic fibrous media. A multi-constituent debris bed was prepared in a temperature controlled column and ICP-OES measurements were taken for the following 20 days as well as continuous head-loss measurements to study the relation between metals in solution and head-loss through a debris bed. This series of testing established a foundation of separate calcium chemical effects studies leached from NUKON fiberglass, and provides a wealth of new information not previously understood about the leaching of calcium from NUKON fiberglass.

4.2 Effect of Fiberglass Destruction on Calcium (4100)

In the event of a LOCA various degrees of fiberglass intactness may exist due to the relation between the piping insulation location with respect to the pipe break and jet impingement angle. NUREG/CR 6224 (Olson, 2014b) determines classes of fiberglass depending on the degree of destruction, ranging from class 7 (intact) to class 1 (untangled individual fibers). These classes were utilized as the boundaries for a bench scale leaching experiment to determine if the level of fiberglass destruction could affect the amount of calcium released

from: (1) unadultered (class 7), and (2) blended (modified class 1 and 2; due to the blending process changing the fiber characteristic length). Seven bottles, three of each destruction level and a blank sample were run for a total test time of eight hours. ICP-OES measurements showed an overall slight difference in the average of the two fiberglass preparation groups. Detailed testing procedures can be found in CHLE-SNC-012(Olson, 2014b). The blank bottle contained a calcium concentration of 0.65 mg/L. The results are shown in Table 11 below.

Table 11: ICP-OES results of [Ca] fiberglass preparation given in mg/L

Unadulterated	Blended
1.2	1.3†
1.4	1.0
1.3	1.1

† The first value for the blender was considered an outlier because upon taking the sample, it was noted that the fiber was still intact, as opposed to the fiber slurry seen in the other two samples.

Results of the fiberglass preparation experiment indicated a small difference in the average release of calcium between the two data sets: 1.3 mg/L for unadulterated fiberglass, 1.1 mg/L for blended fiberglass. A student's 't' test was conducted to investigate the similitude of the results, the full calculation is presented in CHLE-SNC-13 (Olson, 2014c). The student's 't' test confirmed that the two averages were statistically similar within a 95% confidence interval. With this knowledge, future bench tests were conducted with the confidence that the destruction level of the fiberglass did not change the rate of calcium release. This result further implied that the UNM preparation method used to generate the debris bed in the head-loss column testing would have the same calcium release rate from NUKON fiberglass when compared to unadulterated fiber used in bench scale testing. The bench and tank scale differed from the column test in each of them used unadulterated fiberglass. The column fiberglass was prepared using a modified NEI method as described in the debris bed section above.

4.3 Post-LOCA Calcium Orthophosphate Solubility Limit (4200)

The goal of the 4200 series was to determine the solubility limit of calcium in post-LOCA containment solution at 80°C. The expected amount of calcium in solution can be obtained from the thermodynamic modeling (Figure 9). The addition of sufficient quantities of calcium salts to a supersaturated solution will result in the formation of HAp ([Ca] = 0.16 mg/L at 7.1 pH and 80°C). Varying quantities of $CaCl_2$ were added to target pH 7.1 solutions; after three hours, the solution was filtered (to remove precipitates) into a sample bottle for ICP-OES analysis. These results are summarized in Table 12.

The blank bottle results demonstrate a total calcium contamination of 0.18 mg/L from the source water, boric acid, and TSP. This contamination comes from adding 13,600 mg/L of boric acid and 2,220 mg/L of TSP, so very small traces of contamination (i.e., less than 0.01% of the TSP) of the chemicals contributed to the observed calcium. In addition, the chemicals used were "technical grade" chemicals prototypic to the plant, and are of substantially lower quality than "reagent grade" or "ACS grade" that is often used in laboratory research. The technical grade TSP used is only about 98 % pure, which leaves 2% of the mass for impurities, which is fairly substantial (although most of the impurity is NaOH).

HAp was modeled (Chapter 2) with the experimentally measured pH at 80°C, for comparison to 4200 results. The blank bottle concentration compared to the expected HAp concentration indicates that the contamination level may have exceeded the solubility limit (Table 12), and precipitated prior to the addition of $CaCl_2$. If this were the case precipitate ripening could have occurred during the heating period, prior to $CaCl_2$ addition. Increasing the amount of calcium added to solution does not alter the resulting solubility product. The average of the experimental results was within a tenth mg/L compared to the HAp solubility. The measured temperature associated with pH was lower than testing temperature due to the procedure of sample and data collection. When a sample was removed from the bath it was immediately filtered, into the 125 mL nitric treated sample bottle, then the pH of the solution would be taken. This time difference led to the solution cooling to the measured temperature observed in Table 12.

Table 12: Results of salt addition to 4200 series and comparison to thermodynamic prediction

Ca added by $CaCl_2$ [mg/L]	**ICP-OES Measured Ca [mg/L]**	**Final pH**	**Temp. [ºC]†**	**[Ca] (mg/L) Assume HAp 80ºC Final experimental pH**
0	0.18	6.93	63.7	0.21
40.35	0.24	7.11	64.9	0.16
79.99	0.25	7.02	63.6	0.17
161.3	0.33	6.91	61.7	0.21
Average	**0.25**	**6.99**	**63.5**	**0.18**

†Temperture of solution before pH measurement was taken

Comparing the concentration in solution obtained in the 4200 series with the 4100 series, it can be seen that a significantly different concentration was obtained using $CaCl_2$ when compared to using NUKON. These results indicate that the addition of $CaCl_2$ leads to the formation of a different solubility product than that which was formed when calcium is slowly leached from the fiberglass. This has implications into the validity of the defined surrogate preparation technique defined by WCAP-16530-NP (Lane et. al 2006). The formation of a different precipitate will lead to different precipitate size. As indicated before the addition of HAp will seed the solution leading to only HAp formation (Neuman & Mulryan, 1971). Therefore the WCAP-16530-NP defined calcium phosphate surrogate is not prototypic of the calcium product formed in post-LOCA solution, and may change the characteristics of calcium orthophosphate in solution, if added as a chemical head-loss surrogate.

4.4 Separate effects calcium behavior from NUKON fiberglass (4300)

Studies investigating the release of calcium into solution out to 30 days, suggest the occurrence of an interesting phenomenon that has not been reported in previous chemical effects studies. Calcium leached from fiber was expected to reach a maximum concentration in solution. After several days of continual exposure of fiber to heated, borated, TSP-buffered solution at the maximum concentration, a sudden decrease in calcium concentration was measured. Repeated experiments confirmed this result and this

variable in calcium concentration over time was the focus of this research. The 4300 series consisted of four tests comprised of 3 bench test and 1 tank test. The three bench tests were identical 2 g/L experiments conducted at the 7.1 baseline pH, for increasing periods of time (1, 8, 30 day). The tank test was conducted at 1.18 g/L, the expected amount of submerged NUKON fiberglass for a LBLOCA that releases the maximum amount of NUKON into the containment pool. The tank test was performed to provide insight into scaling effects of the 4300 bench series, and provided a baseline for calcium behavior to compare to integrated tank tests conducted as part of the larger CHLE test series, outside the focus of the 4000 series.

Before experimentally studying the effects of calcium leaching from NUKON fiberglass, WCAP (Lane et. al., 2006) was utilized to model the designed experimental conditions. The equation predicts the release rate of calcium and the maximum calcium in solution would increase with increasing temperature and pH. The release rate predicted by the WCAP is sensitive to temperature over the range of interest (doubling as the temperature increases from 40^{o}C to 75^{o}C) but not very sensitive to pH (varying by less than 10 percent between pH 6.5 and 7.5). The release rate of calcium from WCAP was used to help guide initial UNM 4300 series testing.

4.4.1 One Day Leaching from NUKON Fiberglass (4300.P1)

Currently the WCAP-16530 correlation (Equations (11),(12),(13)) (Lane et. al 2006) is utilized to predict the calcium concentration and solubility limit of calcium in post LOCA scenarios. The 4300 series experimentally determines the validity of the WCAP correlation in representative Vogtle post-LBLOCA water chemistry buffered by TSP. Preliminary 4300 series investigations sought to determine the release rate of 1 gram of fiberglass at the baseline pH (7.14 pH) at 80^{0}C over a 24 hour period. The predicted release rate of calcium from NUKON™ using WCAP-16530 indicated that saturation would occur within 3 hours for 1 gram of fiberglass in 500 mL solution at 80^{0}C at 7.14 pH (Figure 29). It was expected that as time increased during the 24 hour period, the concentration of calcium would approach an asymptotic value considered to be the solubility limit. ICP-OES results

(Figure 30) demonstrate a linear increase in calcium concentration over the 24 hour period. The total calcium concentration measured in a solution with TSP after 24 hours corresponded to the WCAP-16530 prediction from an un-buffered solution in the first half hour. Therefore the WCAP-16530 equation is not valid for buffered solution NUKON leaching, and additional experimentation was completed to find the solubility limit under testing conditions.

$$RR = kA(1 - \frac{C}{K}) \quad (11)$$

$$K = 10^{[a+b(pHa)+c\left(\frac{1000}{T}\right)]} \quad (12)$$

$$k = 10^{[d+e(pHa)+f\left(\frac{1000}{T}\right)]} \quad (13)$$

RR = release rate

A= amount of material

k = constant dependent on pH and temperature

C = the concentration of the released species

K = the saturation limit of the released species (a quasi-equilibrium constant)

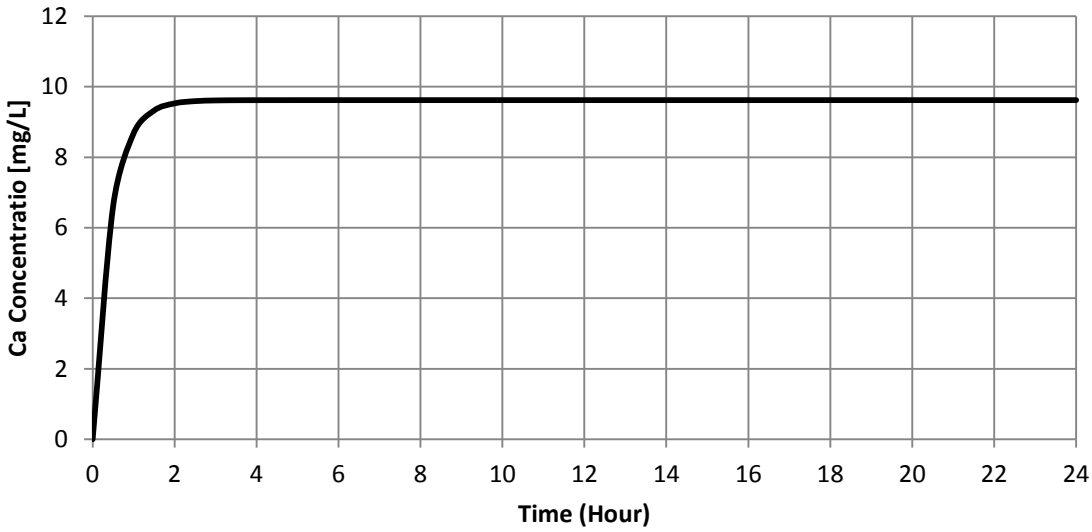

Figure 29: WCAP-16530 (Lane et. al 2006) prediction [Ca] for 1g of NUKON™ in 500 mL H_2O at 80 ^{o}C & pH 7.14

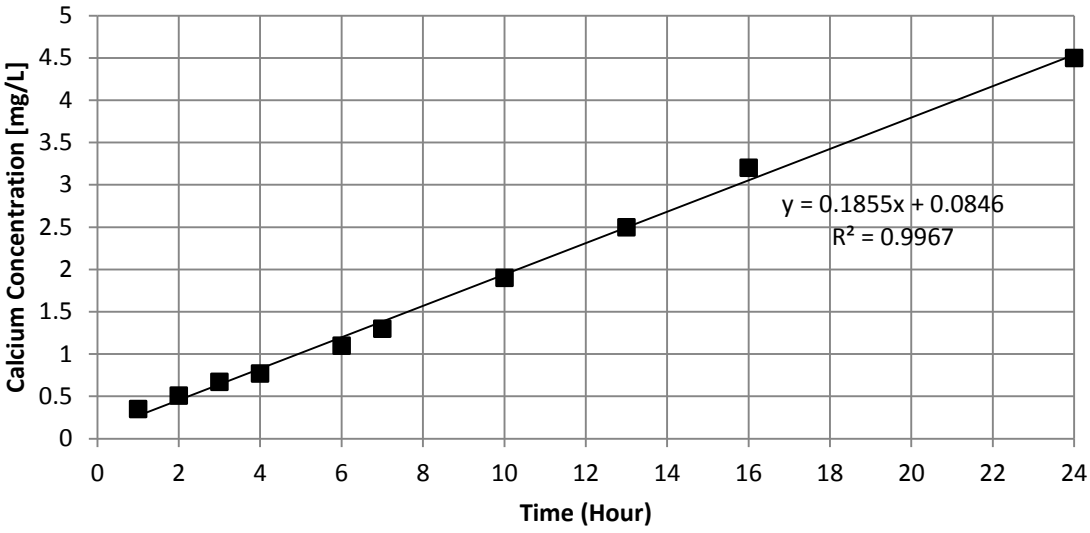

Figure 30: ICP-OES results for UNM 4300 Calcium Leaching at pH 7.14 & 80 ℃

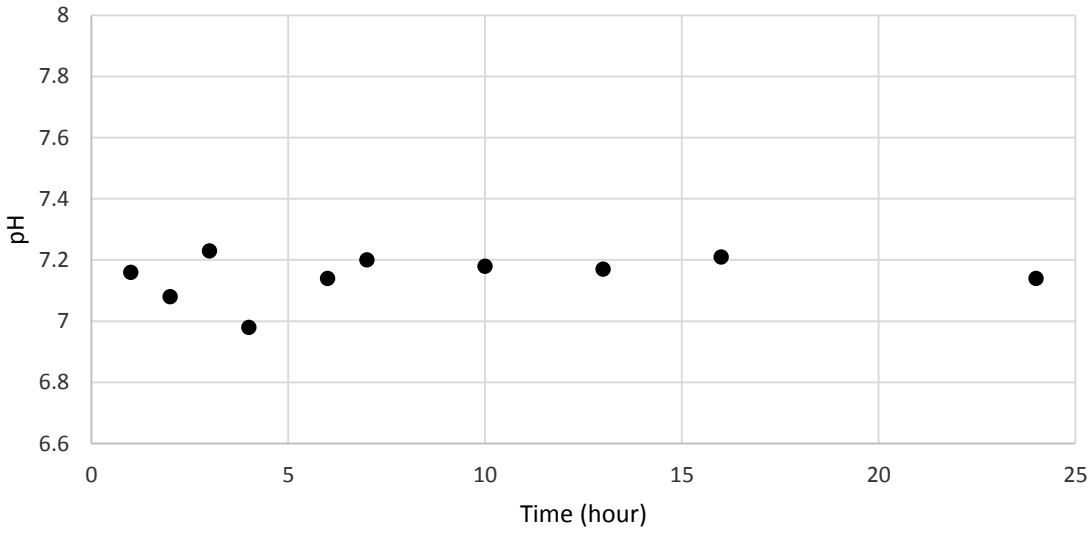

Figure 31: Measured pH at average measured temperature of 69.5°C (temperature loss before measurement) for 4300.P1

4.4.2 Eight Day Leaching from NUKON Fiberglass (4300.P2)

A longer duration (8 day) 4300 series (4300.P2) test was carried out to reach the solubility limit, keeping all other experimental conditions the same. The results showed that the maximum calcium concentration was measured on the second day at 6.5 mg/L. The

expected asymptotic behavior was observed, giving an approximate saturation limit at ~5.5 mg/L. An unexpected and significant decrease in calcium concentration observed on the on the eighth day (Figure 32).

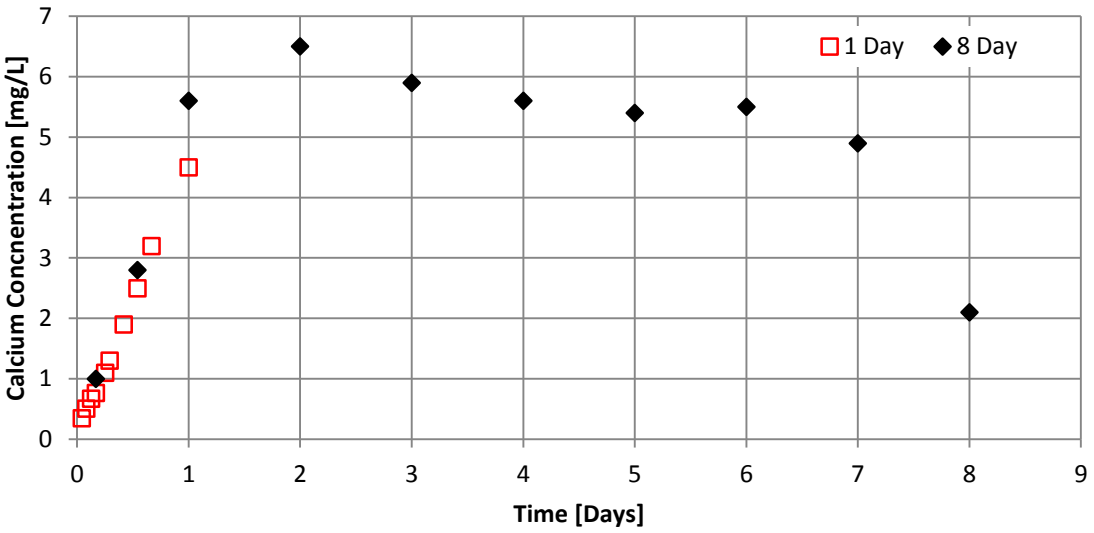

Figure 32: UNM 4300 Ca Leaching at 2g/L NUKON, 7.14 pH, & 80 ℃ for 1 & 8 days

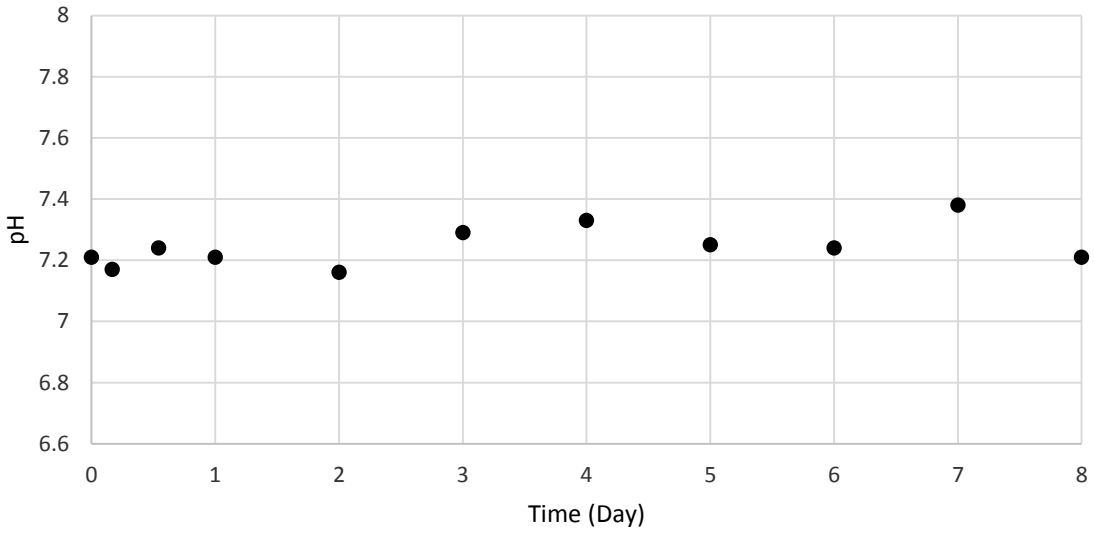

Figure 33: Measured pH at average measured temperature of 70°C (temperature loss before measurement) for 4300.P2

4.4.3 Thirty Day Leaching from NUKON Fiberglass (4300.P3 & 4300.Tank)

After the completion of the 8 day test, two hypotheses were developed to explain the sudden concentration drop on the 8th day of 4300.P2. The first hypothesis (4300.P3) was precipitate aging, which could be investigated by longer testing periods. The second hypothesis considered a decrease in the release rate of calcium from the fiberglass surface and a continued rate of precipitation and is known as the twice leached fiber (TLF) experiment. TLF results are presented following the results of 4300.P3. 4300.P3 was tested using two 30 day tests, one on the bench scale (500 mL) and another on the tank scale (1136 L (300 gallon)).

These 30 day experiments investigated the change in calcium concentration for increased time periods and experimental scaling effects from the bench to the tank scale. The water chemistry in the tank and bench scale were identical. The tank and bench scales differed in fiberglass concentration with designed 2 g/L in the bench tests and 1.18 g/L in the tank tests, both tests were run at constant temperature of 80 °C. The bench scale fiberglass concentration for 4300.P3 was chosen to maintain consistency with previous bench tests (1 gram in 500 mL), while the tank scale was chosen based on the expected amount of fiberglass to be used in future integrated effects tank tests, outside the scope of the CHLE 4000 series.

The previous 8 day bench test (4300.P2) was compared to the 30 day bench test (4300.P3), up to 15 days. During the 30 day bench scale experiment, bottles were prepared so that a sample could be collected every third day for 30 days, with duplicate bottles on days 3, 6, 9, and 18; an additional jar was also prepared for sampling on the first day. 4300.P3 shows an overall similar trend to 4300.P2. The calcium concentration reached on the 1st day is slightly higher for the 30 day test, and this trend is also noted on the 3rd day and one data point for the 6th day. This slightly higher value could be due to the slightly lower starting pH of 7.00 for the 30 day test verse pH 7.21 for 4300.P2. The difference in the pH was not due to chemicals added, as the same quantity of chemicals was added in the preparation of both bulk solutions, and is due to experimental variation possible factors include pH probe calibration, carbonate concentration, and initial nanopure pH. As shown

in Figure 3 and Figure 4, WCAP suggests higher initial release rate of calcium from fiberglass for a higher pH.

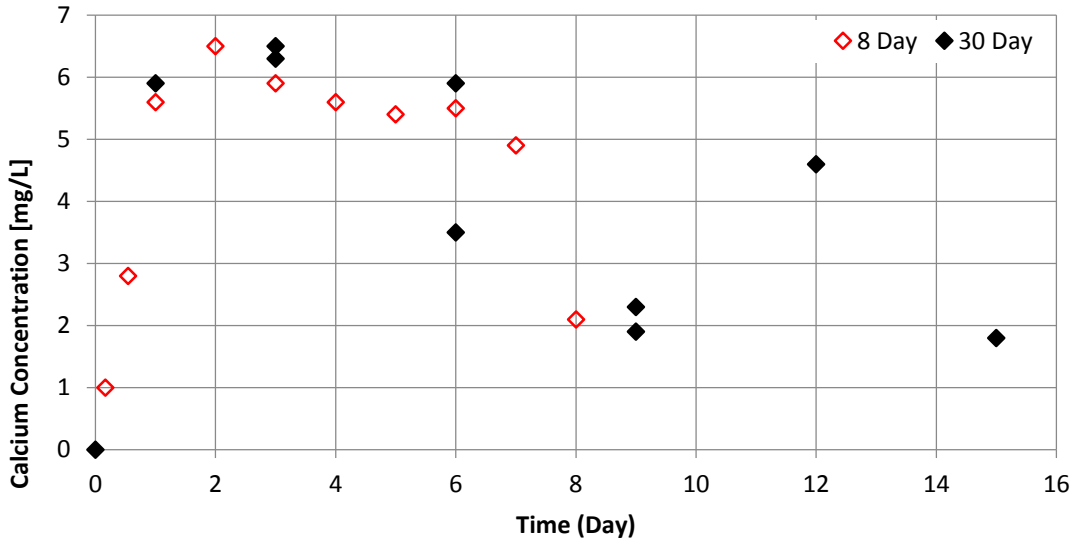

Figure 34: Compares identical bench tests (4300. P2 & 4300.P3) up to 15 days (500 mL, 1 gram NUKON, 80 ^{0}C)

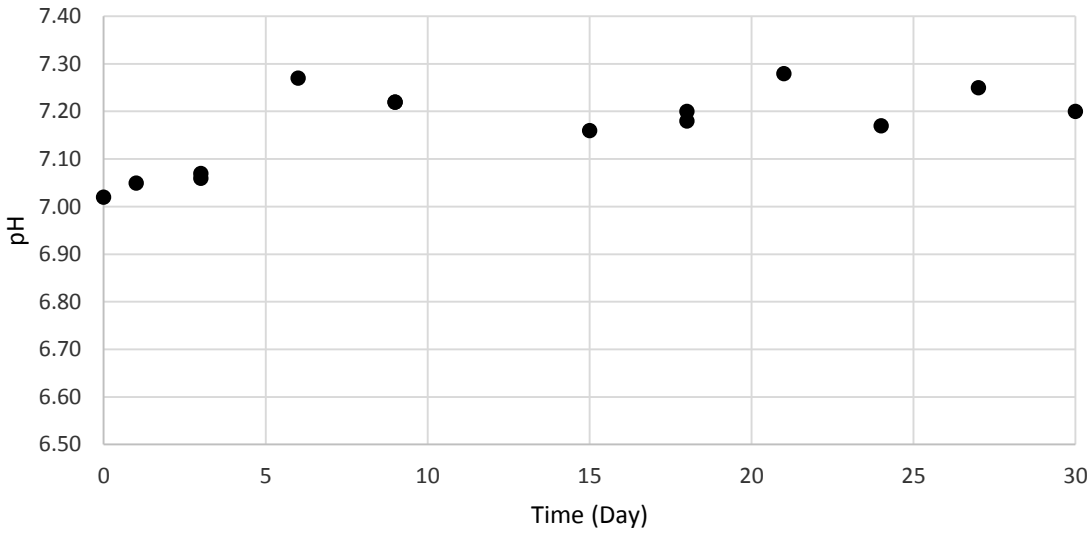

Figure 35: Measured pH at average measured temperature of 49.2^{o}C (temperature loss before measurement) for 4300.P3

An interesting outcome of performing duplicate experiments is observed on the 6th day. One value obtained is slightly higher than that of the 8 day test and the other value is significantly lower. A precipitate aging process can reduce the calcium solubility limit to a lower value as early as day 6 during a bench test. This could be due to calcium contamination leading to HAp formation during the solution heating period prior to fiberglass addition (4200). Another data point to take special note of occurs on day 12 with a value similar to that seen on the 7th day of the 4300.P2. Day 12 calcium concentration is within the expected calcium concentration range, but not for the time period. This result indicates that the precipitate ripening may happen as late as day 12.

For the tank test, samples were collected every day for the first 10 days and every 5 days for the remaining 20 days. Tank test sampling differed from bench test sampling in that the samples were sequentially taken from the same experiment; in bench test experiments every point represents a separate but identically prepared experiment. Figure 36 shows only the first 15 days of the 30 day experiment for comparison with the 8 day bench test. In 4300.Tank, the calcium concentration does not reach a steady-state value until the third day, whereas 4300.P2 reaches a steady-state value on the second day. The tank then follows a similar trend observed in 4300.P2 test where steady state Ca concentration is reached (3rd Day), the observed steady state concentration drops slightly (~7th day), then significantly to 2 mg/L (>10th -15th Day). Days 4-7 of each test show nearly identical behavior. On day eight the tank maintains an approximate calcium concentration of 4.5 mg/L whereas the bench scale drops to 2.1 mg/L. The tank experiment then continues to have approximately 4.5 mg/L for days 9 and 10. Somewhere between the 10th and 15th day of the tank experiment the steady state concentration decreased to 2 mg/L.

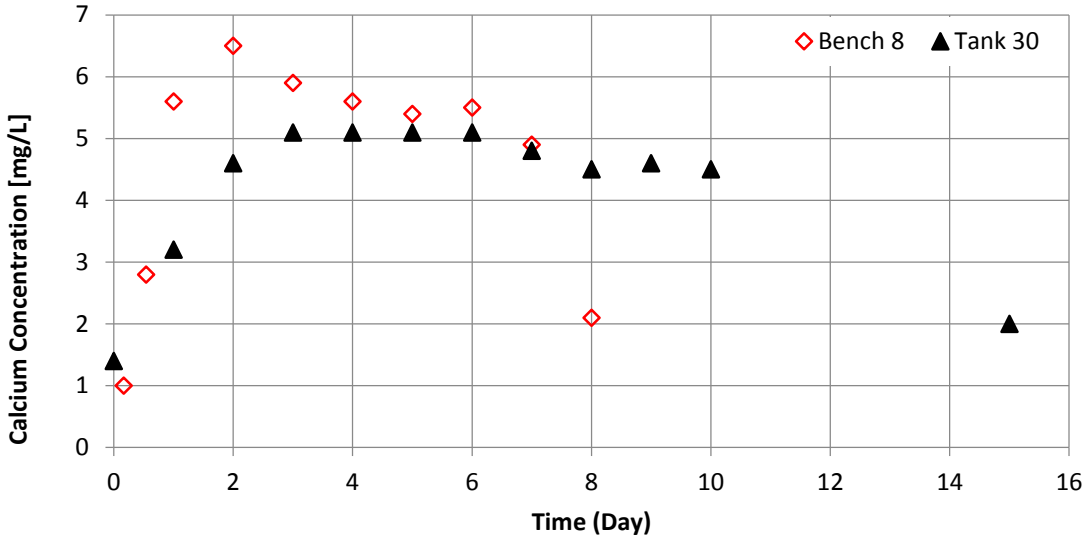

Figure 36: Compares the 4300.P2 to the 4300.Tank test with identical water chemistry but varying fiberglass concentration (Bench 2 g/L vs. Tank 1.18 g/L)

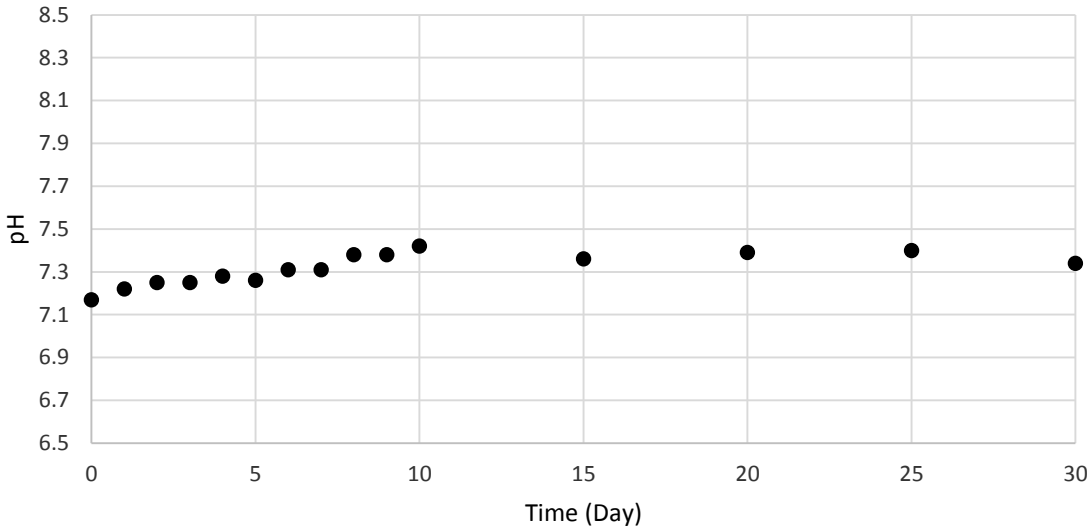

Figure 37: Measured pH at average measured temperature of 63.2°C (temperature loss before measurement) for 4300.Tank

As noted before, the calcium concentration in the 30 day tests for both bench & tank scale follow a similar trend to 4300.P2. Figure 38 compares the 4300.P3 and 4300.Tank and demonstrates that in the 12th day, bench scale has a similar value to that of the 8-10 day tank test of calcium concentration. This result may indicate that the precipitate

formed here is a metastable precipitate, with the possibility of lasting for up to five days. Looking to day 15 of 4300.Tank and 4300.P3, the tank has a calcium concentration of 2 mg/L versus a concentration of 1.18 mg/L on the bench scale. The offset days of data points taken between day 15 and 30, do not allow for direct value comparison but does demonstrate the gradual decrease in concentration down to 1.4 and 1.3 mg/L on the bench and tank respectively. A complete comparison for the 4300.P2, 4300.P3, and 4300.Tank are compared in Figure 39.

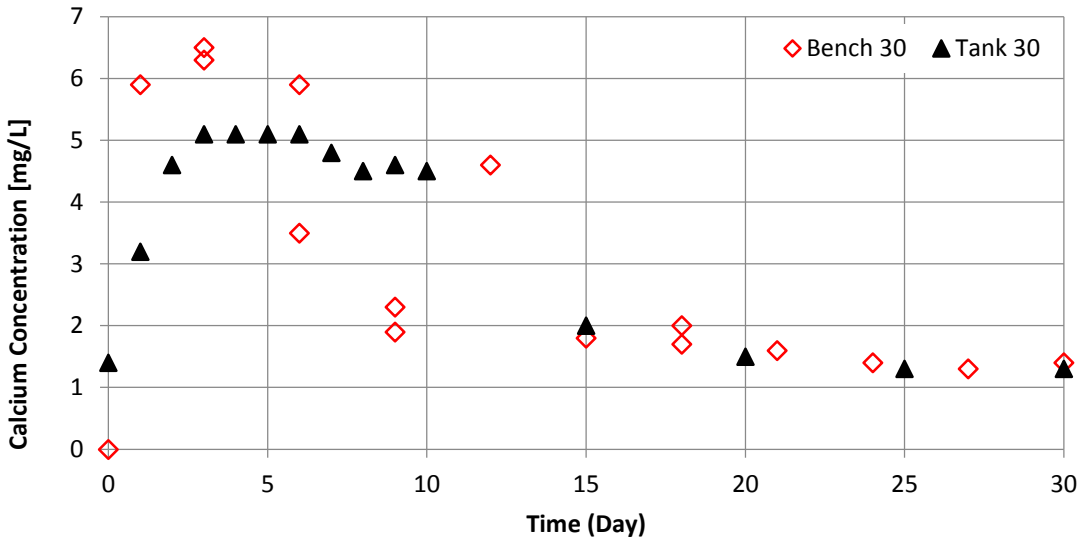

Figure 38: Ca in solution for 30 day fiberglass leaching experiments at pH 7.14 & constant 80 ºC

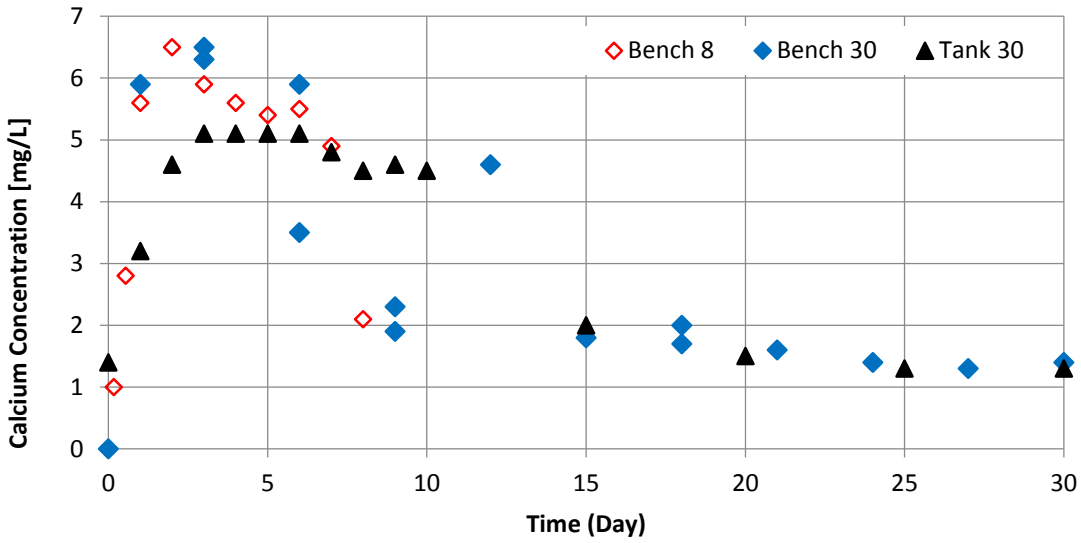

Figure 39: Compares 4300.P2, 4300.P3 and 4300.Tank leaching experiments

4.4.3.1 Twice Leached Fiberglass (4300.P3.TLF)

After the completion of 4300.P2 (8 day leaching), two hypotheses were developed to explain the sudden concentration drop on the 8th day of 4300.P2. The first hypothesis was precipitate aging, which led to the development of the 30 day bench scale test (4300.P3), previously discussed. The second hypothesis was that the release of calcium from the fiberglass slowed, while the rate of precipitation continued, thereby dropping the calcium concentration in solution to a lower value. To test the possibility of a decrease in the release rate of calcium from the fiberglass surface, the twice leached fiber (4300.P3.TLF) experiment was designed with two leaching periods. For a given sample of fiberglass, the initial leaching period was variable (3, 6, 9 & 18 days) while the second leaching period was fixed at 24 hours. The experiment sought to define the release rate of calcium from fiberglass at different periods in time. 4300.P3.TLF allowed separate 1 gram fiberglass samples in 500 mL solution to leach for different initial time periods (e.g. 3, 6, 9, & 18 days). When the initial time period of leaching was completed, the fiberglass was then filtered, added into a new 500 mL solution, and allowed to re-leach for 24 hours. Previous bench scale experimentation (4300.P1) had shown it takes more than 24 hours (Figure 30) for 2 g/L fiberglass to reach the metastable concentration, therefore the amount of calcium

re-leached in the 24 hour period, following the initial leaching period (3, 6, 9, or 18 days), could be compared at different times allowing for observations to be made in changes to the leaching rate.

This experiment utilized the fiberglass samples from the 4300.P3 test. There was concern that if precipitation by heterogeneous nucleation had occurred on the fiberglass surface or in the filtered fines, precipitates filtered from the initial leaching period could be added into the 24 hour leaching experiment. If added to the 24 hour re-leaching bottle they would then dissolve into solution and give an inaccurate fiberglass leaching rate. Therefore for each initial leaching time period (3, 6, 9 & 18 days) two samples were run. One would be added directly into the new 24 hour re-leaching solution and the other would receive a 30 min deionized water (DI) rinse at room temperature, before addition into the re-leaching solution. The DI rise sought to use the retrograde solubility of calcium at low temperatures to speed the release of calcium precipitates back into solution. The results of the twice leached fiber test are shown in Figure 40. There is a clear decrease in the release rate at increased time periods. Noticing that the long periods seem to indicate values similar to that of the original leaching experiments Figure 41 and Figure 42 allows for comparison of the 24 hour re-leaching values (4300.P3.TLF) with initial leaching period results (4300.P3).

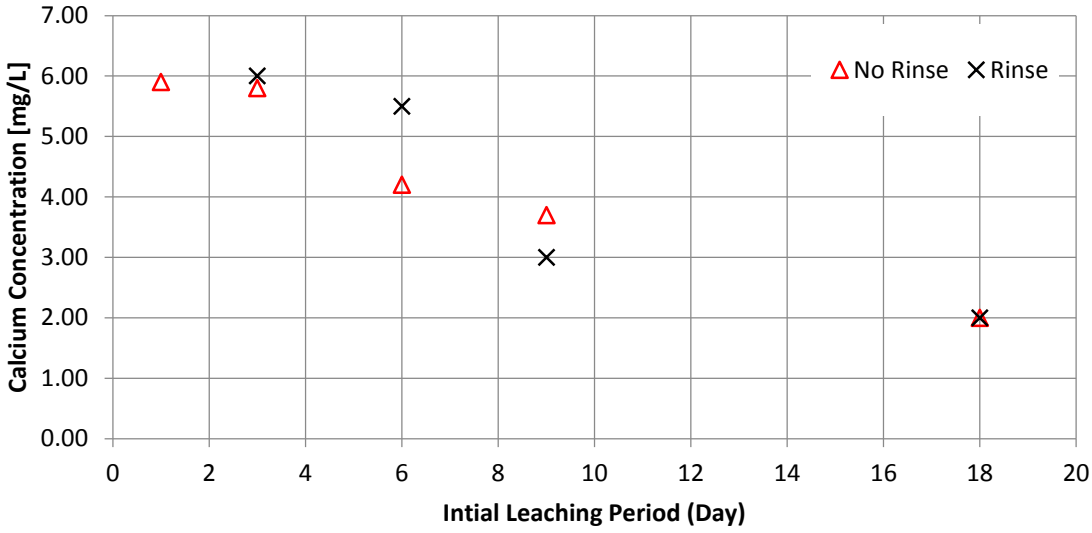

Figure 40: Calcium concentration results for 24 hour re-leaching experiment at varying initial leaching time periods

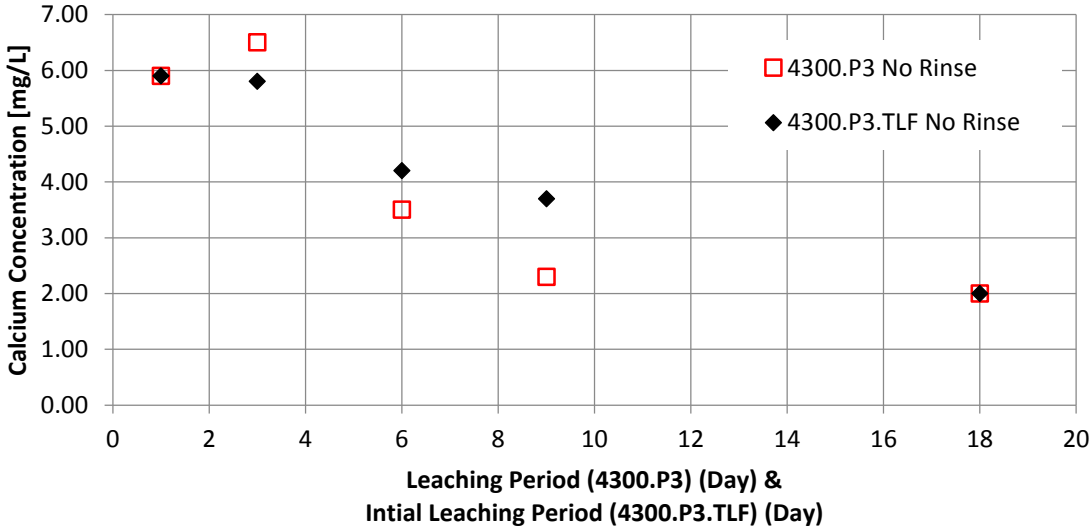

Figure 41: Twice Leached fiber (4300.P3.TLF) results compared to [Ca] of original leached results (4300.P3)

For the no rinse fiber, the 24 hour re-leached fiberglass returned to a [Ca] near the original value in all cases. Days 1 and 18 have exact matches for initial leach and re-leach at 5.9 mg/L and 2.0 mg/ L respectively. Day 1 servers as the baseline for the expected calcium release if there is no change in calcium leaching at increased time periods. Days 3 and 6 have the same difference from the original value at 0.7 mg/L, but the original value

is lower for day three and higher than the re-leached value for day 6. Day nine difference is double that of day 3 and 6 at 1.4 mg/L and in this case the original leaching value is lower than that of the re-leached value.

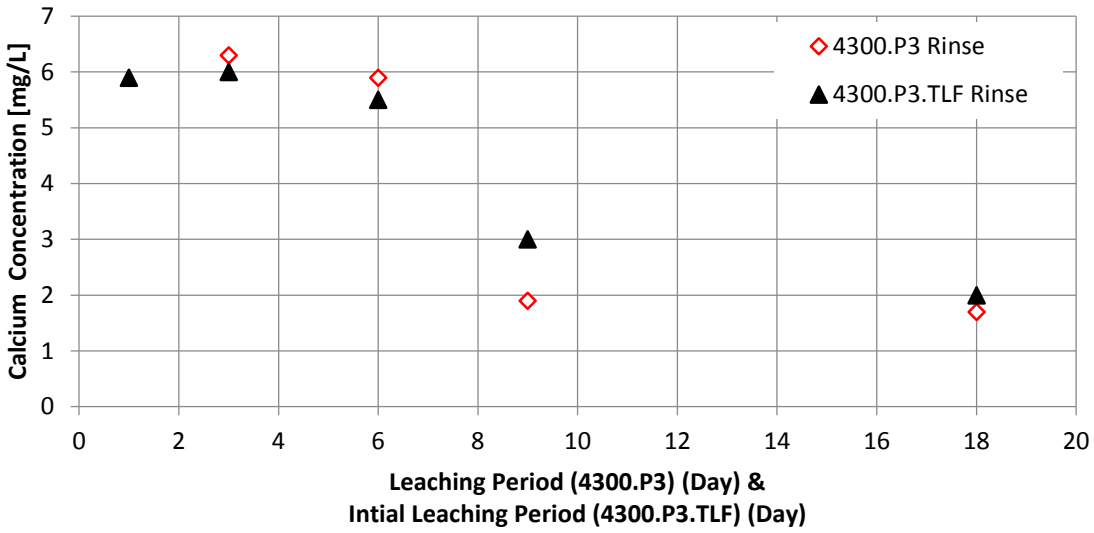

Figure 42: Twice Leached fiber (4300.P3.TLF) results for fiber that received an additional 30 minute DI rinse prior to second leaching period, compared to [Ca] of original leached results (4300.P3)

The rinsed TLF samples [Ca] returned to values similar to that of the original. Days 3 and 6 show higher original values, while days 9 and 18 show lower original values. The difference in values is similar for days 3, 6, and 18 at 0.3 mg/L, 0.4 mg/L, and 0.3 mg/L respectively. The difference in original versus re-leached for day 9 in approximately three times as large as the difference seen on any other days at 1.1 mg/L. The 30 minute DI rinse at room temperature was ineffective at removing precipitates, but calcium was foun to leach into solution during the rinse (Figure 43). This reasonably implies the rate of calcium leaching from fiberglass is more favorable, that dissolution of calcium orthophosphate precipitates. Overall there are 4 data points with lower original concentrations (average difference from original: 0.88 mg/L), 3 data points with higher original values (average difference from original: 0.47), and two data points with the same value. The overall average difference from the original leaching value including higher, lower, and the same as the original is 0.23 mg/L. These results are summarized in Table 13.

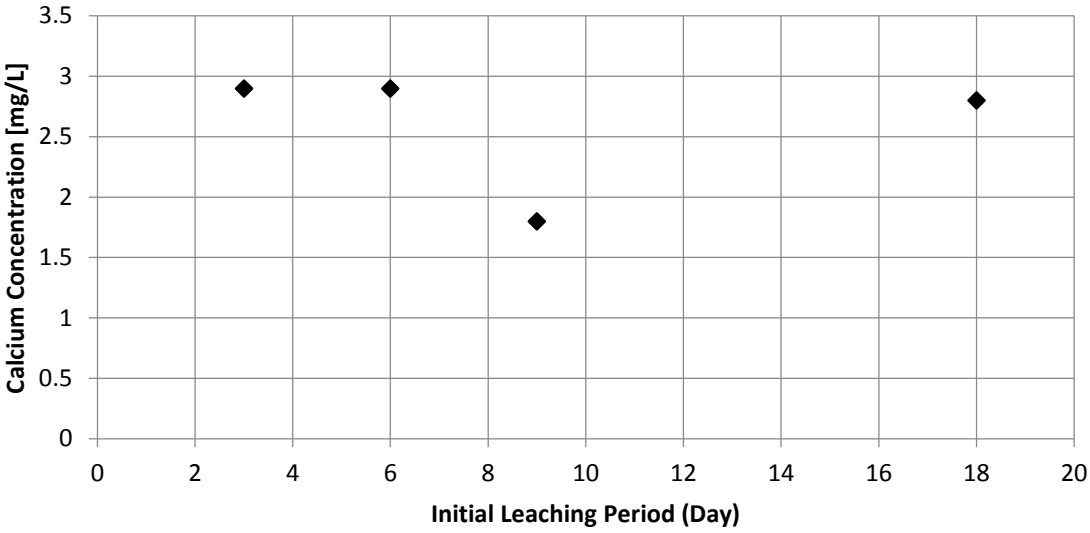

Figure 43: ICP-OES results from 1 gram fiberglass in 500 mL DI water at room temperature for 30 min after leaching for varying initial time periods in borated buffered water at 80°C

Table 13: Summarizes data obtained in the Twice Run Fiberglass Experiment

TWICE LEACHED FIBERGLASS						
NO RINSE						
Initial Leach period (Day)	4300.P3 [Ca] (mg/L)	4300.P3.TLF [Ca] (mg/L)	Δ (mg/L)	Original Concentration		
1	5.9	5.9	0.00	Same		
3	6.5	5.8	0.70	Higher		
6	3.5	4.2	-0.70	Lower	Low Avg	-1.05
9	2.3	3.7	-1.40	Lower	High Avg	0.70
18	2.0	2.0	0.00	Same	No Rinse Overall Avg	0.28
RINSE						
Initial Leach period (Day)	4300.P3 [Ca] (mg/L)	4300.P3.TLF [Ca] (mg/L)	Δ (mg/L)	Original Concentration		
3	6.3	6.0	0.30	Higher		
6	5.9	5.5	0.40	Higher	Low Avg	-0.70
9	1.9	3.0	-1.10	Lower	High Avg	0.35
18	1.7	2.0	-0.30	Lower	Rinse Overall Avg	0.18
		Avg Overall	0.23			
		Avg Overall Low	-0.88			
		Avg Overall High	0.47			

In conclusion, the data collected in the twice leached fiberglass experiment did not provide information on a change in fiberglass release rate. For each of the re-leaching experiments one would expect to find that the solution had re-leached to the same value as the original 24 hour leaching experiment i.e. 5.9 mg/L, if there was no change in release rate. As shown in Table 13 the average difference between original 4300.P3 concentration and the re-leached calcium concentration is 0.23 mg/L. In contrast the overall average difference between the initial 1 day leaching value and the re-leach value for all experiments is 1.67 mg/L (Table 14). Albeit the TLF hypothesized a decrease in the calcium release rate from fiberglass with increased time periods, the similarity between the

re-leach values and the initial leaching period values leads to inconclusive data with respect to the release rate. The data suggests a precipitate was transferred into the re-leaching solution in each case, and that this precipitate did not dissolve into solution but instead acted as a nucleation site for further precipitate formation.

Table 14: Compares 4300.P3.TLF results to the expected value leached at 24 hours if assuming no change in fiberglass leaching rate with increasing time

TWICE LEACHED FIBER						
NO RINSE						
Initial Leach period (Day)	Initial [Ca] Leaching in 1 Day (mg/L)	4300.P3.TLF (24 hr. re-leach) [Ca] (mg/L)	Δ (mg/L)	Original Concentration		
1	5.9	5.9	0.00	Same		
3	5.9	5.8	-0.10	Lower		
6	5.9	4.2	-1.7	Lower	Low Avg	-1.98
9	5.9	3.7	-2.2	Lower	High Avg	N/A
18	5.9	2.0	-3.9	Lower	Overall Avg	-1.58
RINSE						
Initial Leach period (Day)	Initial [Ca] Leaching in 1 Day (mg/L)	4300.P3.TLF (24 hr. re-leach) [Ca] (mg/L)	Δ (mg/L)	Original Concentration		
3	5.9	6	0.10	Higher		
6	5.9	5.5	-0.40	Lower	Low Avg	-2.40
9	5.9	3	-2.9	Lower	High Avg	0.10
18	5.9	2.0	-3.9	Lower	Overall Avg	-1.78
		Avg Overall	-1.67			
		Avg Overall Low	-1.87			
		Avg Overall High	0.10			

Scanning electron microscope (SEM) images (Figure 44) of fiberglass samples allowed to leach for 18 days on the bench scale, do not exhibit noticeable differences. One sample was filtered and then taken for SEM imaging (No Wash: A, B); the other sample was filtered, added to a 30 min DI wash/ rinse then filtered again before SEM Imaging (Wash: C, D). The fibers appear to have particulates on the fiberglass surface. The makeup of the particulate is not detectible as EDS analysis returns the composition of the fiberglass.

The SEM imaging as well as the similarity of results for washed and no wash samples leads to the conclusion that the DI rinse was ineffective. That is not to say that the DI rinse removed no calcium. Figure 43 shows ICP-OES results from samples taken from the DI rinse that demonstrate an average of 2.6 mg/L of calcium was rinsed from the fiberglass. This rinse did not prevent the transfer of aged precipitates to the new solution.

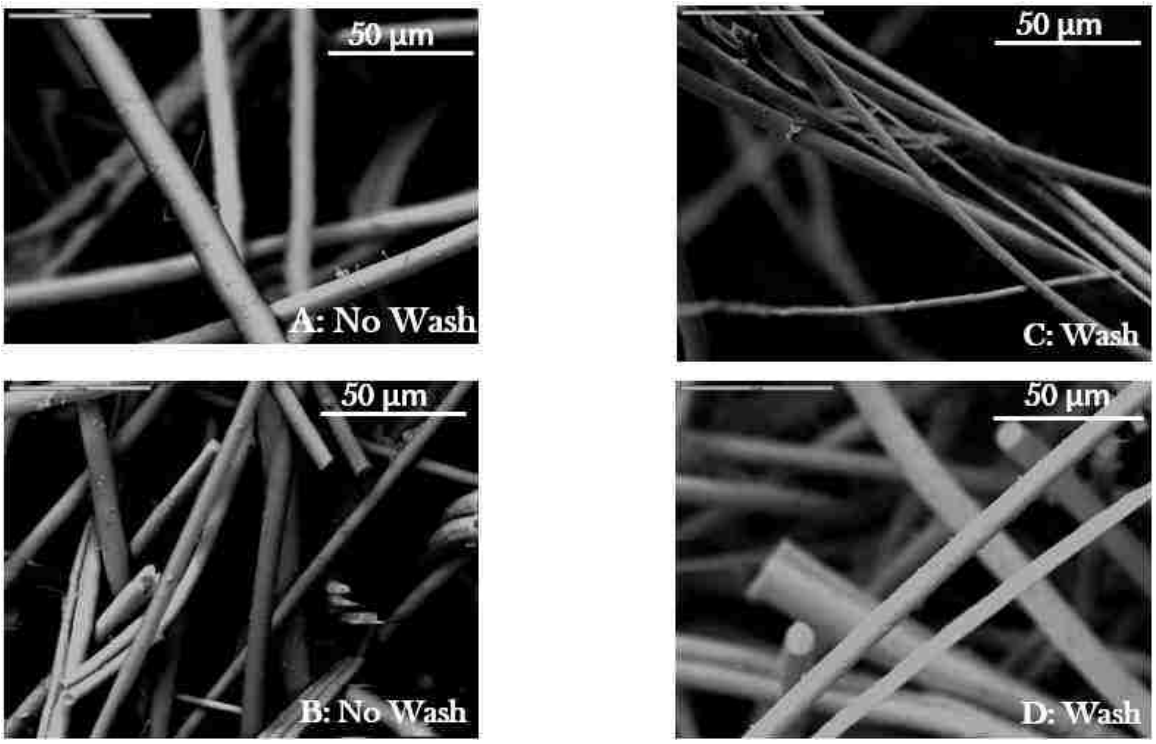

Figure 44: Scanning Electron Microscope (SEM) images of washed and unwashed fiberglass samples from the Twice Run Fiberglass experiment

4.5 Calcium Study in Heated Vertical Head-Loss Column (4400)

The goal of the 4400 series experiment was to explore and measure calcium chemical effects in a heated vertical head-loss column. The test maintained solution chemistry (borated & buffered) and temperature conditions as used in all previous bench tests and tank test (pH 7.1, 80 ^{o}C). The 4400 series test was run for 20 days. The amount of fiberglass was scaled to match the fiberglass concentration (fiberglass mass / water volume ratio) used in the 4300 tank test. A fiberglass mass of 37.2 grams was used to generate debris bed in column with 8.32 gallons of water. In order to create a more prototypic debris bed,

epoxy, inorganic zinc (IOZ), and latent dust/dirt were combined with the prepared NUKON fiberglass debris to form the multi-constituents fibrous bed. The debris materials were scaled to match prototypical values used in the UNM Head Loss (HL) series. The chemicals and debris bed constituents masses used in the 4400 series test are listed in Chapter 3 Table 10. The presence of epoxy in this test led to a higher total inventory of calcium. Leaching tests for epoxy are shown in Figure 45.

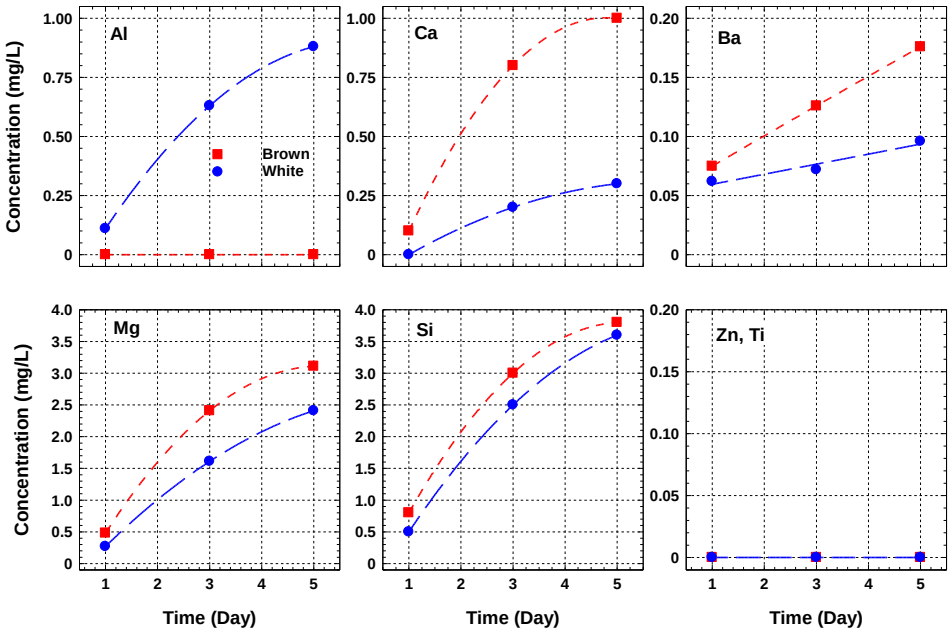

Figure 45: Epoxy 5 day leaching tests for 2 g, pH 7.14, 500 mL at 80 °C

The 4400 series was initiated on 10/31/2014 at 10:20 AM with the loading of the multi-constituents debris bed. The column temperature at debris loading was 86.2°C. The column temperature was set higher to account for temperature losses that were anticipated during debris bed addition to column. The temperature decrease was observed to decrease from 86.2°C to 71°C in 6.5 minutes, and returned to the desired testing temperature of 80°C two hours into the test. The temperature in the column was maintained at 80°C throughout testing. The temperature decrease is observed as shown in Figure 46b, as well as the temperature rise to 80 °C over the next 3 hours. The temperature in the column was kept stable at 80 °C over the period of testing.

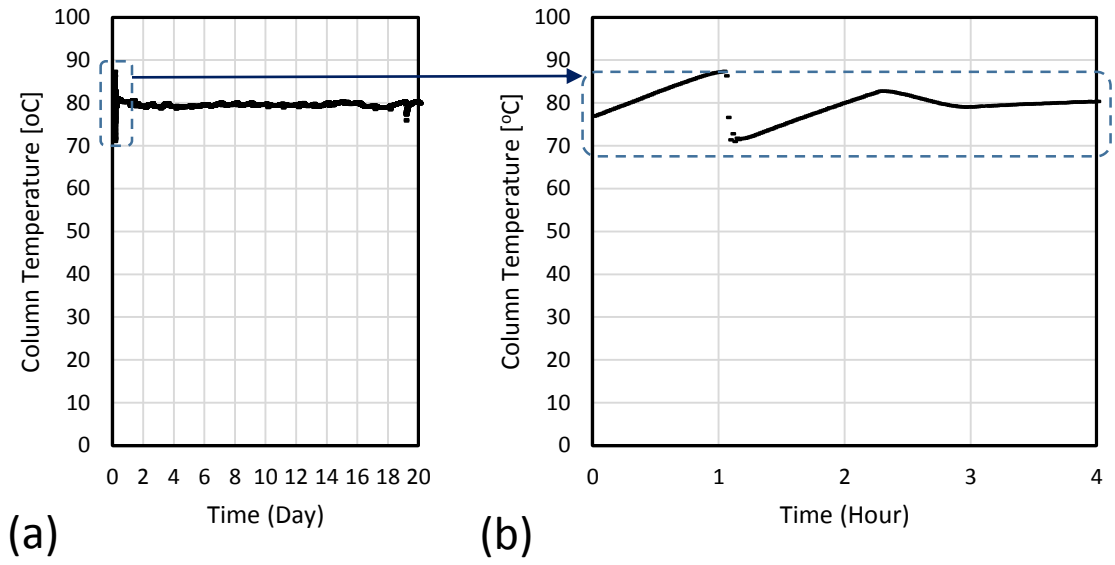

Figure 46: (a) 4400 Series 20 Day Temperature profile and (b) change in the temperature due to debris bed loading

As per HL testing procedure (Ali et al., 2014), the debris bed was loaded at a column approach velocity of 0.05 ft/s, to promote debris settling. The head-loss was allowed to stabilize at 0.05 ft/s, before decreasing to the prototypic approach velocity across the sump screen of 0.013 ft/s. Figure 47 compares the stability criteria to the velocity profile during the high velocity period. The stability criteria was met within the first 24 hours. Due to the stability drifting back above 1%/hr between hours 18-28, the planned decrease in velocity to the testing velocity (0.013 ft/s) was not performed until the 32nd hour of testing.

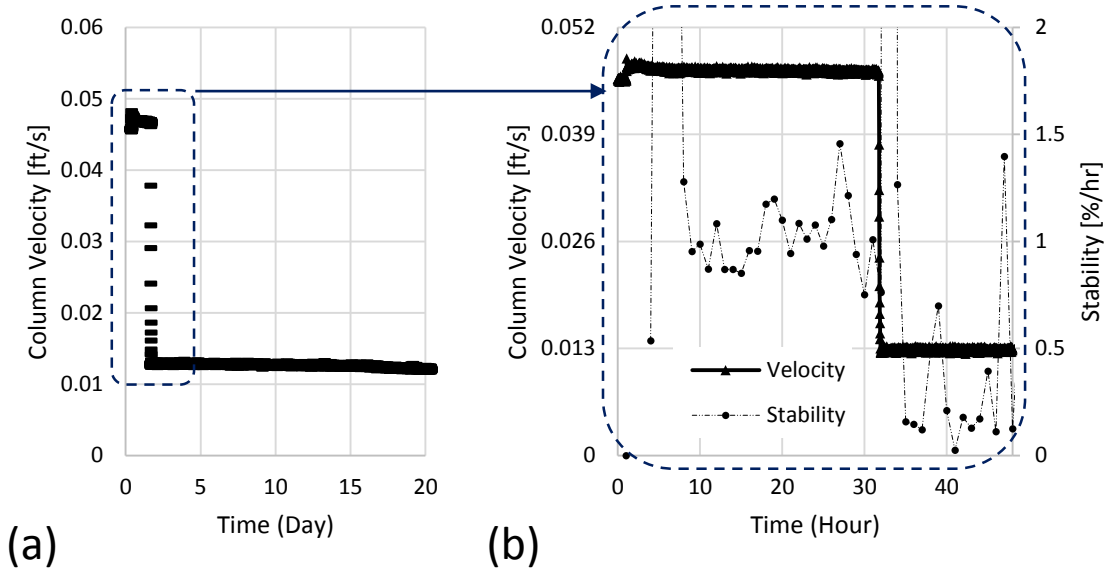

Figure 47: (a) Velocity profile of the 20 day testing period and (b) comparison of the column approach velocity and head loss stability criteria

Figure 48a shows the variation in measured turbidity by sample location. The measured turbidity from top samples were consistently higher than from samples taken from the bottom. There appears to be consistency in the high and low peaks, though this is most likely from variation in floating epoxy particulates. Figure 48b shows the results of turbidity samples taken from the bottom of the column, after debris bed filtration. There is a general decrease in the trend of the turbidity from samples taken from the bottom, with an outlier on the 19th day. Results from the head-loss data (Figure 49) and stability criteria for this outlier indicate that the bed seems to have been significantly disturbed during this pull from the bottom, most likely resulting in particulate removal from the bed. This means that the turbidity reading on day 19 represents a measurement of particulate removed from the bed during the sampling transient and not representative of water turbidity at day 19 under steady state experimental conditions. Figure 49 shows the stability criteria overlaid on a graph of head-loss and includes where the ICP-OES sample was taken for each of the 20 days of testing.

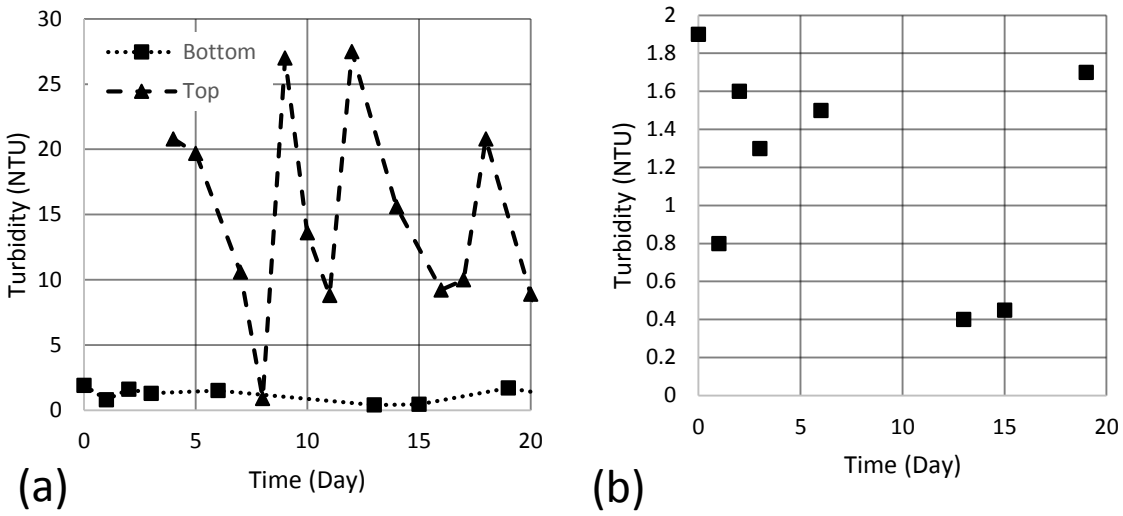

Figure 48: (a) Turbidity data comparison by sample location and (b) turbidity results for samples taken from the drain

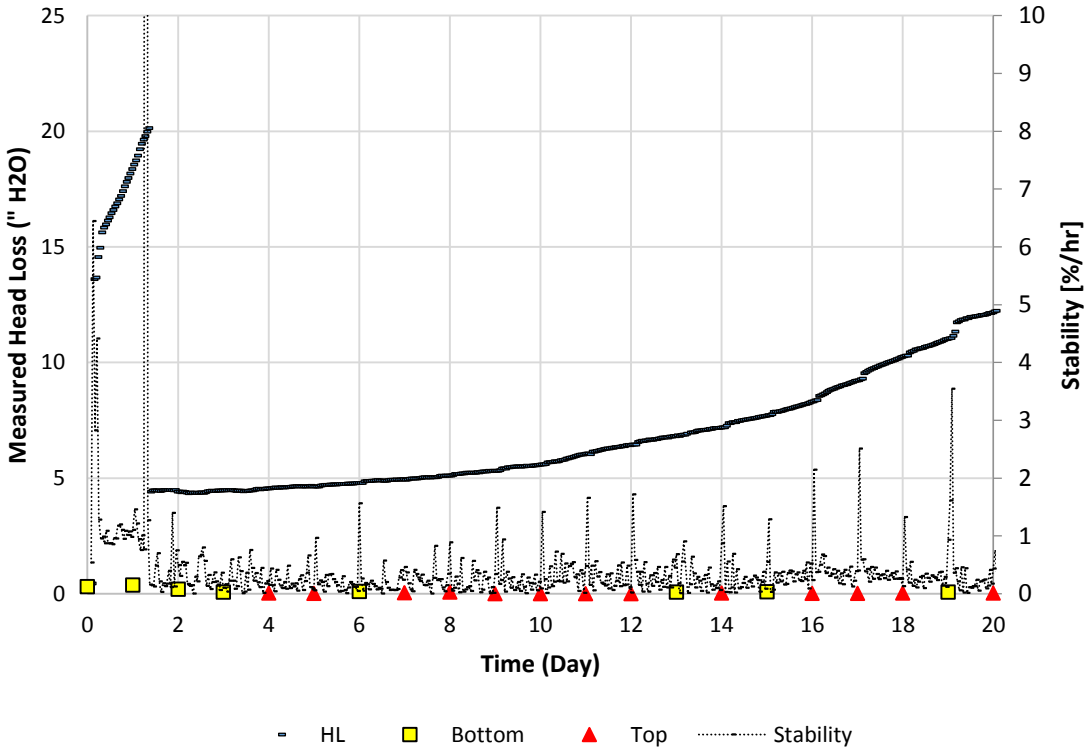

Figure 49: Comparison of Head-Loss and stability criterial with indicators of samples taken from either the top or the bottom of column

The head-loss observed in the column over time is not due to repeated bed disturbance, but due predominantly to chemical effects. Stability spiked (implying the HL was momentarily unstable) on days when samples were taken from both the movable flange (top) and the drain line (bottom). The stability then returned immediately below the < 1%/ hr criteria. There is no clear relation between bed disturbance and sample method i.e. samples taken from the top or the bottom. The change is never more than 3 %/hr divergence from stability for any observed spike, excluding the 19th day. The stability criteria remained stable within 4 %/hr for all testing times and within the 1% stability criteria outside of the spiked regions.

As the head-loss increased due to bed characteristics (porosity) change, resistance to the flow increased, changing the operating condition of the centrifugal pump, which resulted in reduction in the approach velocity (Figure 50). The pump did not compensate the flow resistance by frequency increase to recover the same flow condition (flow rate and velocity). The velocity began to noticeably decrease by the 10th day of the experiment, and had deviated from the prototypic approach velocity to 0.012 ft/s by the end of the test. The exponential fit was done from day 3 because the approach velocity was not decreased from the loading value until day 3. The exponential fit will be utilized to perform a linear regression and compare changes in head-loss slope for regions of interest defined by the behavior of calcium in solution.

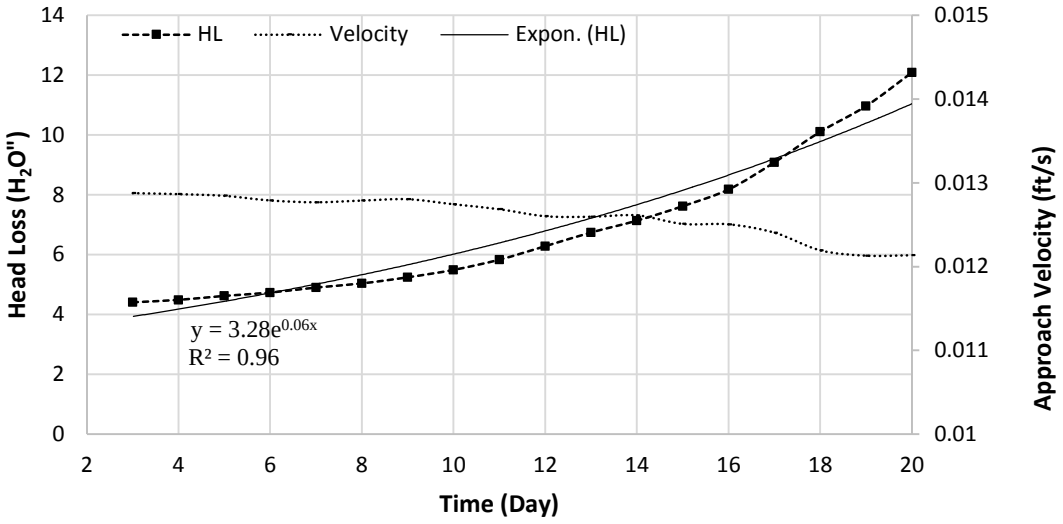

Figure 50: Exponential fit to HL data from day 3 to 20

The pH in solution is fairly stable over the 20 day testing period with an average value of 7.35 (Figure 51). 4400 fiberglass concentration was scaled from the 4300.Tank test and therefore the results were expected to be similar. The 4400 series test differs from previous tests in that the debris bed is multi-constituent - containing epoxy, latent debris and IOZ - in addition to the NUKON fiberglass. 4400 follows the same trend observed in the 4300 bench and tank tests (Figure 52a). The location of the sample extraction does not appear to bias the ICP-OES result (Figure 52b). [Ca] increased in solution up to the third day, then entered a metastable region for the next seven days. The behavior of [Ca] between days 10 & 15 for the tank test is unclear due to a lack of data, but was observed in the 4400 test that the [Ca] in solution drops between days 10 & 11. It is interesting to note that the [Ca] in solution in the column is higher than 4300.Tank before the drop but remains lower after the drop. The final concentration (on day 20) in the 4400 series test is 1.2 mg/L, compared to 1.5 mg/L in the tank.

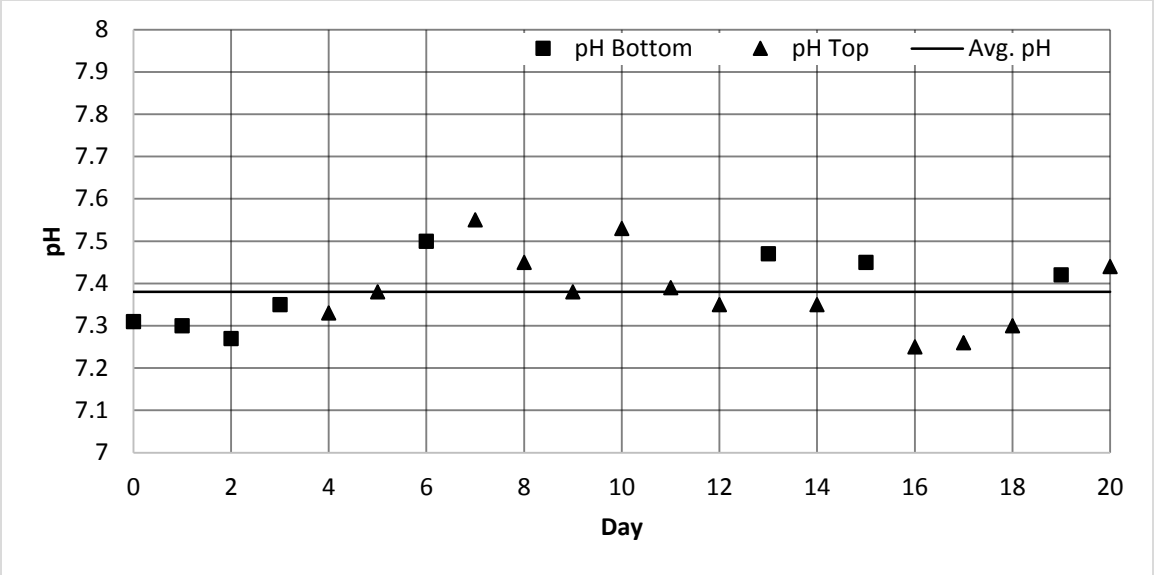

Figure 51: 4400 Series Column testing pH measurements with sample location indicator

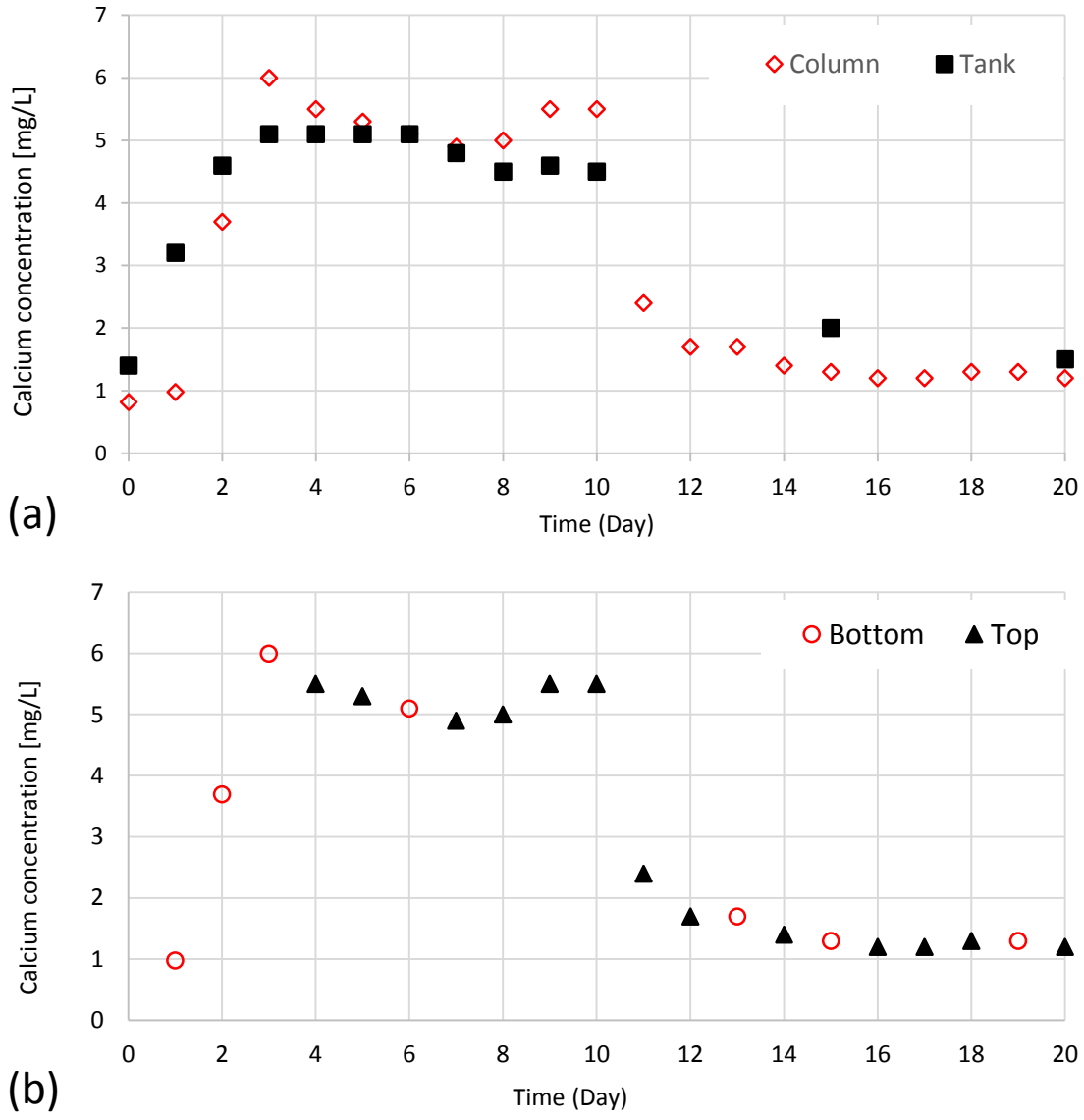

Figure 52: (a) Comparison of ICP-OES Ca results for the 4300.Tank test and the 4400 series column testing and (b) 4400 ICP-OES results by sample location

A comparison was made to determine the relation between the observed change in the measured head-loss and calcium concentration change in the column solution (Figure 53). Calcium concentration follows four distinct regimes between days 3 and 20. Head-loss data is only considered beginning at day three, which corresponds with the time at which the velocity in the column was decreased from the debris bed loading velocity of 0.05 ft/s to the prototypical approach velocity of 0.013 ft/s.

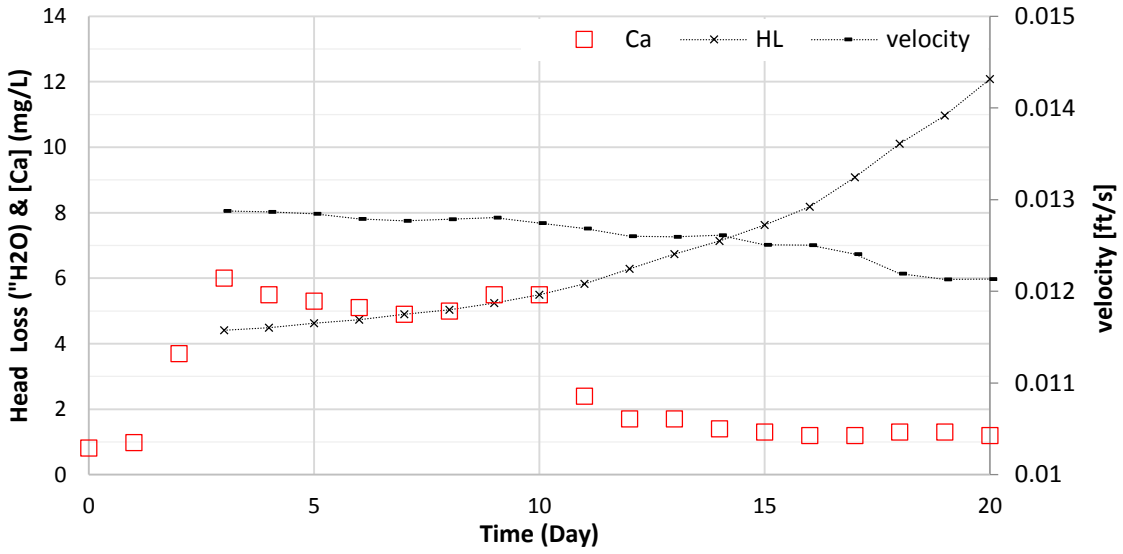

Figure 53: Comparison of [Ca], Head-loss, & velocity in the 4400 column over the 20 day testing period

Analysis of the measured head-loss can be divided into four regions (Figure 54). Region 1 represents a prompt release of calcium which behaves linearly from day 1.3 to 3. Region 2 is the head-loss corresponding to the calcium solubility metastable region from days 3- 10. Region 3 represents the head-loss measured in days 10 to 12, when the calcium concentration drops from 5.5 mg/L to 1.7 mg/L. Region 4 represents recorded head-loss behavior in days 12-20, when the calcium solubility is constant. The slope of the head-loss curve is calculated for each region using a linear regression through all head-loss points within that region. There is a trend of increasing head-loss slope in the three regions: Region 1, 0.17; Region 2, 0.80; and Region 3, 1.30. A greater increase in the head-loss would have been observable, had the velocity of the experiment be maintained constant. It is expected that the porosity of the bed decreases, leading to a resultant head-loss increase through the bed. Head-loss continues to increase in Region 4 due to continued crystal formation and growth of the ripened precipitate

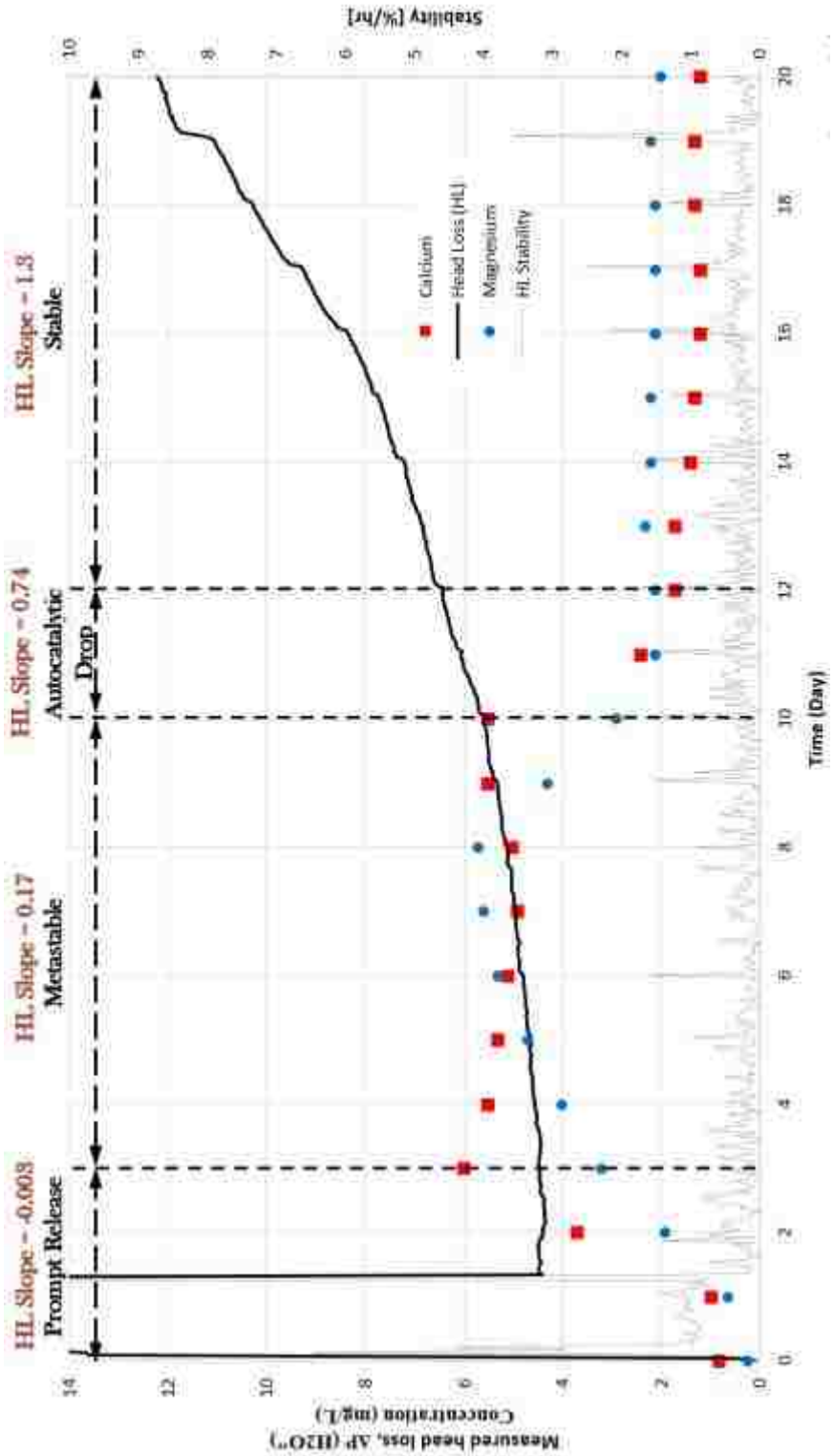

Figure 54: Four region calcium behavior compared to linear regression of HL slope

4.6 Fiberglass Concentration & Magnesium Behavior (4300 & 4400)

Fiberglass concentration and magnesium behavior have been shown to interact control regions of the calcium behavior in post-LOCA solution. Concentration of fiberglass effects the rate at which the prompt release of calcium enters solution. One addition bench test was carried out to see the effects of quadrupling the fiberglass concentration in solution. Magnesium is a known stabilizer of ACP in solution and active species in the calcium orthophosphate system. Magnesium ICP-OES results for the 4300 series (4300.P2, 4300.P3, & 4300.Tank) and the 4400 series demonstrated a codependent behavior of magnesium and calcium in post-LOCA containment solution.

4.6.1 Increased Fiberglass Concentration Bench Test

The typical bench test concentration of 2 g/L was quadrupling (1 gram to 4 grams) in a 500 mL solution. Calcium release over time was expected to scale proportionally to fiberglass mass. In response, the sampling times were reduced by a factor of four. The results of this experiment are shown in Figure 55. The '4 times fiber' test demonstrates that an increase in the fiberglass mass leads to an increase in the rate at which calcium is released into solution. The concentration of calcium in the 4 gram sample reaches 6.9 mg/L at 12 hours, while the maximum concentration of the 1 gram sample is 6.5 mg/L at 48 hours. Due to the test duration of 18 hours, future tests are needed to determine how the calcium in solution will behave after the solubility limit is reached.

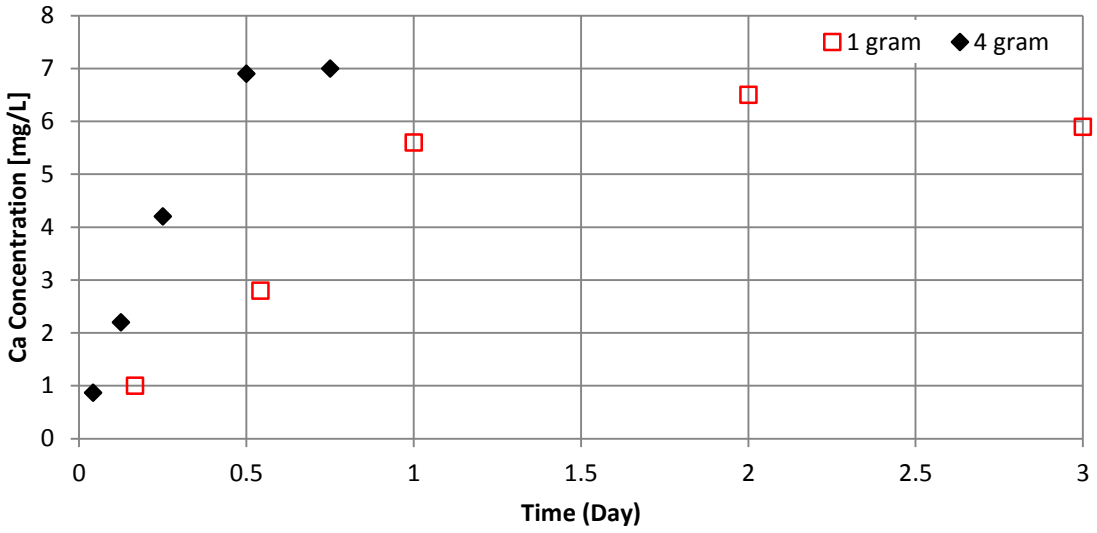

Figure 55: UNM 4300 Ca Leaching at 7.14 pH & 80 ^{0}C for 2 g/L NUKON (square) & 8 g/L NUKON (diamond)

4.6.2 Eight Day NUKON Leaching Magnesium Results (4300.P2)

Magnesium exhibits a slow leaching period into solution over the first 5 days (Figure 56). After approaching the maximum concentration in solution at ~6.1 mg/L magnesium, there is a three day drop in magnesium concentration down to 2.6 mg/L magnesium for day 5 to 8. After the second day of magnesium decrease from solution, calcium drops auto-catalytically from 4.9 to 2.1 mg/L calcium. This result further disproves the TLF hypothesis of decreased rate of calcium leaching from fiberglass leading to the drop in calcium concentration.

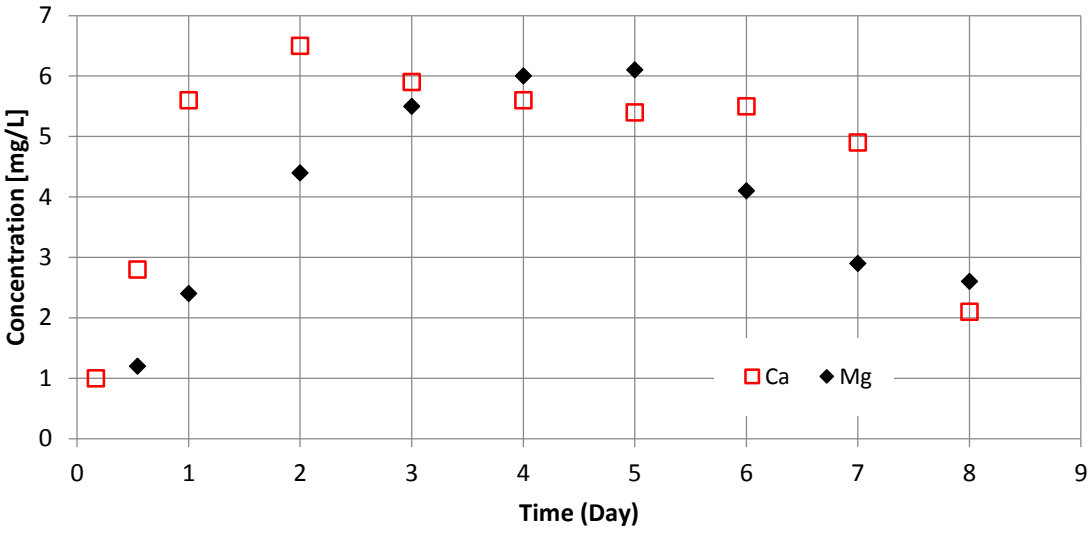

Figure 56: 4300.P2 comparison of ICP-OES results for calcium & magnesium

4.6.3 Thirty Day NUKON Leaching Magnesium Results (4300.P3 & 4300.Tank)

Previously the 30 day bench experiment (4300.P3) had a number of non-typical bench test calcium concentrations, specifically, the variable calcium concentration on day 6 and the high calcium concentration on day 12. Focusing first on the day 6 results the recorded calcium concentration were 5.9 and 3.5 respectively. Experimental conditions between 4300.P2 and 4300.P3 were identical, therefore referring back to Figure 56, the drop magnesium concentration is expected to drop at approximately day 5. The magnesium concentrations correlating to the 5.9 mg/L Ca and 3.5 mg/L Ca, were 3.5 mg/L Mg and 2.7 mg/L Mg respectively. Both magnesium values are lower than those observed from day 6 of 4300.P2 (4.1 mg/L Mg). In the 4300.P2 the calcium concentration did not drop until the magnesium concentration was lower than 2.9 mg/L. Assuming that total magnesium must be less than 2.9 mg/L Mg to allow calcium to drop out of solution; it would be expected for the 4300.P3 higher calcium concentration to not have dropped whereas for the observed lower calcium concentration should have dropped. Lastly turning attention to the day 12 high calcium concentration it can be seen that the magnesium is at 6.8 mg/L therefore the calcium should not have dropped. The experimental conditions which led to the stabilization of the magnesium and the resulting stabilization of calcium concentration are not clear, but this does further the point that the high magnesium concentration and calcium

concentration are correlated, and that magnesium is controlling or at least predeceasing the drop in calcium concentration.

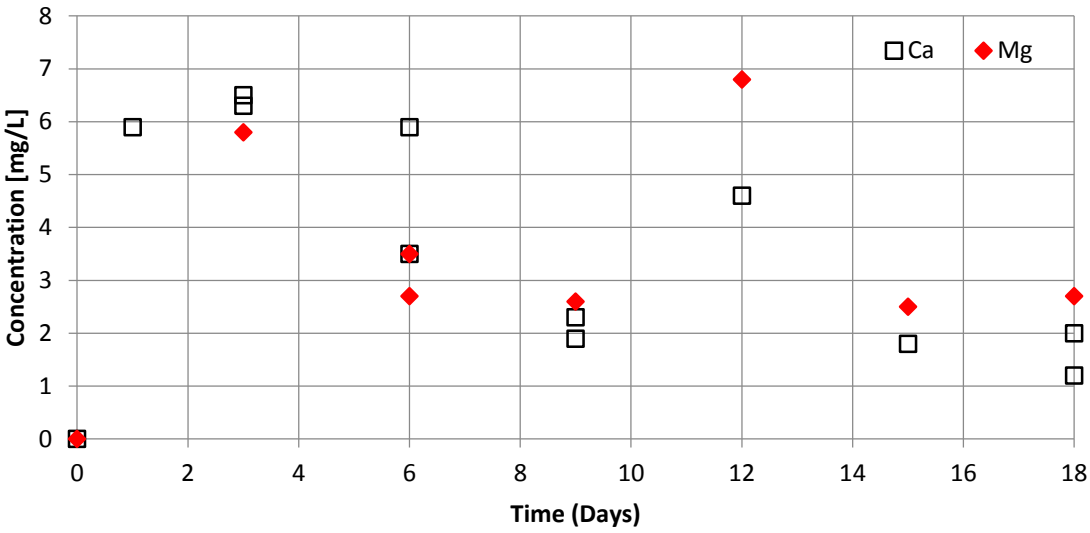

Figure 57: 4300.P3 Bench Test with magnesium data

The correlation of magnesium and calcium in the tank demonstrates again that magnesium follows the same trend observed in the 4400 series. 4300.Tank reaches a known max value of 5.3 mg/L Mg observed on day 10 (Figure 58). The true tank maximum is not known due to lack of data collection between days 10 and 15 of the test. The magnesium concentration has been observed to approach a value near that of calcium and then decrease to a value near that of calcium as well.

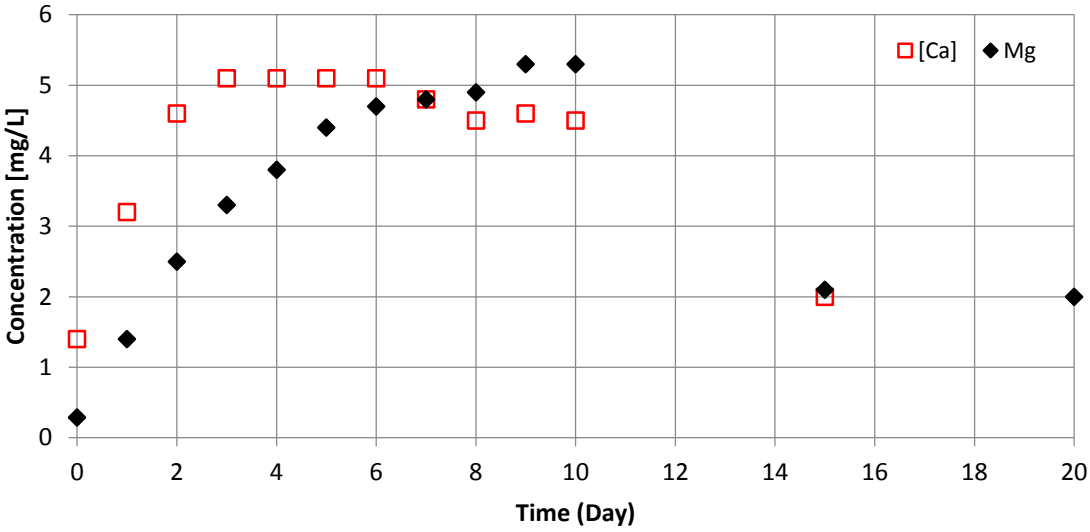

Figure 58: 4300.Tank test with magnesium data

4.6.4 Heated Vertical Head-Loss Column Magnesium Results (4400)

Comparing the concentration change of calcium and magnesium showed that the sudden decrease in calcium concentration in solution is attributed to the presence and change of magnesium concentration leaching into solution from the NUKON fiberglass. After eight days magnesium reached the maximum measured concentration in solution of 5.7 mg/L (Figure 59). Magnesium then drops over a three day period at which point calcium drops. Identical to the result in 4300.P2, the calcium drops following a magnesium concentration of 2.9 mg/L. There was a time period from day 7 to day 10 where an increase in calcium concentration was observed before the drop. This behavior was more pronounced in this experiment than the others, but could indicate the metastable solubility product became destabilized by the decreasing magnesium concentration.

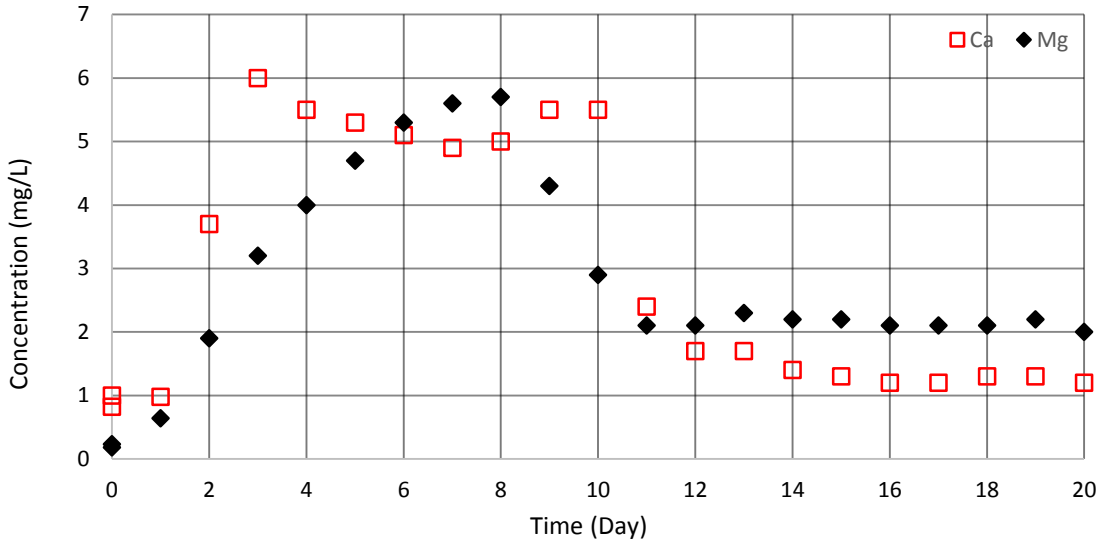

Figure 59: 4400 Ca & Mg ICP-OES results

Chapter 5: Discussion and Conclusion

5.1 Summary

Six major findings were confirmed through experiments carried out in the 4000 series. First, the destruction level of fiberglass did not change the rate of calcium leaching from NUKON. Secondly, the addition of $CaCl_2$ into prototypic LBLOCA chemistry resulted in the formation of HAp. The solubility limit of HAp was not observed in any NUKON leaching experiment. Third, the calcium behavior in solution changed overtime in a predictable 4 region pattern. Fourth, in a constant heat vertical head-loss column, the head-loss associated with chemical effects increased overtime. Higher head-loss was found to occur in regions associated with the growth or increase in precipitates. Fifth, increasing fiberglass concentration displayed a decrease in time to reach the maximum measured calcium concentration. The time to reach the maximum calcium concentration was found to be proportional to changes in calcium concentration. Lastly, the behavior of magnesium was observed to control the metastable calcium position. This chapter integrates the testing efforts of the 4000 series data. The discussion includes a formal investigation of the effects of fiberglass concentration, analysis of the metastable (region 2) and stable (region 4) determining the thermodynamically expected precipitates. Lastly these concepts are applied to interpreting the results of the head-loss test.

5.2 Effects of Fiberglass Concentration

Variable amounts of fiberglass may be dislodged and transported to the containment floor during a LOCA, depending on pipe break size, location, and available fiber inventory. The amount of fiberglass arriving at containment floor and the total volume of water will determine the rate of calcium leaching into solution. The dependence of calcium leaching rate on fiberglass concentration was investigated on the bench scale and large-scale tests investigating three fiberglass concentrations.

The majority of bench scale testing incorporated a fiberglass concentration of 2 g/L; with the exception one short duration test (20 hour), which was run at 8 g/L. Large-scale tests were each run using a fiberglass concentration of 1.18 g/L, though the total available

calcium between the tank and column tests differed due to the presence of epoxy paint in the column debris bed; separate bench scale leaching experiments have demonstrated that epoxy leaches calcium (Figure 45; 4 g/L epoxy, 80°C, 5 days, 1 mg/L Ca total).

A comparison of the time dependency of calcium leaching from NUKON fiber is shown in Figure 60. It is noted that higher initial concentrations of fiberglass in solution resulted in reaching the maximum concentration of calcium in solution faster than lesser fiberglass concentrations. For example, the maximum concentration of calcium in solution for the 8 g/L fiber test occurred four times faster than the 2 g/L fiber test, suggesting an approximately linear release rate to reach maximum calcium concentration in solution. The tank (1.18 g/L) experiment took 3 days to reach its maximum calcium concentration, which was consistent with the overall trend for calcium release into solution, but does not follow the linear relationship noted between the 2 g/L and 8 g/L test samples.

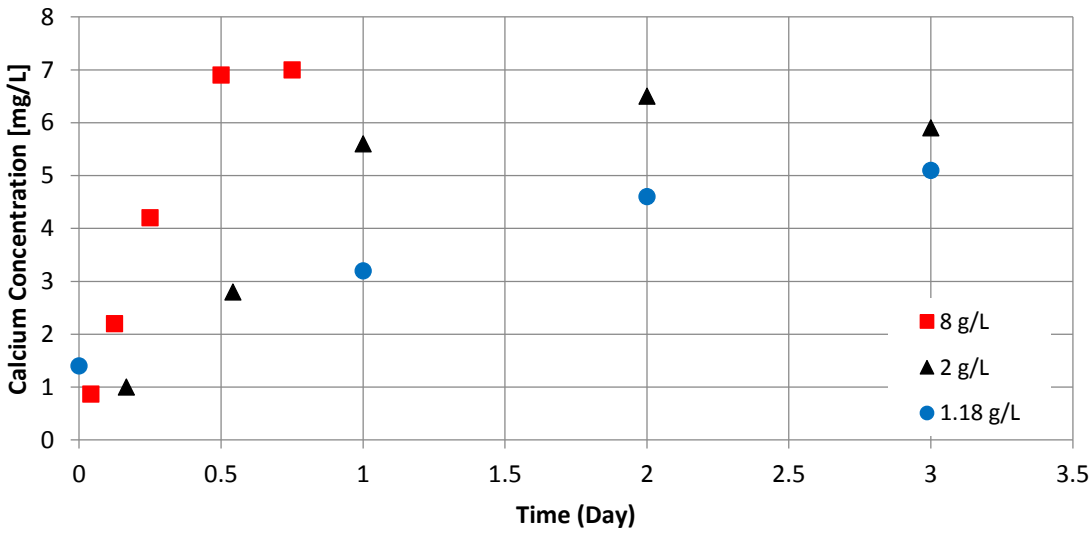

Figure 60: Effects of fiberglass concentration on calcium release in borated TSP-buffered solution

As also shown in Figure 60, increasing the fiberglass concentration increases the maximum calcium concentration reached in solution. The linear relationship in the time taken to reach the maximum calcium, observed between the 2 g/L and the 8 g/L, is not true for all cases. If a linear release rate was assumed to be consistent for 2 g/L and 1.18 g/L fiberglass, there would be a 12% expected deviation from the true value obtained in the

tank test (1.18 g/L). The 2 g/L fiber concentration was from 4300.P2, and the 1.18 g/L fiber concentration was from 4300.Tank. The leaching behavior observed here is the first of four regions of calcium leaching behavior from NUKON fiberglass which will be discussed in the following sections.

5.3 Calcium Orthophosphate Solubility Products from NUKON

The 4000 series investigations beyond the initial leaching period (discussed in Section 5.2) suggested the occurrence of an interesting phenomenon that has not been reported in previous chemical effects studies. First, calcium leached from fiber into solution until a maximum concentration was reached as expected. Then after several days of continual exposure to heated borated and TSP-buffered solution at the maximum concentration, a sudden decrease in calcium concentration was measured. This decrease was followed by a stable phase out to 30 days. Using thermodynamic modeling techniques discussed in chapter 2, this section determines the most probable phases of calcium orthophosphate.

The solubility product formed in region 4 demonstrated a tapering off behavior from the initial drop of ~ 2 mg/L Ca to a final stable value at 30 days of 1.4, and 1.3 mg/L Ca for the 4300.P3 and 4300.Tank respectively. The calcium concentration at 30 days was considered the most stable product, because the tapering off occurred as a gradual perfecting of a more crystal structure. The measured pH on day 30 of 4300.P3 and 4300.Tank was 7.24, and 7.34 respectively. β-TCP had a solubility limit of 1.14 and 1.00 mg/L calcium at the final measured pH values for 4300.P3 and 4300.Tank respectively. The vicinity of the results indicates β-TCP as the precipitate formed for region four of the calcium series. No other calcium orthophosphate species had a representative calcium solubility limit to that measured (Table 7) and the new solubility data reported in Figure 12, agrees well with the data solubility found here further suggesting the formation of β-TCP.

β-TCP cannot be precipitated from aqueous solution (Dorozhkin, 2007) β-TCP is a high temperature phase of calcium orthophosphate that may be prepared e.g. by the thermal decomposition of CDHA at 800^{o}C. Temperature of this magnitude is not expected for a LOCA scenario and is not inside the range experimented here. Production of

fiberglass requires melting of glass such that the molten glass can be poured and spun to create thin strands of glass. PCI states in the NUKON MSDS (PCI, 2015) a melting point of 704ºC. It is proposed that β-TCP formed in the manufacturing of the NUKON could control the solubility, seen in region 4 of calcium leaching experiments. The presence of magnesium is believed to prevent the immediate formation of this product.

Considering the tapering off behavior to hold true for region 2, the representative calcium solubility value for the metastable region was considered to be from the lowest attained value for each test's particular metastable region. For each metastable region measured during 4000 series testing, the lowest measured calcium concentration was tabulated, including the measured value's test day, and the measured pH on that day. Comparing the values tabulated to Table 7, the most likely solubility products were DCPA and CDHA. For each of these calcium orthophosphates the calcium solubility limit was calculated at the measured pH value and at the testing temperature of 80ºC (Table 15) using the process outlined in chapter 2. CDHA has a lack of true crystalline structure resulting in variable stoichiometric coefficients (CDHA: $Ca_{(10-x)}(HPO_4)_x(PO_4)_{(6-x)}(OH)_{(2-x)}$) (Dorozhkin, 2009), where x can vary between 0 and 1. The value for CDHA used for this initial testing assumed a boundary condition of x equal to 1 resulting in a Ca/P ratio of 1.5; the TCP ratio found in region 4.

Table 15: Models the two most likely calcium orthophosphates solubility limit at the test temperature and measured pH for the comparison to metastable calcium concentrations

Test	**Lowest Metastable [Ca] (mg/L)**	**Test Day**	**pH**	**[Ca] (mg/L) Assume DCPA 80ºC Measured pH**	**[Ca] (mg/L) Assume CDHA 80ºC Measured pH**
4300.P2	5.4	5	7.25	6.52	4.95
4300.P3	5.9	6	7.27	6.51	4.80
4300.Tank	4.5	8, 10	7.38, 7.42	6.47, 6.48	4.08, 3.85
4400	4.9	7	7.55	6.54	3.20

In general the calculated solubility was closer to CDHA than to DCPA. In the cases where DCPA was closer (4300.P3, and slightly for the column) both assumed precipitates were off from the measured value by more than 10%. DCPA is more stable at low pH and

was not expected at the pH range measured. CDHA may be produced by adding quantities of calcium and orthophosphates to boiling water, in sufficient quantities to form immediate precipitation, e.g. 4200 series at 100^{o}C. The similarity in the formation of CDHA and ACP (same procedure as CDHA at <100^{o}C) leads to similarities in the properties. CDHA has an undefined stoichiometry, which is proposed to explain the multiple metastable region values have been observed in testing that may be higher or lower based off fiberglass concentration.

The assumed value of x=1 used to generate the thermodynamic modeling is a boundary case where the Ca/P ratio is 1.5, the same as β-TCP. Therefore the precipitate could be arranging in the formation of β-TCP but the high concentration of magnesium is forming magnesium substituted CDHA, or a magnesium substituted β-TCP. To determine how close this CDHA value stoichiometry formed was to the boundary condition of x=1, the x value for the chemical formula of CDHA ($Ca_{(10-x)}(PO_4)_{(6-x)}(OH)_{(2-x)}$) was manipulated to reach the measured calcium concentration at the measured pH (Table 16). The values calculated were near 0.966 except in the case of the column test which differed from other tests in the possibility of additional latent debris leaching.

Table 16: x-value required for theoretical [Ca] to match measure concentration in metastable position

Test	[Ca] assume CHDA	Day	pH	x value
4300.P2	5.4	5	7.25	0.978
4300.P3	5.9	6	7.27	0.948
4300.Tank	4.5	8	7.38	0.978
4300.Tank	4.5	10	7.42	0.96
4400	4.9	7	7.55	0.89

Known to have similar properties to ACP, one observed similarity was the presence of magnesium stabilizing the CDHA in region 2. Posner set a limit of 0.2 molar ratio of Mg:Ca as the limit at which ACP could no longer convert to HAp. To investigate the relation of magnesium and calcium, the molar ratio was plotted for comparison to the changes in calcium concentration. Although the behavior of calcium was seen to be reproducible on the bench scale, results also showed that variations in the drop could occur

e.g. 4300.P3 day 6 and 12. Each bench test represents an identically prepared but separate experiment, whereas large-scale experimentation represent a continuous experiment. Therefore when considering the effects of magnesium on the dropping, each bench test must be considered in isolation (e.g. each result is independent), whereas for large-scale testing, the change in measured calcium concentration represents the progression of a single experiment, and each result may be considered dependent on the previous. Of the two large-scale experiments, only the column test captured the drop in calcium concentration.

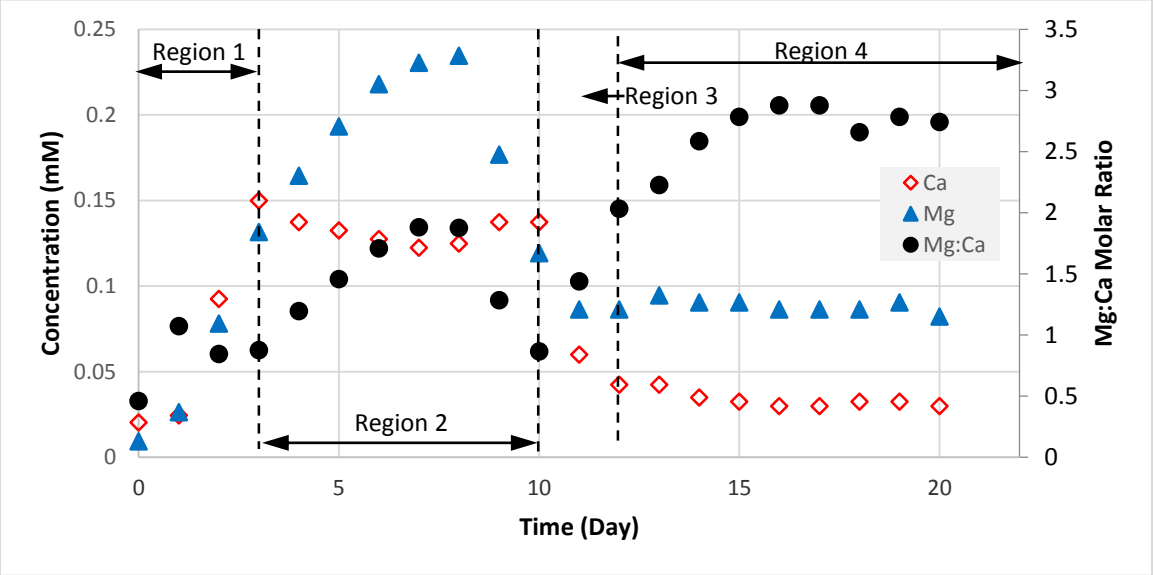

Figure 61: 4400 Series molar concentrations and Mg:Ca molar ratio

The 4400 series was the only continuous experiment to capture the drop in calcium concentration, occurring at a Mg:Ca ratio of 0.87. The drop in magnesium concentration occurred at a Mg:Ca molar ratio of 1.9 for the column test (Figure 61). The drop in the calcium behavior was proposed to be from the decrease in magnesium, therefore destabilizing the CDHA. The final measured molar ratio in region four had a molar ratio of 2.7.

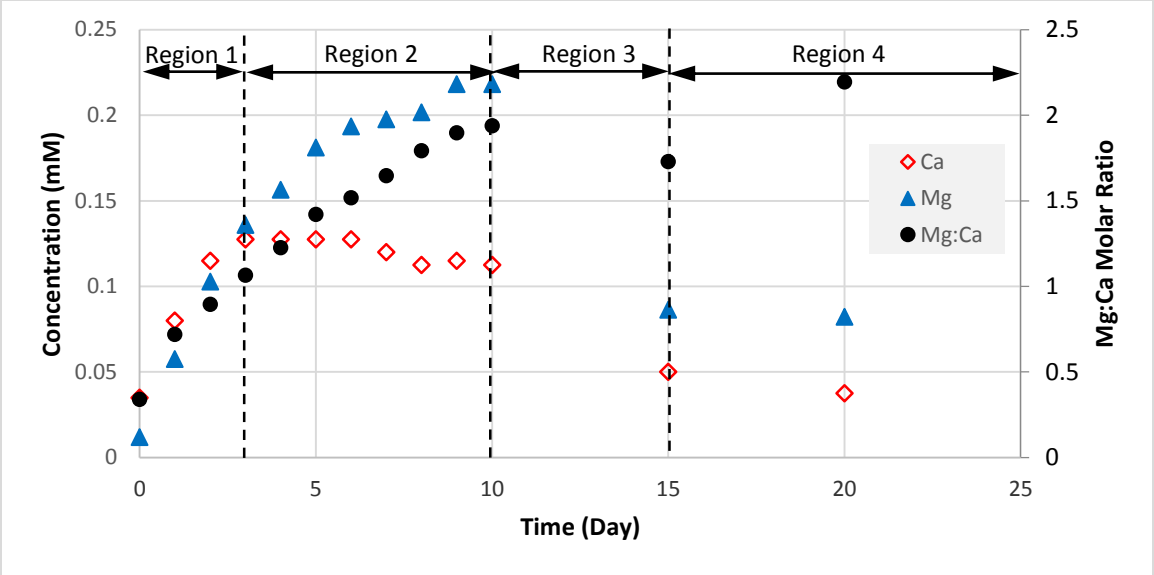

Figure 62: Molar concentrations of 4300.P3 test and Mg:Ca molar ratio

The maximum molar ratio in 4300.Tank was observed to be 1.9, the same as the maximum molar ratio in the column. No data is available until five days after the maximum molar ratio. This 15th day data point for the tank test had a calculated molar ratio of 1.7, compared to 2.2 in the tank. The tank approached a molar ratio of 2.2 by day 20. The presence of addition leaching materials was proposed to lead to decreased time to observe the drop in calcium concentration, and faster rise in the magnesium concentration post drop.

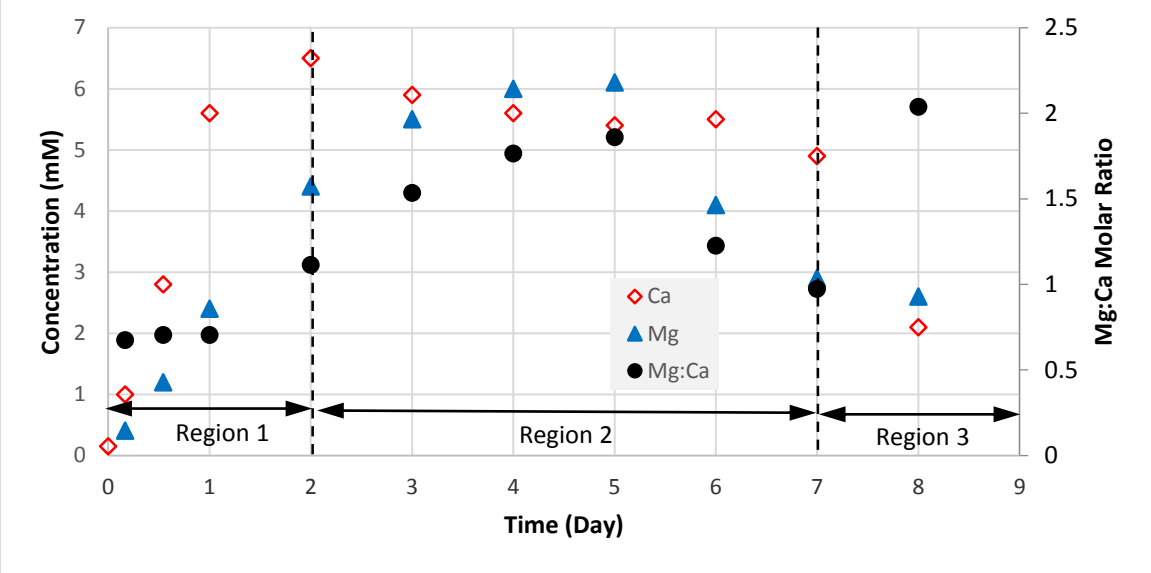

Figure 63: Molar concentrations of 4300. P2 test and Mg:Ca molar ratio

The molar ratio of 1.9 is again observed before the drop in calcium concentration in 4200.P2. Araujo et. al. (Araujo, 2009) prepared a 0.2 Mg:Ca molar ratio CDHA by wet precipitation at pH 9 at 38ºC, using 1.25 M $Ca(OH)_2$, 2.85 M H_3PO_4 and varying amount on $MgCl_2 \cdot 6H_2O$, in 25ºC solution over 24 hour period. The solution was then dried at 40ºC and sintered at 1000ºC to create a maximum of nearly 15 mol% Mg-β-TCP ($Ca_{2.61}(Mg1_{0.28},Mg2_{0.11})(PO_4)_2$). Although the exact precipitate is not known, it is most likely CDHA, which will assist in the explanation of the observed head-loss.

5.4 Effects of Precipitate Ripening on Calcium Concentration

This section will focus on the know properties of the determine solubility products to describe the regional calcium behavior. Analyses for the bench (Figure 64) and large-scale tests (Figure 65) are divided into two graphs due to the difference in fiberglass concentrations (bench: 2 g/L; large-scale: 1.18 g/L) and the previous discussion on the dependence of calcium concentration in solution relative to fiberglass concentration.

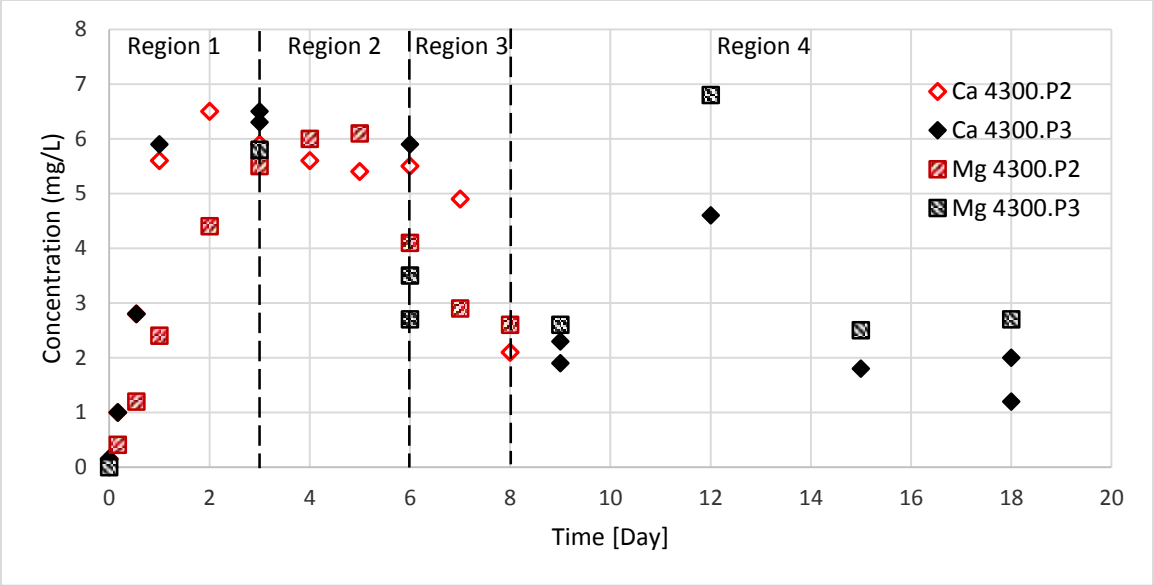

Figure 64: Identical condition bench scale calcium leaching tests with 2 g/L NUKON fiberglass concentration

Region 1 was the prompt release of calcium which was defined by the calcium concentration in solution. The greater the fiberglass concentration the higher observed maximum calcium concentration and the less time taken to reach region 2. In addition to calcium, region 1 corresponded to a prompt release of magnesium as well. The prompt release of magnesium continued into region 2.

Region 2 was defined as the metastable region of calcium. This metastable region was observed from 4 to 7 days. This region was known to be controlled by magnesium, where a maximum Mg:Ca ratio of 1.9, initiated a decrease in magnesium concentration. Magnesium is still in the prompt release stage during calcium region 2. It was proposed that magnesium reaching the maximum value in solution was dependent in the same way as calcium. Higher concentrations of fiberglass will lead to a decrease in the time taken for magnesium to reach the maximum concentration. Therefore, tests with higher magnesium concentrations were expected to have short region 2 durations, in comparison to lower fiberglass concentration experiments. Comparing the 2 g/L (Figure 64) metastable region to the 1.18 g/L (Figure 65) metastable confirms this hypothesis.

Region 3 was the autocatalytic drop in calcium concentration occurring 2 days after the maximum Mg:Ca molar ratio was achieved for 4300.P2 and 4400. The decrease in

magnesium concentration prior to a change in calcium concentration indicated the formation of two separate precipitates, of which the calcium orthophosphate was stabilized by the presence of magnesium. Considering this precipitate to be CDHA, with similar properties to ACP, stabilization by magnesium was reasonable.

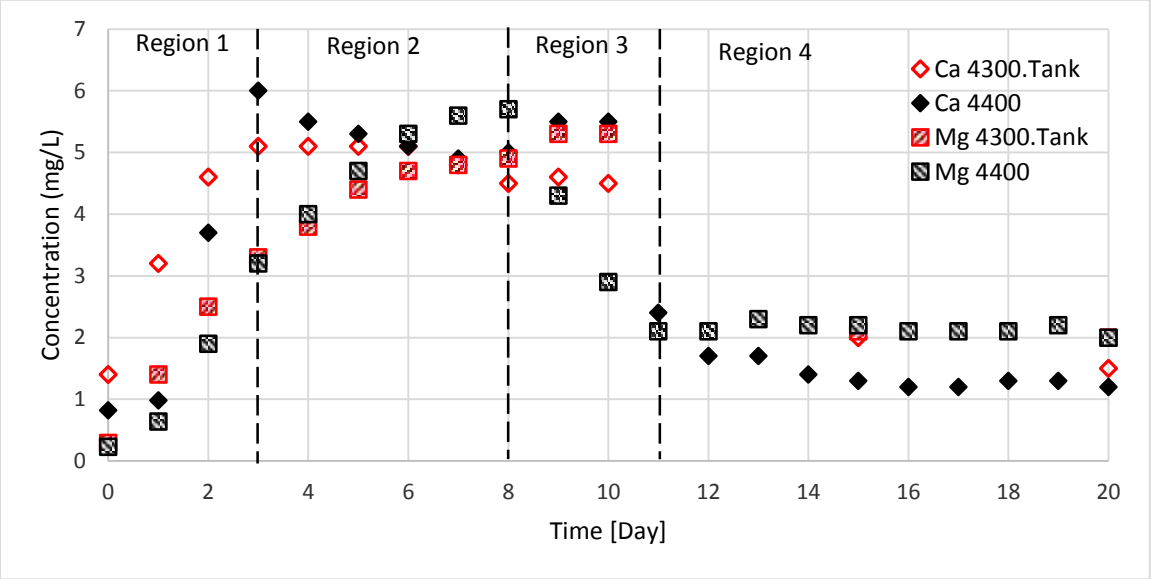

Figure 65: Measured calcium and magnesium in solution for large-scale calcium leaching test with fiberglass concentration 1.18 g/L

Region 4 was the final stable position observed to occur out to 30 days presumed to be β-TCP. Although β-TCP is unable to precipitate from solution, the fabrication of fiberglass could lead contain calcium orthophosphates. If β-TCP is magnesium substituted, the solubility of this phase has been found to depend on the concentration of substituted magnesium in the β-TCP (Li et. al., 2009) as $pKsp = 28.87432 + 1.40348C - 0.3163C^2 + 0.04218C^3 - 0.00275C^4 + 0.0000681659C^5$, where C is the concentration of magnesium in the β-TCP in mol %.

5.5 Effects of Calcium & Magnesium on Measured Head-loss

The fiber leaching experiment conducted in the vertical head-loss column focused on the relationship between changes in calcium concentration and head-loss over extended periods. During the test, samples were collected from the removable flange on top of the

column (before filtration) and from a sampling port at the bottom end of the column (after filtration). Sampling port selection did not affect ICP-OES measurements, but samples taken from the bottom resulted in more reliable turbidity measurements, which showed a decreasing trend on particle size from 1.3 on day 3 to 0.45 on day 15 compared to the top samples. During the test, reduction in the measured column approach velocity was observed as results of head-loss increase and debris bed compaction. The increased head-loss caused a slight change in bed porosity, increased the flow resistance, and changed the operating condition of the centrifugal pump (Approach velocity 0.013 ft/s). The pump does not compensate the flow resistance by increasing its frequency to recover the same flow condition (flow rate and velocity) automatically. Starting on the 10^{th} day experimentation a decrease in the velocity was observed (Figure 18), and by the 20^{th} day of testing, the approach velocity decreased to 0.012 ft/s.

When comparing the measured head-loss across a prototypic debris bed to the regional calcium regional concentrations, each region had a progressively increasing trend in head-loss compared to the previous region. A correlation was developed between the formation of calcium phosphate precipitates and the increase in head-loss; each region is considered as a different stage of the calcium phosphate precipitation process. The region 1 head-loss slope only considers from hour 32 (decrease from loading velocity to prototypic velocity) onward. There was no increase in head-loss observed in region 1. In region 2, the CDHA precipitate had formed and were slowly reaching a stable concentration. As CDHA grows in solution, the debris bed porosity is decreasing, and therefore the head-loss should begin to increase. On days 8-10, a light increase in the calcium concentration was observed, which was attributed to the destabilization of CDHA. In region 3, there was a sharp decrease in calcium concentration in solution. There is also a corresponding increase in the head-loss, by a factor of 4. Region 4 was a recession period as β-TCP continues to form; a continual increase in head-loss is also measured during this period, but at a lesser rate than is observed in the transition from region 2 to region 3.

The resulting head-loss from the chemical behavior was overlain on a graph of the measured calcium and magnesium concentrations. The graph was then divided into five regions corresponding to the behavior of metals in solution. The regions correspond to the

initial four region calcium behavior, but region 2 was divided into 2 regions (A & B) at the maximum Mg:Ca molar ratio. This split in region 2 allowed for head-loss changes associated with the precipitation of magnesium to be observed.

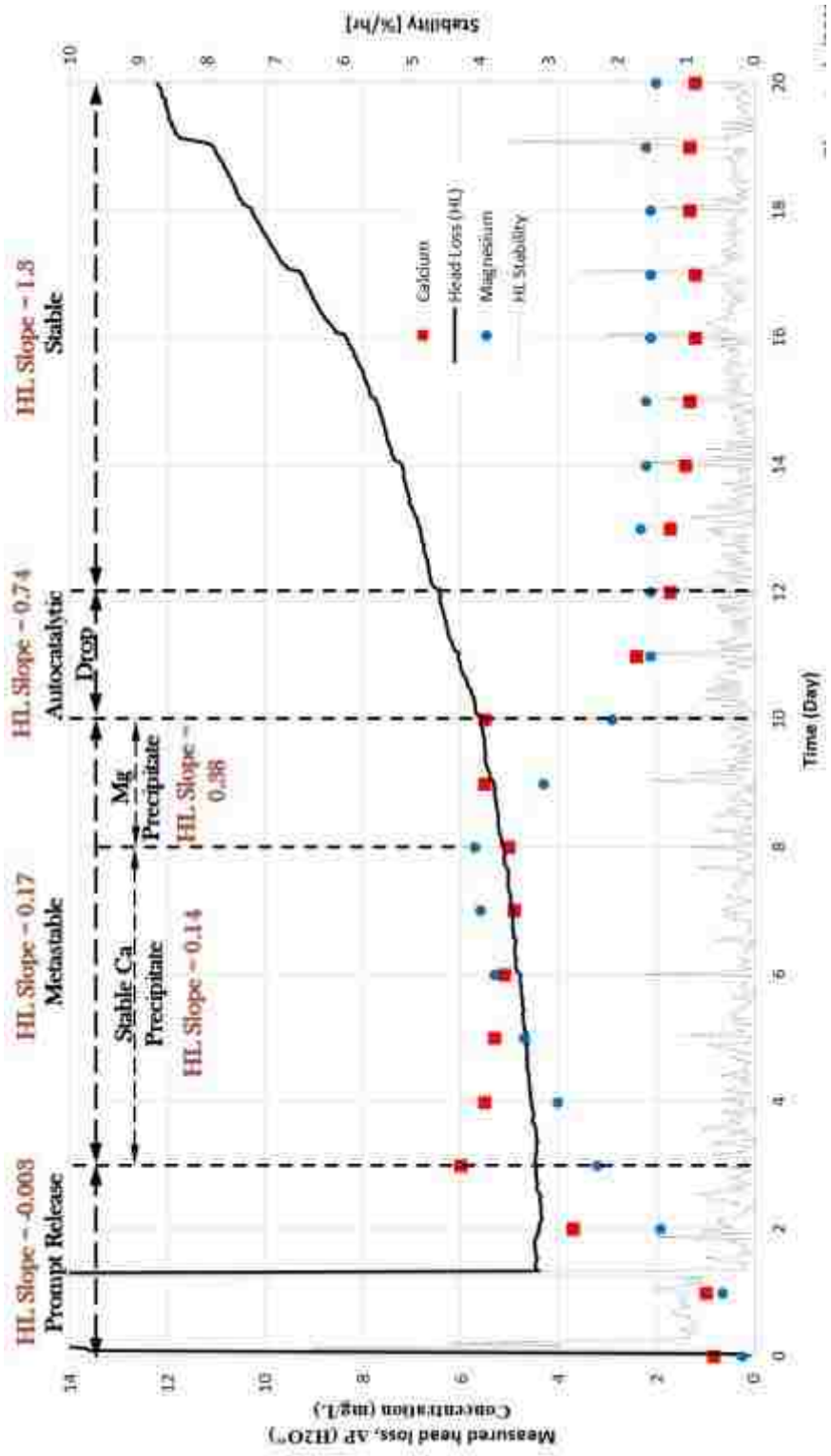

Figure 66: Five-Region column Ca & Mg concentration and the measured corresponding head-loss with stability criteria

The head-loss was observed to increase in each subsequent region. Region 1, region 3, and region 4 had the same head-loss slopes as observed in Figure 22. The total region 2 head-loss slope was 0.17 which now correspond to a head-loss slope of 0.14 and 0.38 for region 2 A, and region 2B respectively. The more than 2.5 times increase in head-loss slope change in region 2 was attributed to the precipitation of magnesium in region 2B. Region 3 would be expected to have an even higher increase in head-loss as magnesium continue to precipitate and CDHA transforms to β-TCP increasing the amount of calcium in the solid phase. A large increase was observed of 2 times increase in head-loss slope.

5.6 Conclusion

In an effort to understand the chemical effects of calcium leaching from NUKON fiberglass, several experiments were performed on three solution inventory scales subjected to a variety of flow profiles. The behavior of calcium in solution was observed to be repeatable for the conditions of the test, and can be divided into four predictable regions: (1) prompt release, (2) metastable region, (3) autocatalytic drop, and (4) stable region. Region 1 was found to be independent of the size distribution of the fiberglass, but sensitive to fiberglass concentration. This result implies that regardless of the fiberglass size distribution following a LOCA, the amount of calcium released from the NUKON will be the same for a given concentration. While independent of size distribution, the approach to region 2 demonstrates an inverse relationship between fiberglass concentration and the time needed to reach maximum calcium concentration in solution and the maximum concentration of leached calcium is dependent on the initial fiberglass concentration.

The duration of region 2 was directly related to the presence of magnesium in solution, since magnesium acts as a stabilizing agent to the ACP that is formed. Magnesium must reach a Mg:Ca molar ratio of 1.9, followed by precipitating out of solution. The initial drop in magnesium concentration occurring independent of changes in calcium concentration suggests that magnesium forms a separate precipitate. As the precipitation continues the magnesium concentration decreased, destabilized the CDHA, and allowing for the autocatalytic transformation to β-TCP. This investigation demonstrates that the

behavior of calcium and magnesium was coupled and that both elements need to be considered as co-dependent for future research.

The drop in calcium concentration observed in region 3 was studied for increases in head-loss in a heated vertical column. Head-loss slope demonstrated a four times increase in region 4 compared to region 2A determined to increase more than four times the head-loss slope observed in region 2. Furthermore outside of the prototypical debris bed constituents the head-loss did not account for the formation of corrosion products from other prototypical containment debris, most notably aluminum and zinc. Therefore, due to the retrograde solubility of calcium phosphates and the exclusion of other containment materials this head-loss test represents an upper bound on the formation of calcium phosphate chemical effects.

References

Ali, A., Williams, C., Blandford, E. D., & Howe, K. (2014) . Proceeding from ANS, 14; *Filtration of Particulates and Pressure Drop in Fibrous Media in Resolution of GSI-191*. Anaheim, CA: Winter Meeting and Nuclear Technology Expo.

Ali, A., Kim, S.-J., Williams, C., (2014). *Column Chemical Head Loss Experimental Procedure and Acceptance Criteria*. Unpublished report, University of New Mexico, Albuquerque New Mexico.

Araújo, J. C., Sader, M. S., Moreira, E. L., Moraes, V. C. A., LeGeros, R. Z., & Soares, G. A. (2009). Maximum substitution of magnesium for calcium sites in Mg-β-TCP structure determined by X-ray powder diffraction with the Rietveld refinement. Materials Chemistry and Physics, 118(2), 337-340.

Austria, "Translational Annex XV Dossier: Disodium tetraborate anhydrous," European Borates Association, Gratz, 2008.

Bachra, B. N., Trautz, O. R., & Simon, S. L. (1965). Precipitation of calcium carbonates and phosphates—III: The effect of magnesium and fluoride ions on the spontaneous precipitation of calcium carbonates and phosphates. *Archives of oral biology*, *10*(5), 731-738.

Benjamin, M. M. (2014). *Water chemistry*. Waveland Press.

Bethke, C. (1996). *Geochemical reaction modeling: Concepts and applications*. Oxford University Press.

Boskey, A. L., & Posner, A. S. (1974). Magnesium stabilization of amorphous calcium phosphate: a kinetic study. *Materials Research Bulletin*, *9*(7), 907-916.

Bum, B. C. (2013). Chemical effects on PWR sump strainer blockage after a loss-of-coolant accident: review on US research efforts. *Nuclear Engineering and Technology*, *45*(3), 295-310.

Dallman, J., Letellier, B., Garcia, J., Madrid, J., Roesch, W., Chen, D., ... & Sciacca, F. (2006). Integrated chemical effects test project: Consolidated Data Report. *United States Nuclear Regulatory Commission report NUREG/CR-6914*.

Dorozhkin, S. V. (2010). Amorphous calcium (ortho) phosphates. *Acta Biomaterialia*, *6*(12), 4457-4475.

Dorozhkin, S. V. (2007). Calcium orthophosphates. *Journal of materials science*, *42*(4), 1061-1095.

Dorozhkin, S. V. Calcium orthophosphates in nature, biology and medicine. Materials 2009; 2: 399-498. *Caracterización preclínica de las espumas de hidroxiapatita autofraguables in situ*, *297*, 300.

Eanes, E. D., Gillessen, I. H., & Posner, A. S. (1965). Intermediate states in the precipitation of hydroxyapatite. *Nature*, *208*(5008), 365-367.

References

Farzadi, A., Bakhshi, F., Solati-Hashjin, M., Asadi-Eydivand, M., & abu Osman, N. A. (2014). Magnesium incorporated hydroxyapatite: Synthesis and structural properties characterization. *Ceramics International*, *40*(4), 6021-6029.

Feenstra, T. P., & De Bruyn, P. L. (1979). Formation of calcium phosphates in moderately supersaturated solutions. *Journal of Physical Chemistry*, *83*(4), 475-479.

Gustafsson, J.P., Visual MINTEQ. www.lwr.kth.se/English/OurSoftware/vminteq/index.html. 2012.

Hart, G. H. (2004). A short history of the sump clogging issue and analysis of the problem. *Nuclear News*, *47*(3), 24-34.

Jain, V., et al. "Corrosion Rate Measurements and Chemical Speciation of Corrosion Products using Thermodynamic Modeling of Debris Components to Support GSI-191". NUREG/CR-6873 (2005).

Lahti, E. A. (2013) An Experimental Approach to Assessing Material Corrosion Rates in a Reactor Containment Sump Following a Loss of Coolant Accident (Unpublished master's thesis). The Ohio State University. Columbus, Ohio.

Lane, A. E., Andreychek, T. S., Byers, W. A., Jacko, R. J., Lahoda, E. J., & Reid, R. D. (2006). Evaluation of Post-Accident Chemical Effects in Containment Sump Fluids to Support GSI-191. *Westinghouse Electric Company LLC*.

Leavitt, J. (2013a). *T1 MBLOCA Test Report* (3rd rev.) . Unpublished report, University of New Mexico, Albuquerque New Mexico. Corrosion/Head Loss Experiment (CHLE) Program Report CHLE-012.

Leavitt, J. (2013b). *T2 LBLOCA Test Report* (2nd rev.) . Unpublished report, University of New Mexico, Albuquerque New Mexico. Corrosion/Head Loss Experiment (CHLE) Program Report CHLE-014.

Lee, J. I., Hong, S. J., Kim, J., Lee, B. C., Bang, Y. S., Oh, D. Y., & Huh, B. G. (2008). Debris Transport Analysis Related with GSI-191 in Advanced Pressurized Water Reactor Equipped with Incontainment Refueling Water Storage Tank. In Proc. of the XCDF4NRS Workshop-" Experiments and CFD Code Applications to Nuclear Reactor Safety.

Levy, S. (1999). Two-phase flow in complex systems. John Wiley & Sons.

Li, X., Ito, A., Sogo, Y., Wang, X., & LeGeros, R. Z. (2009). Solubility of Mg-containing β-tricalcium phosphate at 25 C. *Acta biomaterialia*, *5*(1), 508-517.

McMurray, J., et al. "GSI-191 PWR Sump Screen Blockage Chemical Effects Tests: Thermodynamic Simulations". NUREG/CR-6912 (2006).

Neuman, W. F., & Mulryan, B. J. (1971). Synthetic hydroxyapatite crystals. *Calcified tissue research*, *7*(1), 133-138.

References

Olson, S. (2014). *4000 Series Test Plan*. Unpublished report, University of New Mexico, Albuquerque New Mexico. Corrosion/Head Loss Experiment (CHLE) Program Report CHLE-SNC-011.

Olson, S. (2014). *4000 Series Test Procedure*. Unpublished report, University of New Mexico, Albuquerque New Mexico. Corrosion/Head Loss Experiment (CHLE) Program Report CHLE-SNC-012.

Olson, S. (2014). *4000 Series Test Report*. Unpublished report, University of New Mexico, Albuquerque New Mexico. Corrosion/Head Loss Experiment (CHLE) Program Report CHLE-SNC-012

Pan, H. B., & Darvell, B. W. (2009). Solubility of TTCP and β-TCP by solid titration. Archives of oral biology, 54(7), 671-677.

Park, J. H., Kasza, K., Fisher, B., Oras, J., Natesan, K., & Shack, W. J. (2006). *Chemical Effects Head-Loss Research in Support of Generic Safety Issue 191. The US Nuclear Regulatory Commission*. NUREG/CR-6913.

PCI. (2015, April 13). *Nukon® Insulation* [Material Safety Data Sheet]. Retrieved fromhttp://www.pciesg.com/media_library/NUKON_MSDS.pdf

Posner, A. S., & Betts, F. (1975). Synthetic amorphous calcium phosphate and its relation to bone mineral structure. *Accounts of Chemical Research*, *8*(8), 273-281.

Qiu, S. R., & Orme, C. A. (2008). Dynamics of biomineral formation at the near-molecular level. *Chemical reviews*, *108*(11), 4784-4822.

Shadanbaz, S., Walker, J., Woodfield, T. B., Staiger, M. P., & Dias, G. J. (2014). Monetite and brushite coated magnesium: in vivo and in vitro models for degradation analysis. Journal of Materials Science: Materials in Medicine, 25(1), 173-183.

Stipniece, L., Salma-Ancane, K., Borodajenko, N., Sokolova, M., Jakovlevs, D., & Berzina-Cimdina, L. (2014). Characterization of Mg-substituted hydroxyapatite synthesized by wet chemical method. *Ceramics International*,*40*(2), 3261-3267.

Tomazic, B., Tomson, M., & Nancollas, G. H. (1975). Growth of calcium phosphates on hydroxyapatite crystals: the effect of magnesium. *Archives of oral biology*, *20*(12), 803-808.

Wang, L., & Nancollas, G. H. (2008). Calcium orthophosphates: crystallization and dissolution. *Chemical reviews*, *108*(11), 4628-4669.

Zigler, G., Brideau, J., Rao, D. V., Shaffer, C., Souto, F., & Thomas, W. (1995). Parametric study of the potential for BWR ECCS strainer blockage due to LOCA generated debris. *United States Nuclear Regulatory Commission final report NUREG/CR-6224, Science and Engineering Associates, Inc., report SEA-93-554-06-A*, *1*, 163.